ACOUSTIC DIFFRACTION BY A FINITE
BARRIER; THEORIES AND EXPERIMENT

Gary M. Jebsen

NAVAL POSTGRADUATE SCHOOL
Monterey, California

THESIS

ACOUSTIC DIFFRACTION BY A FINITE
BARRIER; THEORIES AND EXPERIMENT

by

Gary M. Jebsen

March 1981

Thesis Advisor: H. Medwin

REPORT DOCUMENTATION PAGE		READ INSTRUCTIONS BEFORE COMPLETING FORM
1. REPORT NUMBER	2. GOVT ACCESSION NO.	3. RECIPIENT'S CATALOG NUMBER
4. TITLE (and Subtitle) Acoustic Diffraction by a Finite Barrier; Theories and Experiment		5. TYPE OF REPORT & PERIOD COVERED Master's Thesis; March 1981
		6. PERFORMING ORG. REPORT NUMBER
7. AUTHOR(s) Gary M. Jebsen		8. CONTRACT OR GRANT NUMBER(s)
9. PERFORMING ORGANIZATION NAME AND ADDRESS Naval Postgraduate School Monterey, California 93940		10. PROGRAM ELEMENT, PROJECT, TASK AREA & WORK UNIT NUMBERS
11. CONTROLLING OFFICE NAME AND ADDRESS Naval Postgraduate School Monterey, California 93940		12. REPORT DATE March 1981
		13. NUMBER OF PAGES 129
14. MONITORING AGENCY NAME & ADDRESS(if different from Controlling Office)		15. SECURITY CLASS. (of this report) Unclassified
		15a. DECLASSIFICATION/DOWNGRADING SCHEDULE

16. DISTRIBUTION STATEMENT (of this Report)

Approved for public release; distribution unlimited

17. DISTRIBUTION STATEMENT (of the abstract entered in Block 20, if different from Report)

18. SUPPLEMENTARY NOTES

19. KEY WORDS (Continue on reverse side if necessary and identify by block number)

Acoustic Diffraction, noise control, baffle,
impulse wave

20. ABSTRACT (Continue on reverse side if necessary and identify by block number)

The Biot-Tolstoy (B-T) exact impulse solution of diffraction by an infinite half-plane is compared to the usual Helmholtz-Kirchhoff (H-K) integral formulation and to the exact continuous wave (CW) solution of Macdonald. For backscatter the B-T and H-K solutions are found to differ significantly, especially near the surface of the half-plane, where the B-T solution gives close agreement with experiment. For forward scatter the two exact

DD FORM 1473 EDITION OF 1 NOV 65 IS OBSOLETE
1 JAN 73
S/N 0102-014-6601 |
Unclassified
SECURITY CLASSIFICATION OF THIS PAGE (When Data Entered)

1

Item 20:   continued.

solutions and experimental data are in agreement. B-T is found to
agree well with measurements of diffraction by a barrier perpendi-
cular to a rigid base. By considering source and source image in
the base separately the concept of "image of the source in the
barrier" is found to be unnecessary. Use of the time domain form
of B-T solution in calculating the forward diffraction near a
corner and behind a thin strip is shown to give results which agree
well with measured data. Secondary diffraction effects are
observed in the measurements of diffraction by a thin strip, a
non-vertical barrier and a thick edge.

Acoustic Diffraction by a Finite
Barrier; Theories and Experiment

by

Gary M. Jebsen
B.S., Florida Atlantic University, 1969

Submitted in partial fulfillment of the
requirements for the degree of

MASTER OF SCIENCE IN ENGINEERING ACOUSTICS

from the

NAVAL POSTGRADUATE SCHOOL
March 1981

ABSTRACT

The Biot-Tolstoy (B-T) exact impulse solution of diffrac-
tion by an infinite half-plane is compared to the usual
Helmholtz-Kirchhoff (H-K) integral formulation and to the exact
continuous wave (CW) solution of Macdonald. For backscatter
the B-T and H-K solutions are found to differ significantly,
especially near the surface of the half-plane, where the B-T
solution gives close agreement with experiment. For forward
scatter the two exact solutions and experimental data are in
agreement. B-T is found to agree well with measurements of
diffraction by a barrier perpendicular to a rigid base. By
considering source and source image in the base separately the
concept of "image of the source in the barrier" is found to be
unnecessary. Use of the time domain form of the B-T solution
in calculating the forward diffraction near a corner and be-
hind a thin strip is shown to give results which agree well
with measured data. Secondary diffraction effects are ob-
served in the measurements of diffraction by a thin strip, a
non-vertical barrier and a thick edge.

TABLE OF CONTENTS

I. INTRODUCTION

Many practical problems in acoustics are complicated by
the presence of boundaries which influence the sound field
in some way. When the direct path between source and receiver
is not obstructed, these boundaries represent a perturbation
to the free field solution. If the boundaries are infinite
in extent, the image or normal mode methods are often applied.
Finite boundaries introduce the additional phenomenon of
diffraction or scattering, which is often treated as an
additional perturbation to the free-field plus reflection
solution. When the finite boundary is such that it blocks
the direct path the problem is somewhat different.

In this case, the only sound reaching the receiver is
that which has been diffracted at the edge of the finite
boundary (assuming the boundary to be rigid). In terms of
airborne noise control a finite boundary that blocks the
direct path is often called a barrier or screen. When a
similar technique is applied to the reduction of unwanted
sound in a shipboard sonar system, the boundary is generally
called a baffle. The location and size of baffles on sub-
marines and surface ships are severely constrained by the
size of the ships themselves. As a result, the baffle is
often close to the radiating source and the receivers close
to the baffle. Care must be used in selecting a theoretical

approach to solving the diffraction problem under these cir-
cumstances since some of the techniques in general use involve
simplifying assumptions which may not be valid under these
rigorous conditions.

Much work on the solution to the barrier problem may be
found in the noise control literature. In this paper, two
solutions used in noise control are examined, along with the
little known solution by Biot and Tolstoy, and the theoreti-
cal results are compared. In addition, experimental results
relating to the application of theoretical solutions to
finite barriers are presented.

II.   THEORETICAL APPROACH

A.   GENERAL

The usual approach to solving the problem of diffraction
by a plate or barrier is to approximate the barrier mathe-
matically as an infinitely thin, opaque, half-plane. This
problem was first solved by Sommerfeld [Ref. 1] for plane
continuous waves and then by Carslaw [Ref. 2] for spherical
continuous waves. Macdonald's [Ref. 3] work for spherical
continuous waves is often referenced as the rigorous solu-
tion to diffraction by a wedge (and hence the half-plane).
In 1957 Biot and Tolstoy [Ref. 4] published their exact
impulse solution using the normal coordinate formulation.
Despite the fact that the Biot-Tolstoy impulse solution is
in closed form and contains only simple functions, many
authors in the noise reduction field still consider Macdonald
as the only exact solution [Ref. 5].

A second general approach to the problem is Kirchhoff's
approximate solution to the integral equation formulation
of Huygens' Principle. This approach has been used exten-
sively in both optics and acoustics and can be shown to give
reasonable agreement with observed results, within certain
limits, in spite of the fact that the basic simplifying
assumptions are generally acknowledged to be incorrect
[Ref. 6].

9

There are additional approaches to this problem that will not be explored here. A good summary of the various solutions in the context of the noise control barrier can be found in Reference 5.

Rigorous derivation of the three theories will not be attempted, however the development of each will be summarized in order that basic differences can be understood.

B.   BIOT-TOLSTOY FORMULATION

M.A. Biot and I. Tolstoy published their landmark paper [Ref. 4] on the normal coordinate approach to wave propagation in infinite media in 1957. Within this paper was an application of the normal coordinate approach in solving the problem of diffraction from an infinite wedge which forms the basis for the theoretical results in this paper. The important features of their work in the present application are as follows:

    a.   The solution is exact and in closed form.

    b.   The solution can be expressed in elementary functions.

    c.   The use of an impulse source provides insight into the contributions from various edges and a means of separating the diffracted from reflected and direct components.

The extension of their results to other types of sources is straightforward.

The normal coordinate approach is related to the normal mode description in acoustics which is most often encountered

in the solution of problems where the medium is bounded such
as room acoustics, shallow water sound propagation, and
speaker enclosures. In these cases the normal coordinates
are the allowable modes of vibration (normal modes) of the
system. The overall response of the system is the super-
position of these discrete normal modes. Stated another way,
an external source excites all modes at various amplitudes
and phases and the solution then is the coherent sum of all
these individual excitations. The essence of the normal
coordinate approach to the solution of general diffraction
problems is the extension of the principle of superposition
of normal modes to infinite media. As the boundaries of the
"enclosure" are removed toward infinity the spacing between
normal modes becomes progressively less, with the limit
being a continuous response spectrum with the boundaries at
infinity. If we now introduce a source which "turns on" at
time $t = 0$ (a transient source), the solution contains only
waves traveling outward and no radiation condition need be
imposed. The solution summarized here is taken primarily
from Reference 7.

In order to formulate the problem of diffraction by a
wedge, a cylindrical coordinate system is chosen with the
origin at the wedge crest and the z-axis along the crest as
shown in Figure 1. In this system the acoustic wave equation,
in terms of displacement potential ϕ, is written as

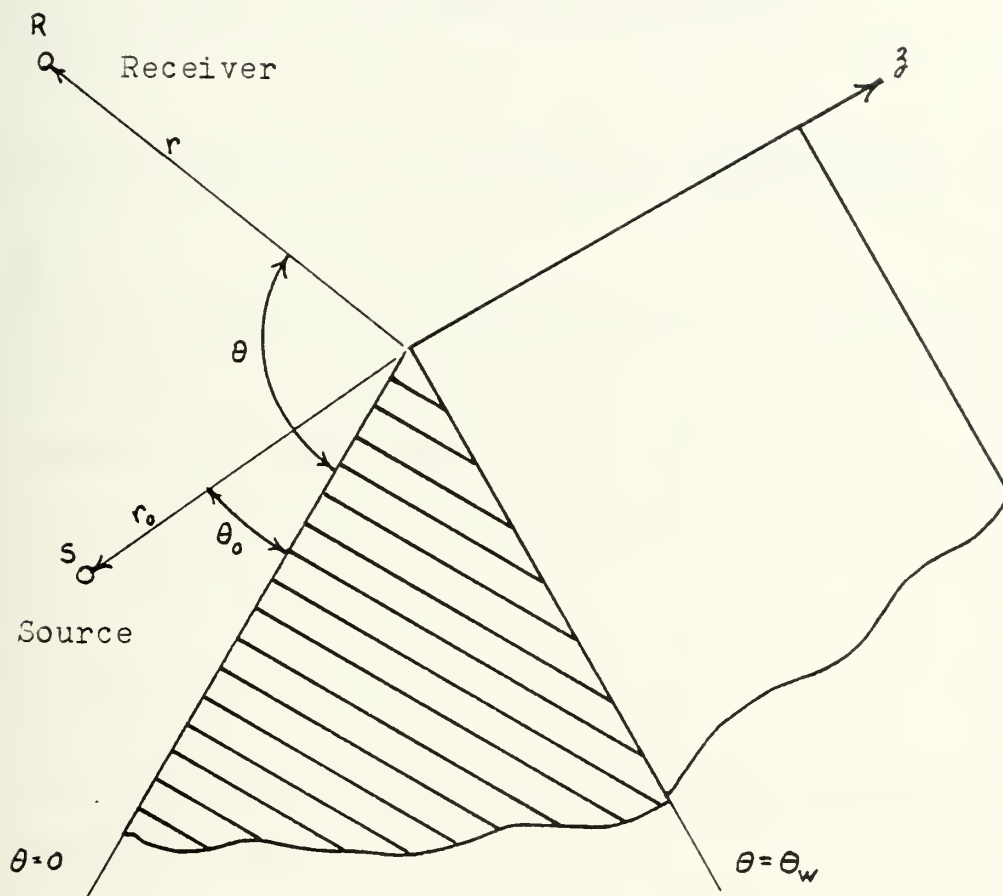Figure 1.   General Infinite edge Diffraction Coordinate
            System.

$$\frac{\partial^2\phi}{\partial r^2} + \frac{1}{r}\frac{\partial\phi}{\partial r} + \frac{1}{r^2}\frac{\partial^2\phi}{\partial\theta^2} + \frac{\partial^2\phi}{\partial z^2} - \frac{1}{c^2}\frac{\partial^2\phi}{\partial t^2} = 0 \qquad\qquad \text{(II-1)}$$

By separation of variables the harmonic solutions are

$$\phi = e^{\pm i\nu\theta}H_\nu{}^{(1,2)}(\kappa r)\ e^{\pm i\gamma z}e^{\pm i\omega t} \qquad\qquad \text{(II-2)}$$

where the separation constants are related by

$$\gamma^2 = \frac{\omega^2}{c^2} - \kappa^2, \qquad k = \frac{\omega}{c}$$

Applying the boundary conditions for a rigid wedge,

$$\frac{\partial\phi}{\partial\theta} = 0 ; \quad \theta = 0, \ \theta = \theta_w$$

restricting the amplitude to be finite at $r = 0$, and choosing a location for our point source ($r = r_0$, $\theta = \theta_0$, $z = 0$) that will result in z-axis symmetry, the solution is written as

$$\phi_n = J_{\nu_n}(\kappa r)\cos\nu_n\theta\ \cos\gamma_n z e^{\pm i\omega t} \qquad\qquad \text{(II-3a)}$$

$$\nu_n = \frac{n\pi}{\theta_w} \qquad\qquad \text{(II-3b)}$$

The solution can be separated into space-dependent and time dependent parts,

$$\phi_n = q_n\psi_n \qquad\qquad \text{(II-4a)}$$

$$\psi_n = J_{\nu_n}(\kappa r)\cos\nu_n\theta\cos\gamma z \qquad\qquad \text{(II-4b)}$$

The q_n are the normal coordinates which satisfy the differential equation

$$\ddot{q}_n + \omega^2 q_n = \frac{Q_n}{u_n} \qquad\qquad \text{(II-5)}$$

here Q_n is the generalized source function and u_n is proportional to the kinetic energy in each mode. The series represented by (II-4) is known to be orthogonal and may be normalized by the condition

$$u_n = \rho \int_0^{\theta w} d\theta \int_{-\infty}^{+\infty} dz \int_0^{\infty} (\nabla \psi_n)^2 r \, dr$$

The medium is infinite in the r and z directions resulting in divergent integrals. These are handled by Tolstoy using a symbolic limiting procedure (discussed in detail in Reference 7, section 8-2) resulting in the following expression

$$u_n = \frac{\rho}{2} \theta_w \frac{\omega^2}{c^2} \frac{\pi}{\kappa \frac{d\kappa}{d\gamma}} \qquad (II-6)$$

It is at this point that we must choose an appropriate form for the generalized source, Q_n.

The usual approach (and the one which we will ultimately use) is to choose the delta function or unit impulse source. It has two distinct advantages over other forms. First, it will result in a solution identical to that achieved via the Green's function approach, at least for those modes which are physically realizable. Second, it provides a simple building block with which the solution for other source forms can be constructed through the application of Duhamel's theorem. The result is analogous to analysis of electronic filters: the response of the system to a unit impulse input is the

14

system impulse response. The system transfer function is
the Fourier transform of this impulse response.

Biot and Tolstoy choose the source such that the displace-
ment potential at a distance R is of the form

$$\phi = - \frac{1}{4\pi R} \, 1(t - {}^R/C) \qquad\qquad (II-7)$$

where $1(t - {}^R/C)$ is the unit step function having the value
zero for $(t-{}^R/C)<0$ and one for $(t-{}^R/C)>0$. This represents
the instantaneous injection of a unit volume at the source
coordinates and is commonly used as a mathematical approxima-
tion to an explosion. Since the pressure and displacement
are related by

$$p = - \rho\frac{\partial^2\phi}{\partial t^2} \qquad\qquad (II-8)$$

the pressure at a distance R due to the source function of
Equation (II-8) will be

$$p = \frac{\rho}{4\pi R} \frac{d}{dt} \, [\delta(t-{}^R/C)]$$

However, Medwin [Ref. 8] derives the solution for an impulse
source directly from Biot-Tolstoy by simply taking the pres-
sure to be proportional to the Biot-Tolstoy expression for
particle velocity, since the two source functions differ by
a first derivative. Medwin shows that this is equivalent to
assuming a point source of strength S (volume per time) which
flows uniformly beginning at time t = 0. The acoustic
pressure at range R due to this source is given by

15

$$Q_n = -\lambda 1(-t)[\nabla^2 \psi_n]_o \qquad \qquad (II-10)$$

where λ is the bulk modulus of the fluid, and ψ_n is the space
dependent solution for the free modes (Equation II-4). The
Lapacian of ψ_n, in brackets, is evaluated at the location of
the source. Substituting (II-4) into (II-10) and utilizing
(II-6), the differential Equation (II-5) can be written as

$$\ddot{q}_n + \omega^2 q_n = \frac{2C^2}{\pi\theta_w} 1(-t) \, J_{\nu_n}(\kappa r_o)\cos\nu_n\theta_o \kappa d\kappa d\gamma \qquad (II-11)$$

The solution to (II-11) represents the normal coordinates for
the problem,

$$q_n = \frac{\cos \omega t}{\omega^2} \frac{2C^2}{\pi\theta_w} J_{\nu_n}(\kappa r_o)\cos\nu_n\theta_o \kappa d\kappa d\gamma \quad t \geq 0 \qquad (II-12)$$

Substituting into (II-4a) and taking the time derivative, the
solution can be written as

$$\frac{\partial\phi}{\partial t} = -\frac{2C^2}{\pi\theta_w} \sum_n \cos\nu_n\theta \, \cos\nu_n\theta_o \int_0^\infty \int_0^\infty J_{\nu_n}(\kappa r)J_{\nu_n}(\kappa r_o) \, \cos\gamma z \, X$$

$$\frac{\sin \omega t}{\omega^2} \kappa d\kappa d\gamma \qquad \qquad (II-13)$$

Equation (II-13) represents an exact solution to the
perturbation of a propagating wave by the presence of a
rigid wedge, assuming Equation (II-10) as the form of the
source. Its present form is not particularly useful, how-
ever the application of two known integral transforms to
Equation (II-13) reveals its simplicity and its close re-
lationship to the physical problem in an intuitively

16

satisfying way. The application of these transforms is discussed next.

Equation (II-13) contains integrals with respect to both the z-axis wavenumber γ and the radial wavenumber κ. Considering the integration over γ first,

$$\int_0^\infty \cos\gamma z \ \frac{\sin \omega t}{\omega^2} \ d\gamma = \frac{1}{c} \int_0^\infty \cos\gamma z \ \frac{\sin ct(\gamma^2+\kappa^2)^{\frac{1}{2}}}{(\gamma^2+\kappa^2)^{\frac{1}{2}}} \ d\gamma \qquad (II-14)$$

and the relationship of the separation constants

$$\omega^2 = c^2(\gamma^2+\kappa^2)$$

The integral on the RHS of Equation (II-14) represents a known integral transform, as follows [Ref. 7]:

$$\frac{1}{c} \int_0^\infty \cos\gamma z \ \frac{\sin ct(\gamma^2+\kappa^2)^{\frac{1}{2}}}{(\gamma^2+\kappa^2)^{\frac{1}{2}}} \ d\gamma = \frac{\pi}{2c} \ J_0[\kappa(c^2t^2-z^2)^{\frac{1}{2}}] \quad ct>z$$

$$= 0 \quad ct<z \qquad (II-15)$$

The existance of two distinct forms of the solution, one of which is zero, is a direct consequence of the choice of a transient source, i.e. if the source is turned on at t = 0 there can be no effect at the receiver until a time equal to the source/receiver separation distance divided by the propagation speed. In this case, z is one component of that separation vector.

Using the result of (II-15) the remaining integral of (II-13) may be written as

$$I_n = \int_0^\infty J_{\nu_n}(\kappa r) J_{\nu_n}(\kappa r_o) \; J_o[\kappa (c^2 t^2 - z^2)^{\frac{1}{2}}] \kappa \, d\kappa \qquad (II\text{-}16)$$

This integral has a known solution which takes on three different forms depending upon the relationship of the variables r, r_o, and $(c^2 t^2 - z^2)^{\frac{1}{2}}$. Tolstoy [Ref. 7] defines these three regions in terms of the propagation time of a pulse emitted by the source at t = 0. The time of arrival (at the receiver) of the earlist possible direct pulse is given by

$$t_1 = \frac{1}{c}[(r-r_o)^2 + z^2]^{1/2}$$

The earliest time of arrival of the pulse which has traveled from source to receiver via the crest of the wedge is

$$\tau_o = \frac{1}{c}[(r + r_o)^2 + z^2]^{1/2}$$

With these new variables, the three regions of the solution are given by

I. $t < t_1$ $I_n = 0$

$$\qquad (II\text{-}17)$$

II. $t_1 < t < \tau_o$ $I_n = (\pi r r_o \sin X)^{-1} \cos \nu_n X$

$$X = \arccos \frac{r^2 + r_o^2 + z^2 - c^2 t^2}{2 r r_o} \qquad 0 \le X \le \pi$$

$$\qquad (II\text{-}18)$$

III. $\tau_o < t$ $I_n = -(\pi r r_o \sinh Y)^{-1} \sin(\nu_n \pi) e^{-\nu_n Y}$

$$Y = \operatorname{argcosh} \frac{c^2 t^2 - (r^2 + r_o^2 + z^2)}{2 r r_o}$$

$$\qquad (II\text{-}19)$$

18

These three regions have a strong intuitive foundation. In Case I. it is obvious that a pulse transmitted by the source cannot be received until a finite time has elapsed, that time being equal to the separation divided by the propagation speed. Case II. represents that time during which reflections from the face of the wedge are received. Tolstoy [Ref. 7] shows that when this expression for I_n is substituted into Equation (II-13), the solution takes the form of images of the source in the reflecting wall. Finally, Case III. is the diffracted wave. It is characterized by an arrival time which is later than the last possible image source arrival, as seen from Figure 1.

The same results can also be interpreted geometrically, as discussed by Watson [Ref. 9]. If we rename the variables r, r_o, and $(c^2 t^2 - z^2)^{\frac{1}{2}}$ in (II-16) as b, c, and a, respectively, Watson points out that the three regions of the solution can be described in terms of the geometry of Figure 2 (z is taken to be zero for simplicity). The solution of Case II. applies whenever the value of side a is such that a triangle can be formed having sides a, b, c. It is obvious that this will be the case whenever a has the values

$$(b-c) < a < (b+c)$$

and, from the law of cosines, the angle A will be given by

$$A = \arccos \frac{b^2 + c^2 - a^2}{2bc} \qquad \text{(II-20)}$$

where A can take on values between o and π. The comparison with Equation (II-18) is immediate. In Case III., a is
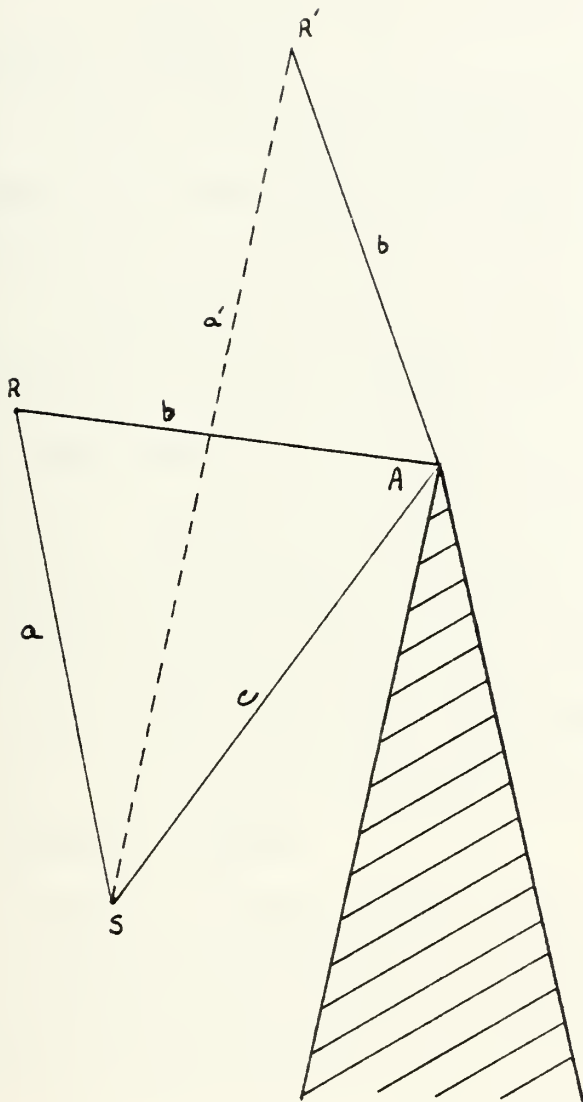
19

Figure 2.   Source, Receiver, and Wedge Crest Geometry.

20

greater than (b+c), the angle A becomes imaginary, and the expression corresponding to (II-20) must come from hyperbolic trigonometry:

$$A = \text{argcosh } \frac{a^2 - b^2 - c^2}{2bc} \tag{II-21}$$

It can be seen from this discussion that the Biot-Tolstoy formulation in the time domain decomposes into direct/reflec-ted and diffracted components in an intuitively satisfying way. This is apparently due to the use of the normal coor-dinate formulation, which considers only modes which are physically realizable, and the choice of the transient form of the source. However, because of this distinct division between direct and diffracted solutions, considerable care must be exercised when working with a geometry where the arrival times of the direct and diffracted waves are close, such as near the boundary between the "illuminated" region and the geometric shadow.

To arrive at the final solution for the diffracted wave, the result of Equation (II-19) is applied to the general solution (II-13) as follows:

$$\frac{\partial \phi}{\partial t} = \frac{c}{\pi \theta_w} (rr_0 \sinh Y)^{-1} \sum_{n=0}^{\infty} \cos \nu_n \theta_0 \cos \nu_n \theta \sin \nu_n \pi e^{-\nu_n Y}$$
$$\nu_n = \frac{n\pi}{\theta_w} \tag{II-22}$$

Expressing the sum in terms of exponentials, regrouping, and collecting in conjugate pairs, the solution can be written in exact, closed form as

21

$$\frac{\partial \phi}{\partial t} = \frac{c}{4\pi\theta_w}(rr_o \sinh Y)^{-1} e^{-\frac{\pi Y}{\theta_w}} \{\frac{\sin\,(\frac{\pi}{\theta_w}(\pi\pm\theta\pm\theta_o))}{1-2e^{-\frac{\pi Y}{\theta_w}}\cos(\frac{\pi}{\theta_w}(\pi\pm\theta\pm\theta_o))+e^{-\frac{2\pi Y}{\theta_w}}}\}$$

$$(II-23a)$$

$$Y = \text{argcosh}\,\frac{c^2 t^2 - (r^2 + r_o^2 + z^2)}{2rr_o}\qquad (II-23b)$$

where the term $(\pi\pm\theta\pm\theta_0)$ indicates that the entire expression within the curly brackets is the sum of four terms, each of which corresponds to a unique combination of $(\pi\pm\theta\pm\theta_0)$.

Recalling the discussion concerning the forms of the impulse source, Equation (II-23) can now be used in place of the second partial derivative in (II-8) and the solution of the diffracted wave in terms of pressure can be written as

$$p(t) = -\frac{\rho cS}{4\pi\theta_w}(rr_o \sinh Y)^{-1} e^{-\frac{\pi Y}{\theta_w}} \cdot \{\beta\}$$

$$(II-24)$$

where Y is given by Equation (II-23b) and β represents the term in curly brackets in Equation (II-23a).

Equation (II-24) represents the diffracted pressure as a function of time due to a unit impulse source. To within a constant representing the source strength, this is analogous to the impulse response, h(t), of a general linear system. This impulse response is often Fourier transformed to obtain the transfer function $H(\omega)$ and examined in the frequency domain. Since there is no known analytical transform of

22

of Equation (II-24), the numerical technique of computing the impulse response in discrete time steps and then transforming using the Fast Fourier Transform (FFT) is employed. To avoid the problem of infinite values of h(t) for the earliest diffracted arrival, Medwin uses an approach which computes the first time point by a numerical integration. All of the Biot-Tolstoy theoretical results presented in this paper are calculated in this way.

C. HELMHOLTZ-KIRCHHOFF FORMULATION

The Helmholtz-Kirchhoff formulation is a mathematical statement of the heuristic description of wave propagation due to Huygens. Simply stated, a source at some distance from the surface (in this case a plate which has one straight edge and extends to infinity in three directions) insonifies all points on the surface S. Each small area element, ds, on the surface then acts as apoint source of spherical waves. At some observation point Q, the acoustic field is due to the incoming waves from the source directly plus the sum of the contributions from all of the point sources on the surface. Neglecting the effect of the direct incoming waves at Q, the field can be determined by integrating over the surface. To construct an exact solution in this manner one would have to know the amplitude and phase of each point "source" on the surface. This not possible, in general, and therefore the Kirchhoff approximation is used. The brief development

given herein follows that in Clay and Medwin [Ref. 10]. A

detailed derivation can be found in most optics texts and

in a book by Baker and Copson [Ref. 6].

From Green's theorem, assuming a source of time dependence

$e^{i\omega t}$, the filed at the observation point Q can be expressed

as

$$U(Q) = \frac{1}{4\pi} \int_S [U\frac{\partial}{\partial n}(\frac{e^{-ikR}}{R}) - \frac{e^{-ikR}}{R}(\frac{\partial U}{\partial n})]_S \, ds \qquad (II-25)$$

where R is the distance from each element ds to the observa-

tion point Q and $\frac{e^{-ikR}}{R}$ is the free space Green's function.

That the integrand is evaluated on the surface is denoted

by the subscript s on the brackets. This known as the

Helmholtz-Kirchhoff integral. It describes the relationship

of the field at Q to the field on S, but the problem of

evaluating the field on S is not yet resolved.

Equation (II-25) can be used to evaluate the diffracted

wave field on either side of the surface. Our primary in-

terest is the diffracted field when source and receiver are

on opposite sides of the surface, however, when they are on

the same side (herein referred to as backscatter) the result-

ing expressions can be somewhat simplified. Since the purpose

of this development is to compare the results with those of

the normal coordinate approach, the simpler case will be

used. For a complete treatment of this Helmholtz-Kirchhoff

integral equation approach, see Baker and Copson [Ref. 6].

If U_s is defined as the incident wave field at the loca-
tion of the surface, with the surface removed, then the
quantity U within the integral can be approximated by

$$U = MU_s \qquad \text{(II-26)}$$

where M is the plane wave reflection coefficient. From
equation (II-26) the normal derivative can be written as

$$\frac{\partial U}{\partial n} = - M \frac{\partial U_s}{\partial n} \qquad \text{(II-27)}$$

By Equation (II-26), the restriction has been imposed that
the only wave field that can exist on the insonified surface
of the barrier is that due to reflection of the incident
wave field (i.e., there can be no scattered field on the
surface). The consequence of this assumption will be seen
when the diffracted field near the surface is examined.

The additional assumption that is required to make the
integral in (II-25) tractable concerns the reflection co-
efficient M. Kirchhoff's assumption considers it to be
equal to the plane wave reflection coefficient for an infi-
nite plane interface. Here the surface is assumed to be
perfectly rigid and M = 1. Equation (II-25) can now be
written as

$$U(Q) = \frac{1}{4\pi} \int_s \frac{\partial}{\partial n}(U_s \frac{e^{-ikR}}{R}) \ ds \qquad \text{(II-28)}$$

When the integral in Equation (II-28) is taken over the
surface of the half-plane, the U(Q) represents the backscat-
tered wave field. If, on the other hand, the integral in
Equation (II-28) is taken over the portion of the plane not

25

occupied by the surface (generally referred to as the aperture in optics literature), U(Q) would represent the wave field scattered forward into the shadow region on the side of the half-plane opposite the source. (Note that this approach would also require a change of sign due to Equation (II-27).

D. MACDONALD'S FORMULATION

The final theoretical development to be considered here is that of Macdonald [Ref. 3]. His solution, like Biot-Tolstoy, is an exact solution for the infinite rigid wedge, except that Macdonald assumes a continuous wave (cw) source. A derivation of his solution will not be attempted, instead, the results of Kawai, Fujimoto and Itow [Ref. 11) will be used. The calculations in their paper are based on an approximate form of Macdonald's solution given by Bowman and Senior [Ref. 12] but only the form of the exact solution is presented below.

From Reference 11 the exact solution can be written in terms of the velocity potential as

$$v = V(\theta_o) + V(-\theta_o)$$

$$v = ik \int_{-T_R}^{\infty} \frac{H_1^{(1)}(T^2 + kR)}{(T^2 + 2kR)^{1/2}} \, dT + ik \int_{-T_{R'}}^{\infty} \frac{H_1^{(1)}(T^2 + kR)}{(T^2 + 2kR)^{1/2}} \, dT \qquad (II-29)$$

where

$$T_R = \text{sgn}(\pi - \theta - \theta_o)(kR_1 - kR)^{1/2} \qquad (II-30a)$$

26

$$T_{R'} = \text{sgn}(\pi - \theta - \theta_o)(kR_1 - kR')^{1/2} \qquad (II-30b)$$

$$\text{sgn}(X) = \begin{cases} + 1 & X > 0 \\ - 1 & X \leq 0 \end{cases}$$

$$R = (r^2 + r_o^2 + z^2 - 2rr_o \cos(\theta + \theta_o))^{1/2} \qquad (II-31a)$$

$$R' = (r^2 + r_o^2 + z^2 - 2rr_o \cos(\theta + \theta_o))^{1/2} \qquad (II-31b)$$

$$R_1 = ((r + r_o)^2 + z^2)^{1/2} \qquad (II-31c)$$

$$k = \omega/c$$

r, r_o, z, θ, θ_o as defined in Figure 1

and $H_1^{(1)}$ is the first order Hankel function of the first kind.

The significant feature of this solution, first pointed out by Macdonald [Ref. 3], is that it consists of the sum of two velocity potentials, $V(\theta_0)$ and $V(-\theta_0)$. These are identified in the noise control literature as the source and the "image of the source in the barrier", respectively. This important interpretation of the solution will be discussed in a later section.

III. COMPARISON OF SOLUTIONS

A. BIOT-TOLSTOY AND HELMHOLTZ-KIRCHHOFF

Biot-Tolstoy (B-T) and Helmholtz-Kirchhoff (H-K) solutions will be compared by choosing a geometry in which both can be expressed in closed form. The backscatter case is chosen wherein source and receiver are in the same location. For this case the time domain solution for the H-K formulation is derived from Equation (II-28), once again following the development in Clay and Medwin [Ref. 10] with some minor changes in notation.

Taking source and receiver to be in the same location (backscatter only) and assuming an impulse source, U_s in Equation (II-28) can be written as

$$U_s = \frac{e^{-ikR}}{R} \tag{III-1}$$

Making this substitution and transforming the surface integral into an integral along the edge [Ref. 10, pg. 323] Equation II-28) can be written as follows:

$$
U(Q) = \frac{y}{4\pi} \int_{-\frac{\pi}{2}}^{\frac{\pi}{2}} \int_{\infty}^{r} d\, [\frac{e^{-2ikR}}{R^2}] d\alpha
$$

$$
= \frac{y}{4\pi} \int_{-\frac{\pi}{2}}^{\frac{\pi}{2}} [\frac{e^{-2ikR}}{R^2}]_{\infty}^{r} d\alpha \tag{III-2}
$$

here y, α, and R are defined as shown in Figure 3. If the
y axis line through Q intersects the rigid half-plane, the
integrand of equation (III-2) is represented by

$$[\quad]_{\infty}^{y} + [\quad]_{r}^{y}$$

(Case I)

If not, the integrand becomes

$$[\quad]_{\infty}^{r}$$

(Case II)

Taking the inverse Fourier transform of (III-2), and denoting
the time domain solution by a small u,

$$u(Q) = \frac{v}{4\pi} \int\limits_{-\infty}^{\infty} \int\limits_{-\frac{\pi}{2}}^{\frac{\pi}{2}} \frac{e^{-2ikR}}{R^2} \bigg|_{\infty}^{r} e^{i\omega t} \; df \; d\alpha$$

(III-3)

For Case I this becomes

$$u(Q) = [\frac{\delta(t - \frac{2y}{c})}{4\pi y}] + [\frac{\delta(t - \frac{2v}{c})}{4\; y\pi} - \frac{v}{4\pi} \int\limits_{-\infty}^{\infty} \int\limits_{-\frac{\pi}{2}}^{\frac{\pi}{2}} \frac{e^{i(\omega t - 2kr)}}{r^2} d\alpha df]$$

(III-4)

Where δ represents the Dirac delta function, a consequence
of the choice of the Green's function of the Helmholtz equa-
tion for the incident wave field.

   The first bracket on the right hand side of (III-4)
represents the reflection from one half of an infinite plane.
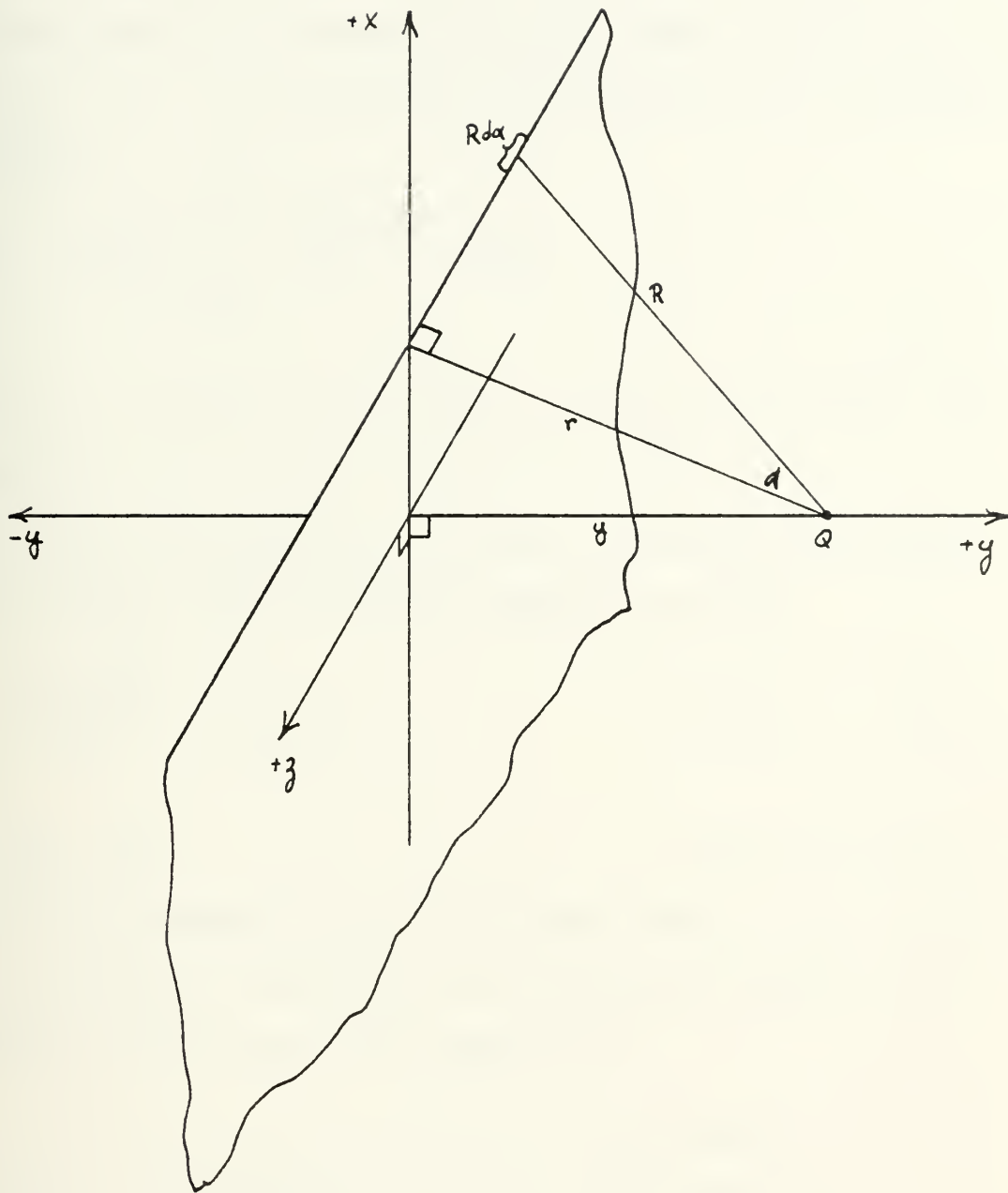
Figure 3.   Coordinate System for Backscatter from an
Infinite Edge.

The second bracket contains the specular reflection from the other half of the plane but reduced by the integral expression representing the fact that the plate is finite. This is in the form of an integral along the edge. Following Clay and Medwin [10], this is called the boundary wave and defined as follows:

$$D(t) = \frac{c^2}{4} \int_{-\infty}^{\infty} \int_{-\frac{\pi}{2}}^{\frac{\pi}{2}} \frac{e^{i(\omega t - 2kr)}}{r^2} \, d\alpha df$$

(III-5)

Case II results in a similar expression but without the reflection.

In terms of Equation (III-5) the following expressions are written for the time domain impulse solution:

$$u(Q) = [\frac{\delta(t - \frac{2y}{c})}{2y} - \frac{y}{\pi c^2} D(t)]$$
   (Case I)   (III-6)

$$u(Q) = \frac{y}{\pi c^2} D(t)$$
   (Case II) (III-7)

Taking advantage of the time domain form of the solution and separating the reflected and diffracted (boundary wave) components of the wave field results in

$$u(Q) = \mp \frac{y}{\pi c^2} D(t)$$

(-) Case I
(+) Case II

This can be written in terms of the geometry of Figure 3 as follows (from reference 10, section 10.2.3)

$$u(Q) = \frac{y}{\pi c^2} \left\{ \frac{2T_x}{t(t^2 + T_x^2 - \tau_0^2)(t^2 - \tau_0^2)^{1/2}} \right\} \qquad t \geq \tau_0 \qquad \text{(III-8a)}$$

$$= 0 \qquad\qquad\qquad t < \tau_0 \qquad \text{(III-8b)}$$

where

$$T_x = \frac{2x_1}{c} = -\frac{2r}{c} \cos\theta = -\tau_0 \cos\theta$$

$$y = \frac{ct_0}{2}$$

$$\tau_0 = \frac{2R}{c}$$

Finally, through trigonometric substitutions,

$$u(Q) = -\frac{2}{\pi c^3} \left\{ \frac{r^2 \sin 2\theta}{t(t^2 - t_0^2)(t^2 - \tau_0^2)^{1/2}} \right\} \qquad\qquad \text{(III-9)}$$

The diffracted pressure at Q as a function of time is given by

$$p_d(t, Q) = -P_\delta R_0 u(Q) \qquad\qquad \text{(III-10)}$$

where P_δ is the source pressure spectral density and R_0 is the reference distance. Taking the product $P_\delta R_0 = 1$ Pascal meter, the diffracted pressure at Q, as a function of time, can be written as

$$p_d(t, Q) = -u(Q)$$

$$= -\frac{2}{\pi c^3} \left\{ \frac{r^2 \sin 2\theta}{t(t^2 - t_0^2)(t^2 - \tau_0^2)^{1/2}} \right\}$$

$$\text{(III-11)}$$

The corresponding expression for the Biot-Tolstoy for-
mulation can be obtained from equation (II-22). For the
thin plate $(\theta_w = 2\pi)$,

$$\frac{\partial\phi}{\partial t} = \frac{c}{2\pi^2}(rr_o \sinh Y)^{-1}\sum_n \cos\frac{n\theta}{2}\cos\frac{n\theta_0}{2}\sin\frac{n\pi}{2}e^{-\frac{nY}{2}}$$

(III-12)

Working with the sum and noting that $\theta = \theta_o$ (source and re-
ceiver coincident),

$$S = \sum_n \cos^2\frac{n\theta}{2}\sin\frac{n\pi}{2}e^{-\frac{nY}{2}} = \sum_n \frac{1}{2}\left(1 + \frac{e^{in\theta} - e^{-in\theta}}{2}\right)\sin\frac{n\pi}{2}e^{-\frac{nY}{2}}$$

Multiplying terms and observing that $\sin\frac{n\pi}{2}$ is zero for n
even and ±1 for n odd, the sum can be evaluated as

$$S = \frac{1}{2}\left(e^{-\frac{Y}{2}} - e^{-\frac{3Y}{2}} + e^{-\frac{5Y}{2}} - \ldots\right) +$$

$$+ \frac{1}{4}\left(e^{-u_1} - e^{-3u_1} + e^{-5u_1} - \ldots\right) +$$

$$+ \frac{1}{4}\left(e^{-u_2} - e^{-3u_2} + e^{-5u_2} - \ldots\right)$$

$$= \frac{1}{4}\operatorname{sech}\frac{Y}{2} + \frac{1}{8}\operatorname{sech}u_1 + \frac{1}{8}\operatorname{sech}u_2; \quad \operatorname{Re}(\frac{Y}{2}) > 0$$

(III-13)

where

$$u_1 = \frac{Y}{2} - i\theta$$

$$u_2 = \frac{Y}{2} + i\theta$$

33

After considerable manipulation the sum can be written as

$$s = \frac{1}{4} \left[\frac{2 \cosh^2\frac{Y}{2} \cos \theta + \cosh Y + \cos 2\theta}{(\cosh Y + \cos 2\theta) \cosh\frac{Y}{2}} \right]$$

(III-14)

From the geometry of Figure 3 the following can be defined

$$t_0 = \frac{2y}{c} \qquad y = \frac{ct_0}{2}$$

$$\tau_0 = \frac{2r_0}{c} = \frac{2r}{c} \qquad r_0 = r = \frac{c\tau_0}{2}$$

The various trigonometric quantities in equation (III-4) can now be expressed in terms of these as follows:

$$\sin \theta = \frac{y}{r_0} = \frac{t_0}{\tau_0}$$

$$\cos 2\theta = 1 - 2 \sin^2\theta = 1 - 2 \frac{t_0^2}{\tau_0^2}$$

For $r = r_o$ equation (II-23b) can be written as

$$Y = \text{argcosh} \ (V)$$

where $V = (\frac{1}{2} \frac{c^2 t^2}{r^2} - 1) = (2 \frac{t^2}{\tau_0^2} - 1)$

Using the half angle relations for hyperbolic functions leads to

$$\cosh \frac{Y}{2} = (\tfrac{1}{2}(V+1)^{1/2}) = t/\tau_0$$

Similarly,

$$\sinh Y = (V^2 - 1)^{1/2}$$

$$= 2\frac{t}{\tau_o^2} \ (t^2 - \tau_0^2)^{1/2}$$

And finally, to within a factor of 2,

$$p(t) = - \frac{S\rho r}{2\pi^2 c^2} \left(\frac{t^2(\cos\theta + 1) - t_0{}^2}{t^2(t^2 - t_0{}^2)(t^2 - \tau_0{}^2)^{1/2}} \right) = - P_\delta R_0 \frac{2r}{\pi c^2} (\quad)$$

$$(III-15)$$

Letting $P_\delta R_0$ be unity, as before, results in an expression for the diffracted pressure wave in the time domain which can be compared directly to the H-K result.

Biot-Tolstoy:

$$p(t)_{BT} = - \frac{2r}{\pi c^2} \left(\frac{t\tau(\cos\theta + 1) - t_0{}^2}{t(t^2 - t_0{}^2)(t^2 - \tau_0{}^2)^{1/2}} \right) \qquad t > \tau_0$$

$$(III-16)$$

Helmholtz-Kirchhoff:

$$p(t)_{HK} = - \frac{2r}{\pi c^3} \left(\frac{r\sin 2\theta}{t(t^2 - t_0{}^2)(t^2 - \tau_0{}^2)^{1/2}} \right) \qquad t > \tau_0$$

$$(III-17)$$

Equation (III-16) and (III-17) are similar in overall form but differ in several important ways. When τ_0 is much greater than t_0, the time dependence of both expression is determined by the $(t^2 - \tau_c{}^2)^{-\frac{1}{2}}$ factor. (for t_0 approaching τ_c, the behavior is more complex and is treated in detail in Appendix A).

Since the impulse source has an infinite amplitude, the leading edge of the diffracted pressure signal ($t = \tau_0$) must also be infinite. After this infinite leading edge, the time behavior can be described as follows:

$$\Delta t = t - \tau_0 \qquad\qquad t^2 = \Delta t^2 + 2t\tau_0 - \tau_0{}^2$$

For the 'early diffracted signal, $\Delta t \ll \tau_0$ and

$$(t^2 - \tau_0{}^2)^{1/2} \approx (2t\tau_0 - 2\tau_0{}^2)^{-1/2} = (2\tau_0(t-\tau_0))^{-1/2} = (2\tau_0\Delta t)^{-1/2}$$

The initial diffracted time signal decays as $\Delta t^{-\frac{1}{2}}$ for both

solutions. Since the amplitude is highest in the early time

portion of the signal, this $\Delta t^{-\frac{1}{2}}$ dominates the Fourier trans-

form of the signal and the frequency dependance of both

solutions takes the form $f^{-\frac{1}{2}}$ which is characteristic of many

diffraction problems. As time increases, however, the H-K

solution approaches the form t^{-4} while the B-T form approaches

t^{-3}.

Both solutions have been implemented on the IBM computer

system at NPS. The diffracted time signals for a representa-

tive geometry are shown in Figure 4. Care should be exer-

cised in comparing the magnitude of the first point ($t = 0$)

since the "infinite" values here were handled differently in

the two solutions. The approach used in the B-T computation

is the numerical integration technique discussed earlier

while the approach for the H-K results are taken directly

from Clay and Medwin [Ref. 10].

The behavior of the two solutions as a function of θ is

also fundamentally different. Examination of the numerators

of Equations (III-16) and (III-17) over the region of θ from

0 to 180° (the problem of the thin plate being symmetrical

with respect to 180°), reveals three apparent zero values

for the H-K solution (θ, 90°, 180°) vice two for B-T (90°,

180°). Actually, the zero in the numerator at 90° is offset,

in the limit, by the term $(t^2 - t_o^2)$ in the denominator which

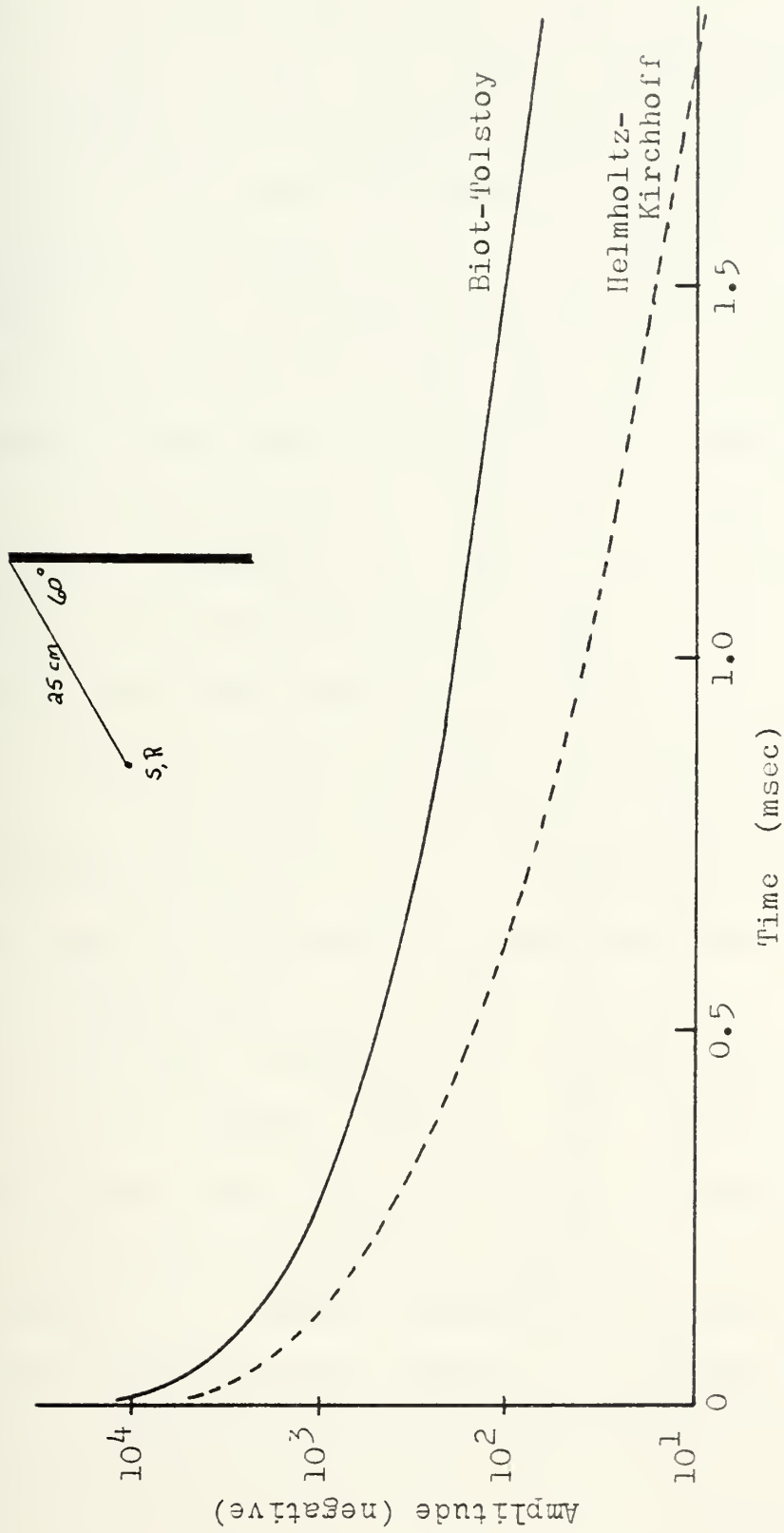goes to infinity at $t = t_o$. Physically, this means that

Figure 4. Comparison of Time Dependence of Biot-Tolstoy and Helmholtz-
Kirchhoff Backscatter Solutions.

37

when source and receiver are directly over the edge, perpen-
dicular to the plate, the solution consists of reflection
only. In order to show the detailed θ dependence, the time
domain solution has been computed for a variety of geometries
and each time solution transformed to the frequency domain.
These results are plotted versus θ for several frequencies
in Figures 5 and 6. The amplitudes are in dB with the
reference being twice the range from source to edge. The
differences between the two solutions are significant, with
the only region of agreement being near 90° where both solu-
tions appear to approach the value of -6dB. This is the
expected result and represents one half of the pressure
amplitude that would result from reflection by an infinite
plane. Actually, the H-K formulation produces the correct
result at θ = 90° while the B-T solution appears to fail in
the immediate vicinity of 90°. As θ approaches 90°, the
travel time of the reflection t_o approaches the travel time
of the leading edge of the diffracted pulse τ_o.

In this region, equivalent to approaching the shadow
boundary in the forward scattering case, the B-T solution is
approaching the delta function form and the approximation
used to calculate the first time point may not be valid
(see Appendix A). The B-T diffraction solution can only be
used for θ approaching 90° since at θ = 90° the separate
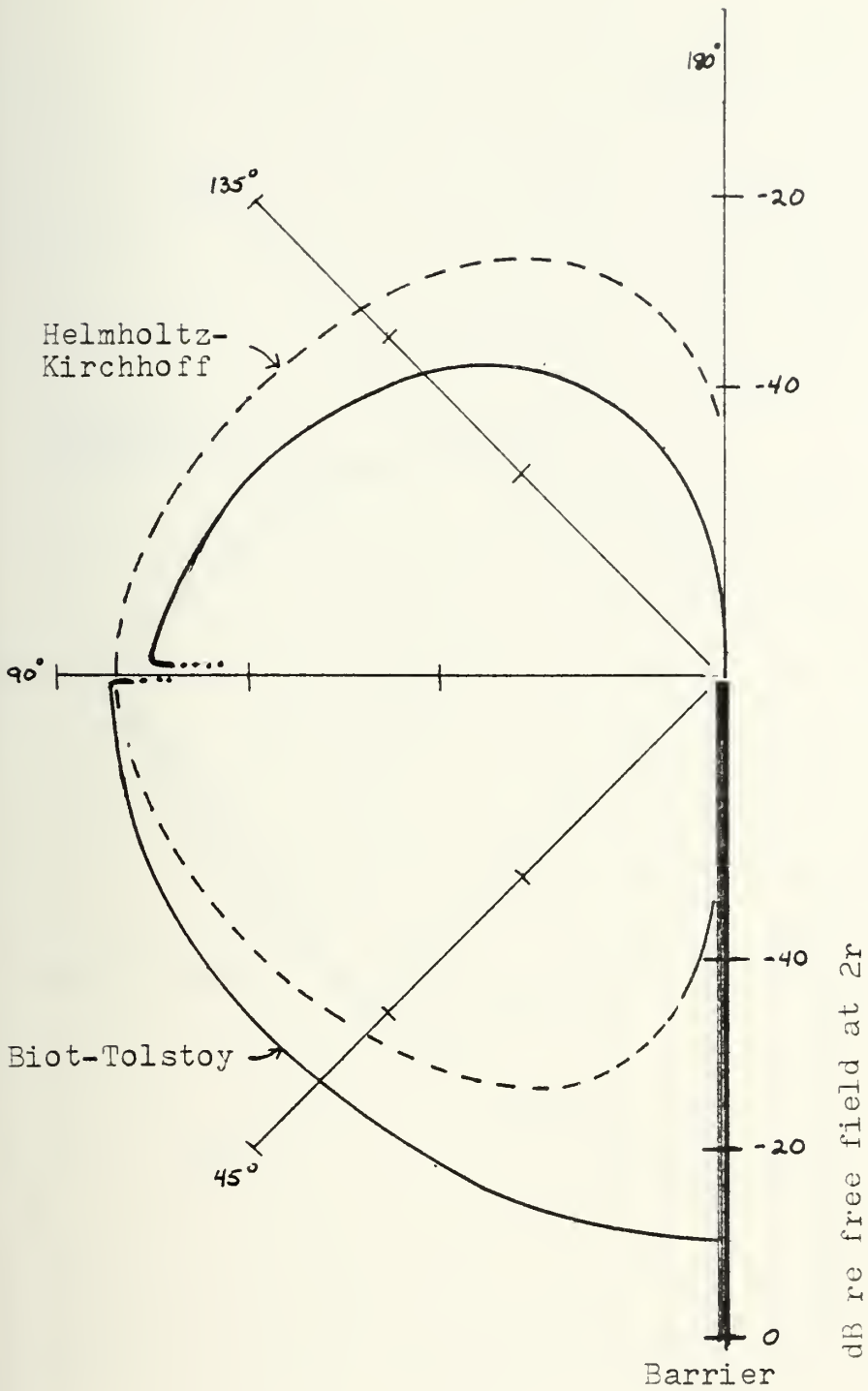reflection solution would apply (Equations II-18 and II-19).

Figure 5.   Comparison of B-T and H-K Backscatter Solutions
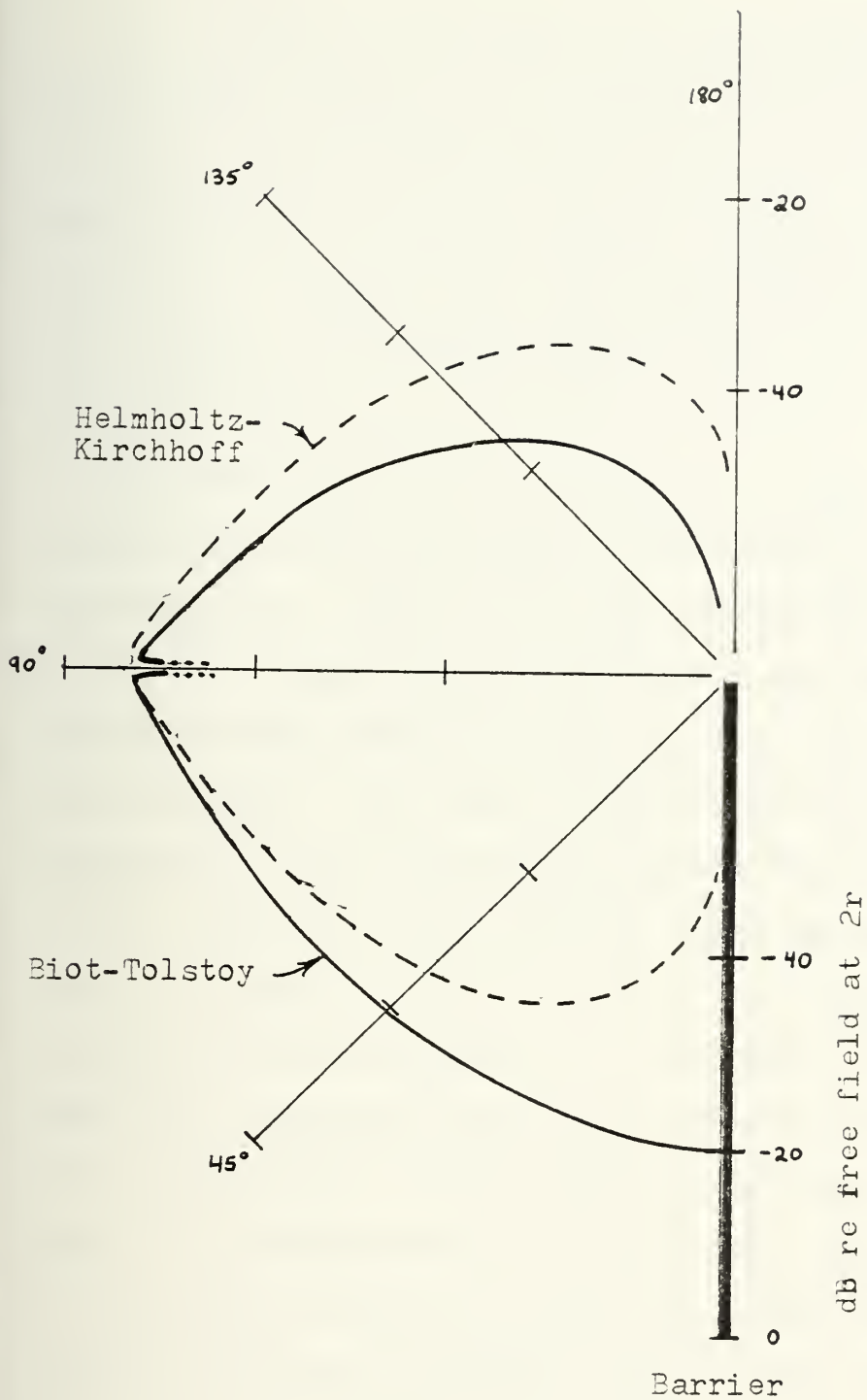as a Function of Θ at r = 20 cm and a Frequency
of 781 Hz.

Figure 6.   Comparison of B-T and H-K Backscatter Solutions as a Function of Θ at r = 20 cm and a Frequency of 10,100 Hz.

40

As the source and receiver are moved away from 90° the
disagreement between the solutions is dramatic. It is in-
tuitively correct that both solutions go to zero as θ
approaches 180°, since the plate is infinitely thin and
would not be "sensed" by a wave from this direction. The
way in which the solutions approach this zero value is
quite different.

The most significant disagreement between the solutions
is seen when source and receiver are close to the plate (θ
approaching 0). The H-K solution approaches zero near the
plate (it is symmetrical, except for sign, about 90° due to
the $\sin 2\theta$ term) while B-T approaches a constant value for
each frequency. This zero in the H-K solution appears as a
consequence of the simplifying assumption stated in Equation
(II-26), where the total pressure field in the plane of the
plate is assumed to be the value of the incoming wave field
evaluated at that location ($M = 1$ assumed). This "boundary
condition" therefore forces the diffracted pressure field
to be zero anywhere in the plane of the plate. It will be
shown in the experimental portion of this paper that the
B-T solution is correct in this region near the plate.
Although not shown in Figures 5 and 6, both solutions exhibit
the proper sign behavior, i.e., the direct and diffracted
pulses are opposite in sign in the region 0 to 90° but have
the same sign for 90 to 180°.

41

The summary, the B-T and H-K solutions simplified for the case of coincident source and receiver, are dramatically different. They approach agreement, in general, only in the region near, but not at, $\theta = 90°$.

The final consideration before leaving the topic of backscatter is an examination of the form of the B-T solution. Multiplying out the numerator and regrouping terms, Equation (III-16) can be written as

$$p_d(t)_{BT} = - \frac{2r}{\pi c^2} \left(\frac{\cos \theta}{(t^2 - t_0^2)(t^2 - \tau_0^2)^{1/2}} + \frac{1}{t^2(t^2 - \tau_0^2)^{1/2}} \right) t > \tau_0$$

(III-18)

When written in this way, the solution is seen to have an interesting characteristic. The solution is the sum of two terms, one which takes into account the overall geometry of source/receiver and plate (the first term in III-18) and a term which depends on the distance from the edge of the plate to the source/receiver. This seems to be a characteristic of exact solutions of the problem of diffraction by a half-plane and is directly related to the "image in the barrier" first mentioned by Macdonald [Ref. 3]. This "image" approach will be discussed in some detail in the next section.

B. BIOT-TOLSTOY AND MACDONALD

In comparing the B-T and Macdonald half-plane diffraction solutions, an approach similar to that of the previous section will be used. However, the solutions will not be limited to backscatter but will be kept general and the emphasis will

42

be on "forward scatter", i.e., diffraction of sound into the geometric shadow region (source and receiver on opposite sides of the half-plane). The purpose of the comparison is twofold: to show that computations based on the two "exact" solutions, one impulse and one CW do, in fact, produce the same results, and to gain some insight into the use of the "image in the barrier". As discussed in section II, the Macdonald's solution form and computations are from Kawai's excellent paper [Ref. 11].

The comparison between B-T and Macdonald computational results requires some manipulation of geometric quantities. Kawai's results are converted to the notation of this paper for consistency, however, this results in only 2-3 points per frequency spectrum. To alleviate this problem somewhat, the geometry is selected in such a way that several different B-T runs result in basically the same values. Figure 7 shows this geometry and the comparison between B-T and Macdonald results. The reference pressure is the free-field pressure that would be measured at a distance of $r + r_o$ from the source with the plate removed. Data referenced in this manner are labeled "dB re free field at 2r". This combination of geometry and reference results in B-T theoretical values which vary only one dB over the range $\theta = 330°$ to $\theta = 360°$. Kawai's computations are then converted from his normalized presentation [Ref. 11, Figure 3] to the format of Figure 6 in 5° increments of θ between 330° and 360° inclusive and
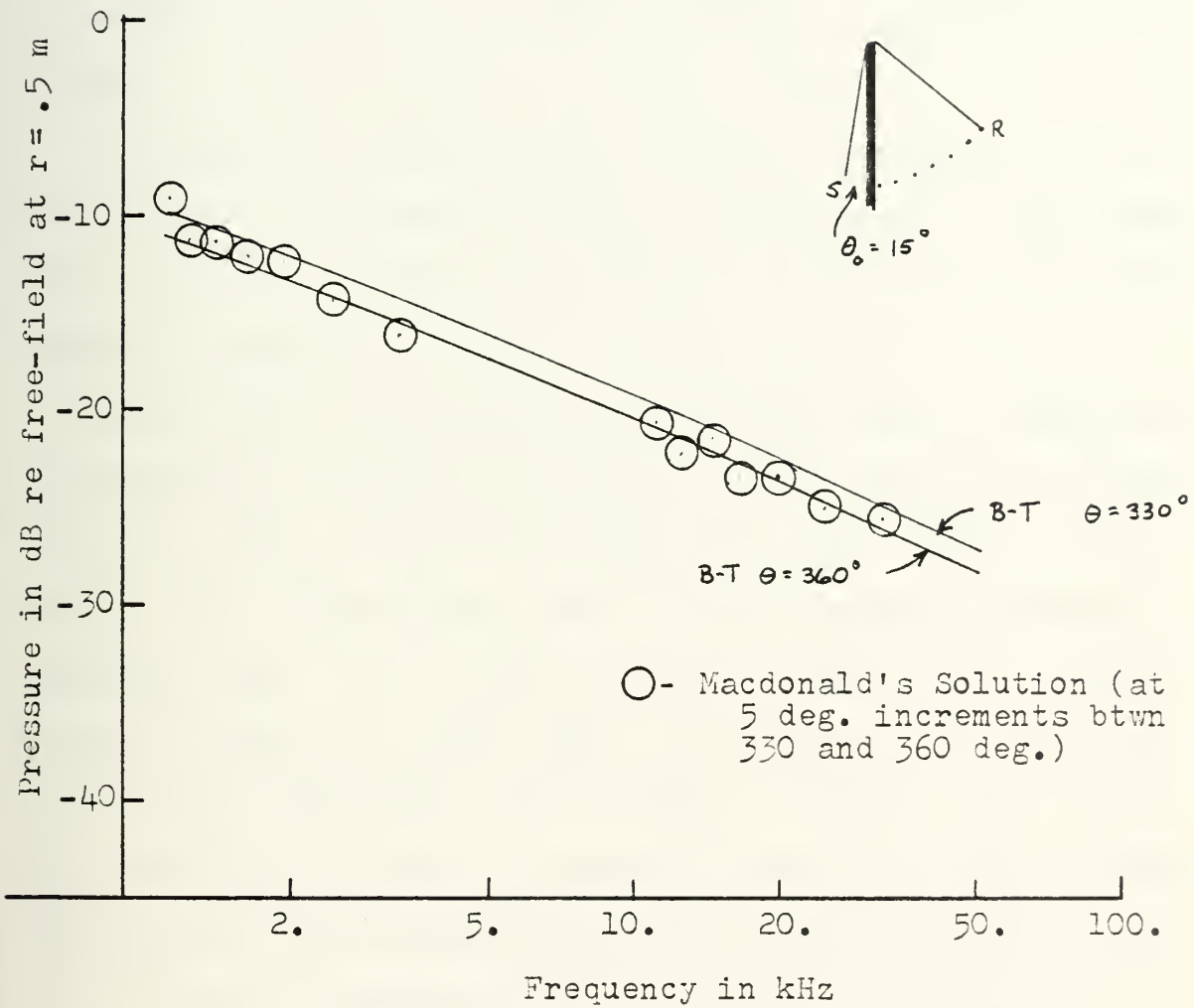
Figure 7. Comparison of B-T and Macdonald's Forward
Diffraction solutions for Various Θ's at
r = 25 cm as a Function of Frequency.

44

plotted in Figure 7 as discrete points. The agreement between the two solutions is seen to be very good. The scatter in the Kawai points is almost certainly attributable to the process of reading these values from the graphs of Ref. 11. Additional comparisons were made over a wide range of different geometries using the B-T theoretical results of Bremhorst [Ref. 12] with agreement similar to that shown in Figure 7 observed in all cases.

It should be noted, however, that the comparisons were not made for the general case of high frequency, large range, near the shadow boundary (R_N large and N small in the presentation of Kawai).

Kawai [Ref. 11] actually presents two sets of computations of Macdonald's theory; one for the "real" source only (referred to as ATT_{θ_o}) and one for the "real" plus "image" source (ATT). This terminology appears to be traceable directly to Macdonald [Ref. 3]. In his solution he separates a complex integral [Ref. 3, p. 422] into two integrals, performs the integrations separately, and recombines the two into an overall solution for velocity potential [Ref. 3, p. 425]. Bowman and Senior's approximate form of this overall solution [Ref. 1]] is given as equations (II-29), (II-30), and (II-31). The comparison of B-T and Macdonald in Figure 7, is based on Macdonald's complete solution, ATT. Indeed, if the complete solution of the half-plane problem is the sum of these two terms, it is not clear why one would want to consider them

45

separately. Yet this is precisely what is done by many authors in the noise reduction field [cf. Ref. 5].

In order to examine the "real" and "image" terms in Macdonald's solution more closely, equations (II-30) and (II-31) are repeated here with a slight change in the way θ and θ_o are expressed;

$$T_R = \text{sgn}(\pi - (\theta - \theta_o))(kR_1 - kR)^{1/2} \qquad\qquad \text{(II-30a)}$$

$$T_{R'} = \text{sgn}\,(\pi - (\theta + \theta_o\,))(kR_1 - kR')^{1/2} \qquad\qquad \text{(II-30b)}$$

$$R - (r^2 + r_0{}^2 + z^2 - 2rr_o\cos(\theta - \theta_o))^{1/2} \qquad\qquad \text{(II-31a)}$$

$$R' = (r^2 + r_0{}^2 + z^2 - 2rr_o\cos(\theta + \theta_o))^{1/2} \qquad\qquad \text{(II-31b)}$$

The primed values represent the "image" source terms. The real source terms are a function of the difference between θ and θ_o while the "image" terms are a function of their sum. The significance of this is shown graphically in Figure 8. Figures 8(a) and 8(b) show two different geometries, both of which have the same value of the quantity $\theta - \theta_o$. Since $(\theta - \theta_o)$ is only form in which the quantities θ and θ_o enter real source portion of the solution, it is easily seen that the real source solution is independent of the orientation of the plate. It depends only on the locations of source and receiver relative to the edge. However, the geometries of Figures 8(a) and 8(b) are different in terms of $(\theta + \theta_o)$. It is this term which retains the information concerning the orientation of the plate (half-plane) relative to source and
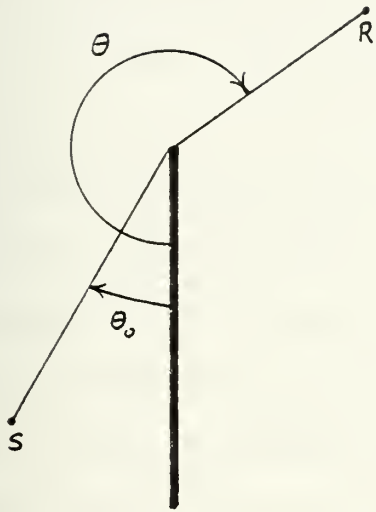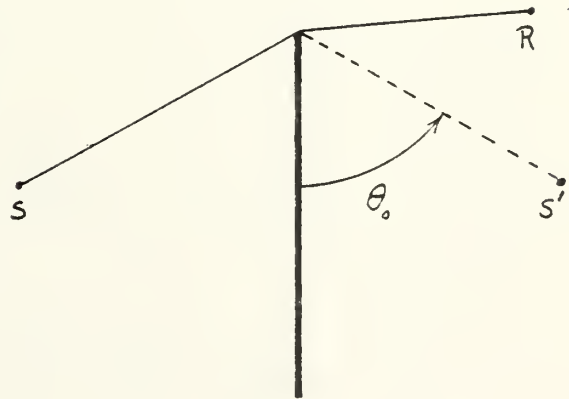
(a)
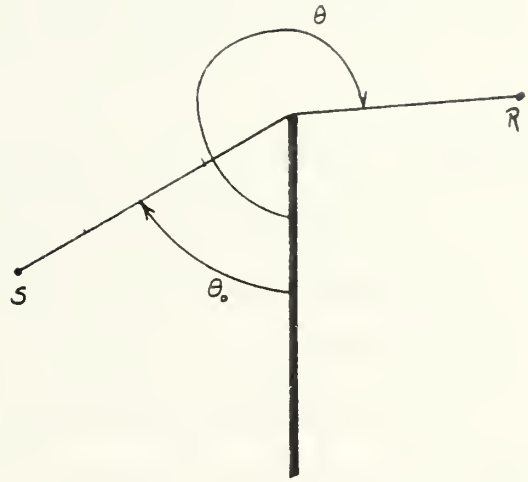
(b)
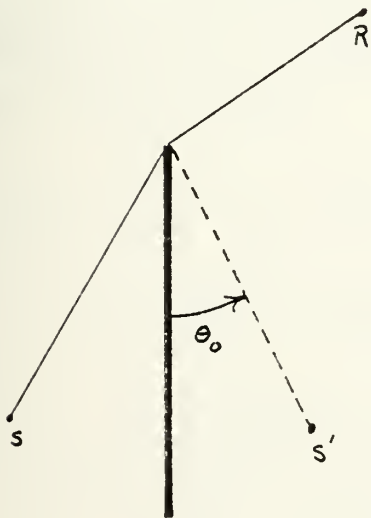
(c)

(d)

Figure 8.   Geometry of the Image of the Source in the
             Barrier.

47

receiver. Since changing the sign of θ_o is the same, geometrically, as moving the source to the opposite side of the barrier, one can easily see why the second term of the solution is associated with the "image of the source in the barrier". This interpretation is shown in Figures 8(c) and 8(d).

This interpretation is not unique to Macdonald's solution. Recalling equation (III-18), is was shown that the B-T solution, for the case of coincident source and receiver, could be written as the sum of two terms, one which depended only on the orientation of the edge and one which also considered the location of the plate. Indeed, the general form of the B-T solution given by equation (II-24) could be written as the sum of a term that is a function of $\theta - \theta_o$ and another that is a function of $\theta + \theta_o$. This would be done in the following way:

$$p(t) = p(t, \theta_o) + p(t, -\theta_o)$$

$$= -\frac{S\rho c}{4\pi\theta_w} (rr_o \sinh Y)^{-1} e^{-\frac{\pi Y}{\theta_w}} \{\beta_{\theta_o} + \beta_{-\theta_o}\}$$

$$\beta_{\theta_o} = \frac{\sin \frac{\pi}{\theta_w} [\pi \pm (\theta - \theta_o)]}{1 - 2 \exp(\frac{\pi Y}{\theta_w}) \cos \frac{\pi}{\theta_w} [\pi \pm (\theta - \theta_o)] + \exp(-\frac{2\pi Y}{\theta_w})}$$

$$\beta_{-\theta_o} = \frac{\sin \frac{\pi}{\theta_w} [\pi \pm (\theta + \theta_o)]}{1 - 2 \exp(\frac{\pi Y}{\theta_w}) \cos \frac{\pi}{\theta_w} [\pi \pm (\theta + \theta_o)] + \exp(-\frac{2\pi Y}{\theta_w})}$$

where each β term is actually the sum of two terms, one with the term in brackets evaluated using the (+) sign and the other using the (-) sign. There appears to be no advantage to writing the B-T solution in this way except to show the geometrical similarity to Macdonald's result. Indeed, Biot and Tolstoy specifically identify both terms as diffraction not reflection. True reflections have separately been identified by B-T as occurring before the diffraction; an interpretation that is direct and obvious in their impulse solution, but which is obscured in Macdonald's CW solution.

In summary, the B-T and Macdonald exact solutions have been found to be in very close agreement for all of the cases examined. Real and image sources have been shown to be a valid, if not particularly useful, interpretation of both solutions.

IV. EXPERIMENTAL APPROACH

A. GENERAL

The measurements reported herein were made in the NPS anechoic chamber utilizing pulse techniques. The anechoic chamber provided the low noise, low reverberation environment necessary to make precise amplitude measurements at low source levels. The use of a pulsed source provided a signal that was both wideband and deterministic and made it possible to control the effects of extraneous scattering by judicious choice of the sampling window. Detailed descriptions of the anechoic chamber and the data acquisition hardware may be found in Reference 12, and will not be repeated here, except when necessary to explain the results.

B. DATA ACQUISITION

A block diagram of the overall experimental data acquisition process is shown in Figure 9. Overall timing of the acquisition process is controlled by the programmable timing simulator. A typical sequence is as follows. The waveform generator is triggered by the timing simulator, sending a single replica of the preprogrammed pulse to the power amplifier. This pulse is amplified to approximately 50 volts peak, added to the 150 volt D.C. bias voltage, and applied to the source (source and receiver characteristics will be
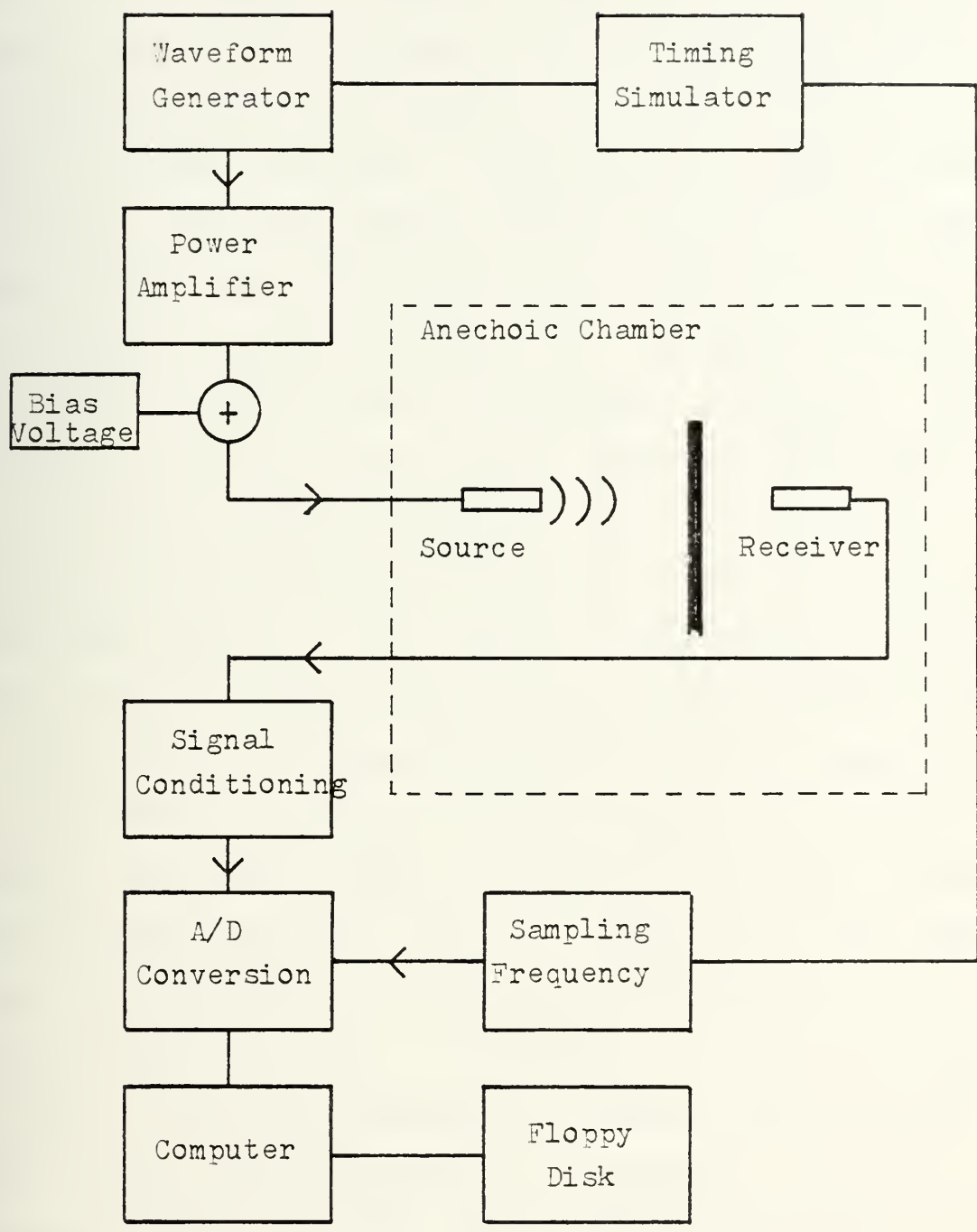
Figure 9.   Experimental Data Acquisition General Block
            Diagram.

51

discussed separately). The transmitted signal is received by the ½ inch condenser microphone (B+K 4133) and sent to the signal conditioning equipment. Here the signal is amplified, filtered to remove low frequency noise and to prevent aliasing in the sampling process, further amplified and digitized (12 bits). Here the timing simulator determines the start time and duration of the sampling of each pulse. By selecting the sampling frequency and duration, the number of samples available to the FFT can be determined. In practice, the number of samples is set slightly higher than the number to be transformed since the computer begins with the first sample and disregards those coming after the specified number have been acquired. This process is repeated for each pulse with a pause of approximately 80 milliseconds between pulses.

The computer accumulates the samples by averaging up to 10,000 samples in the time domain and then computes the Fourier transform of this averaged waveform using a standard software FFT algorithm. Since the FFT must be taken only once, the system runs in real-time, which allows a very large number of pulses to be averaged in a reasonable amount of time. Since this averaging is coherent, the signal-to-noise ratio is proportional to N, the number of pulses, rather than the usual $N^{\frac{1}{2}}$. The averaged time waveform or FTT results are stored on a floppy disk for later use.

C. SOUND SOURCE

The ideal sound source for these experiments would be a point source capable of high acoustic output over very short time durations, with zero output at all other times. These characteristics can only be approached with a real source. The obvious choice of a spark source is rejected in order to avoid finite amplitude effects. Fortunately, the extremely low noise levels of the anechoic chamber plus coherent averaging makes accurate measurements possible with a source of relatively low intensity. The search for a useful source of small dimensions and narrow time response has been a continuing one at NPS [cf. Ref. 14]. The source chosen for the experimental work in this paper were the B & K ½ inch and 1 inch condenser microphones. The use of these microphones as sound sources is described in Reference 12 and in a B & K technical pamphlet [Ref. 15]. In general, the ½ inch source covered the higher frequencies (6-40. kHz) while the 1 inch source was used to provide additional low frequency coverage (down to approximately 1.5 kHz). The 1 inch source is actually capable of providing sufficient output over the entire frequency range but directivity does become significant at the higher frequencies.

Typical source waveform and frequency spectra are shown in Figures 10 through 13. In Figure 10, the waveform at the output of the power amplifier is the top curve with the received waveform shown below. The received waveform (and

Source   -   ½" B+K

Receiver -   ½" B+K

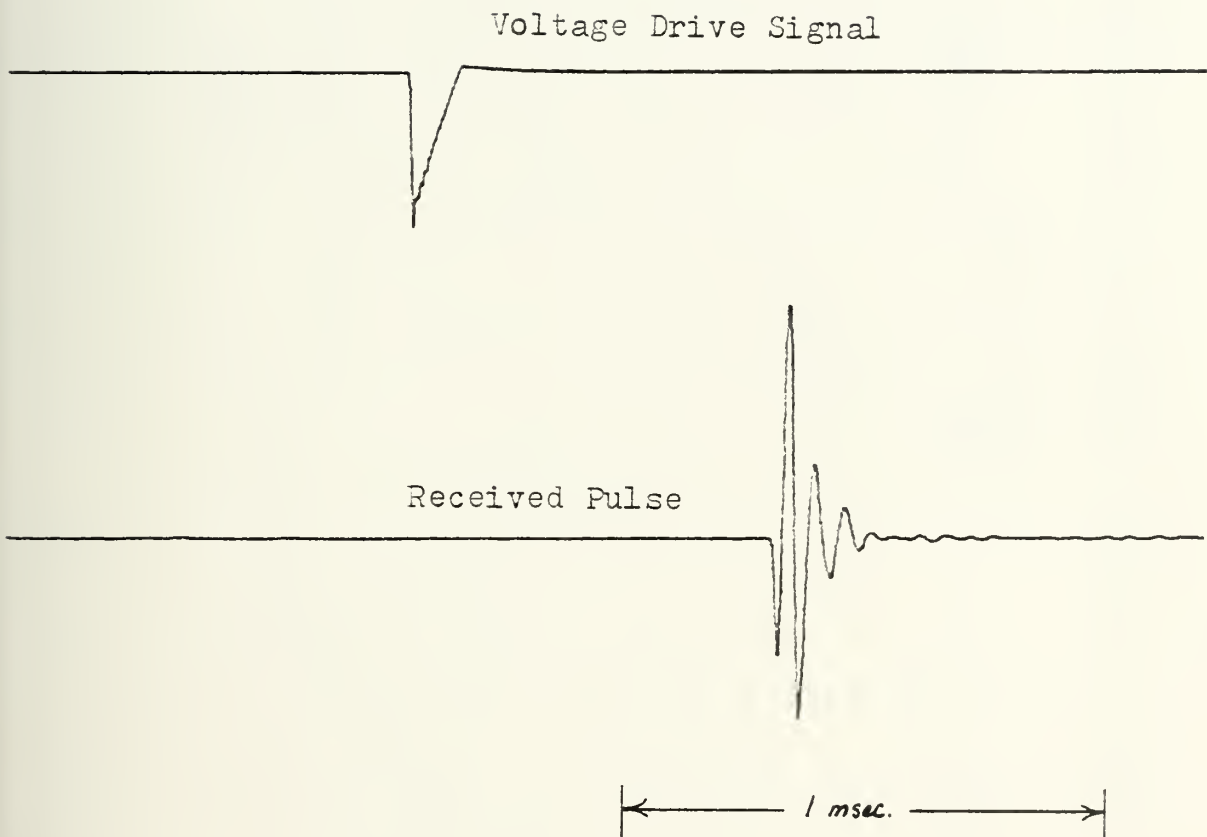Voltage Drive Signal

Received Pulse

|← ─────── 1 msec. ───────→|

Figure 10.   Typical Time Domain Signal, ½" Source.

54
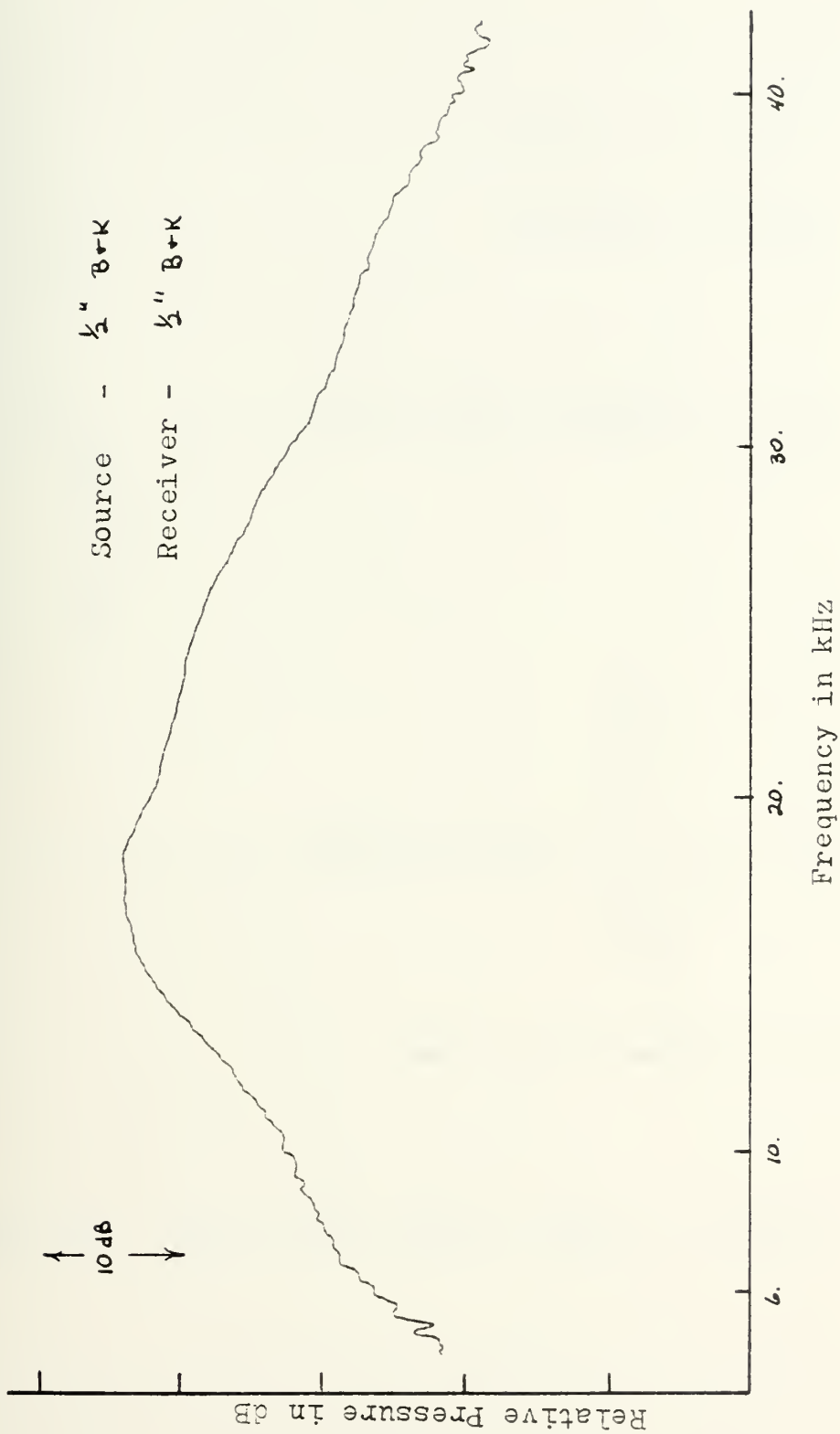
Figure 11. Typical Frequency Spectrum of Acoustic Pulse, $\frac{1}{2}$" Source.

55

Source — 1" B+K

Receiver — ½" B+K

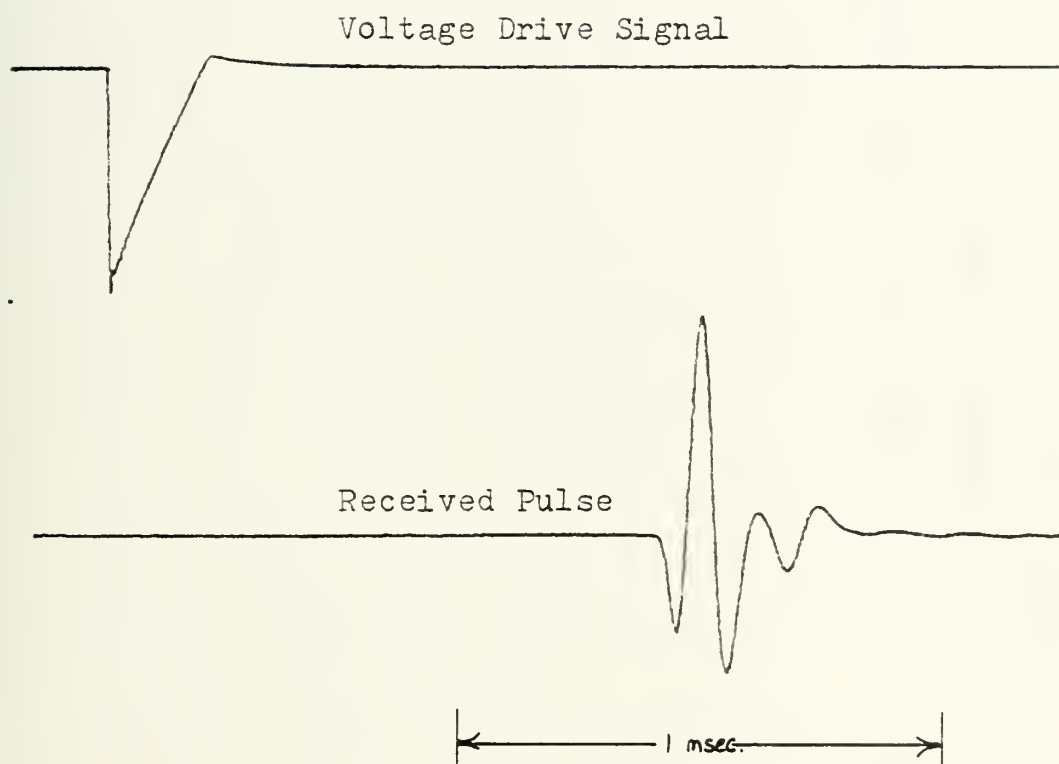Voltage Drive Signal

Received Pulse

|← —— 1 msec. —— →|

Figure 12. Typical Time Domain Signal, 1" Source.

56
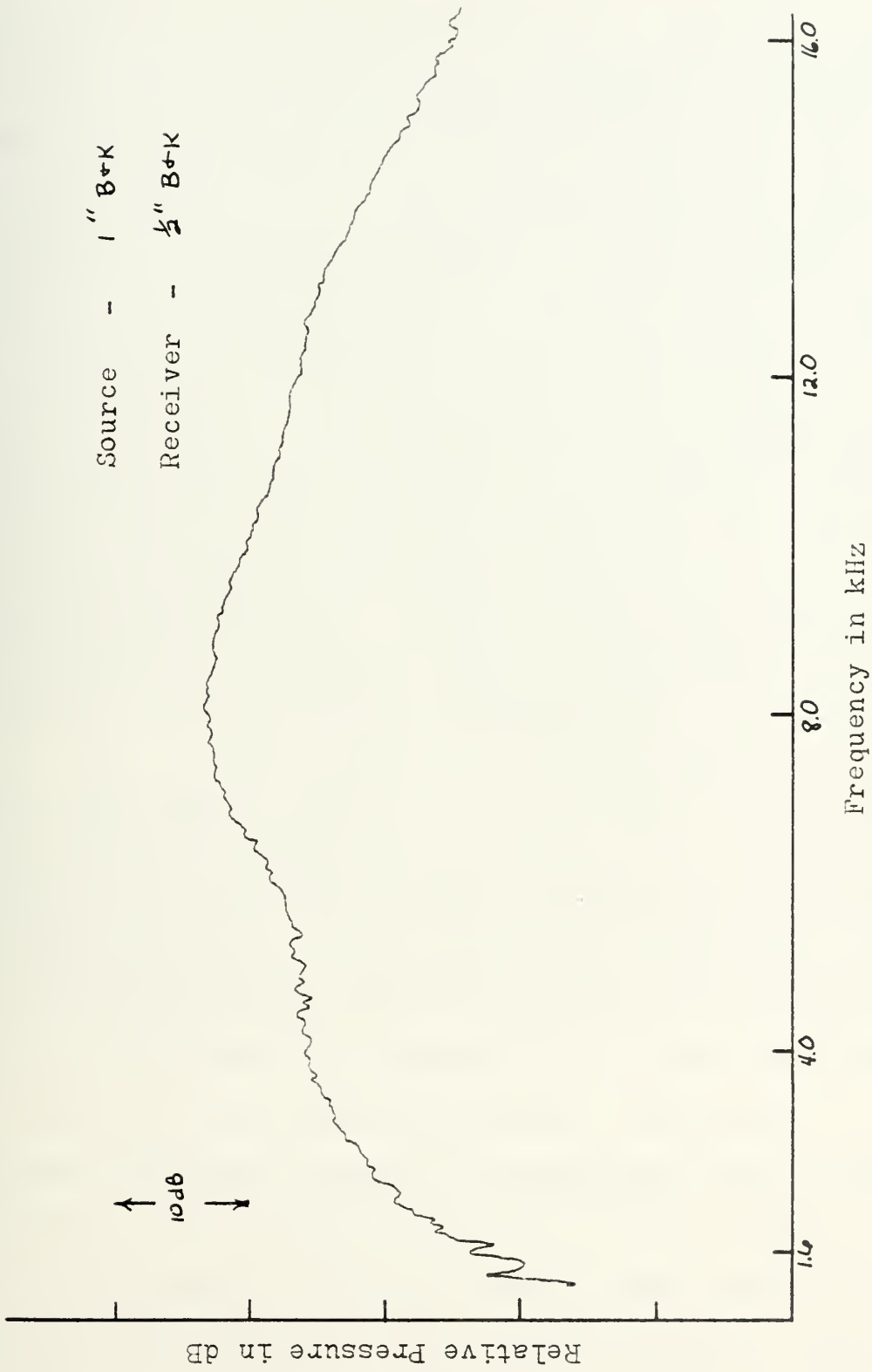
Figure 13. Typical Frequency Spectrum of Received Pulse, 1" Source.

57

associated frequency spectrum) is actually due to a combination of source and receiver response, however, the relative contributions of each are not particularly important since all results are normalized by an appropriate reference measurement using the same source and receiver. The time duration (or "ringing") of the pulse is important since all of the desired diffracted pulse must be sampled before the unwanted arrivals from the other edges of plate. The longer the acoustic pulse, the larger the specimen must be to separate the pulses. This ringing is especially important in measuring backscatter since the low amplitude diffracted pulse will arrive after the direct/reflected pulse which is much higher in amplitude. Figure 11 shows the energy spectral density of acoustic pulse in Figure 10.

Figures 12 and 13 present the same data as Figures 10 and 11, with the same receiver, but using the 1 inch source. In this case, the received pulse was low pass filtered at 14 kHz in order to enhance the low frequency portion of the spectrum.

Once an acceptable source and receiver were selected, a mounting system had to be devised which allowed the micophones to be positioned accurately yet present a minimum of additional scattering surface. The approach used is shown in Figure 14. The diffracting object (in this case a thick plate) was suspended with nylon fishing line from a frame attached to the ceiling of the achechoic chamber. Heavier
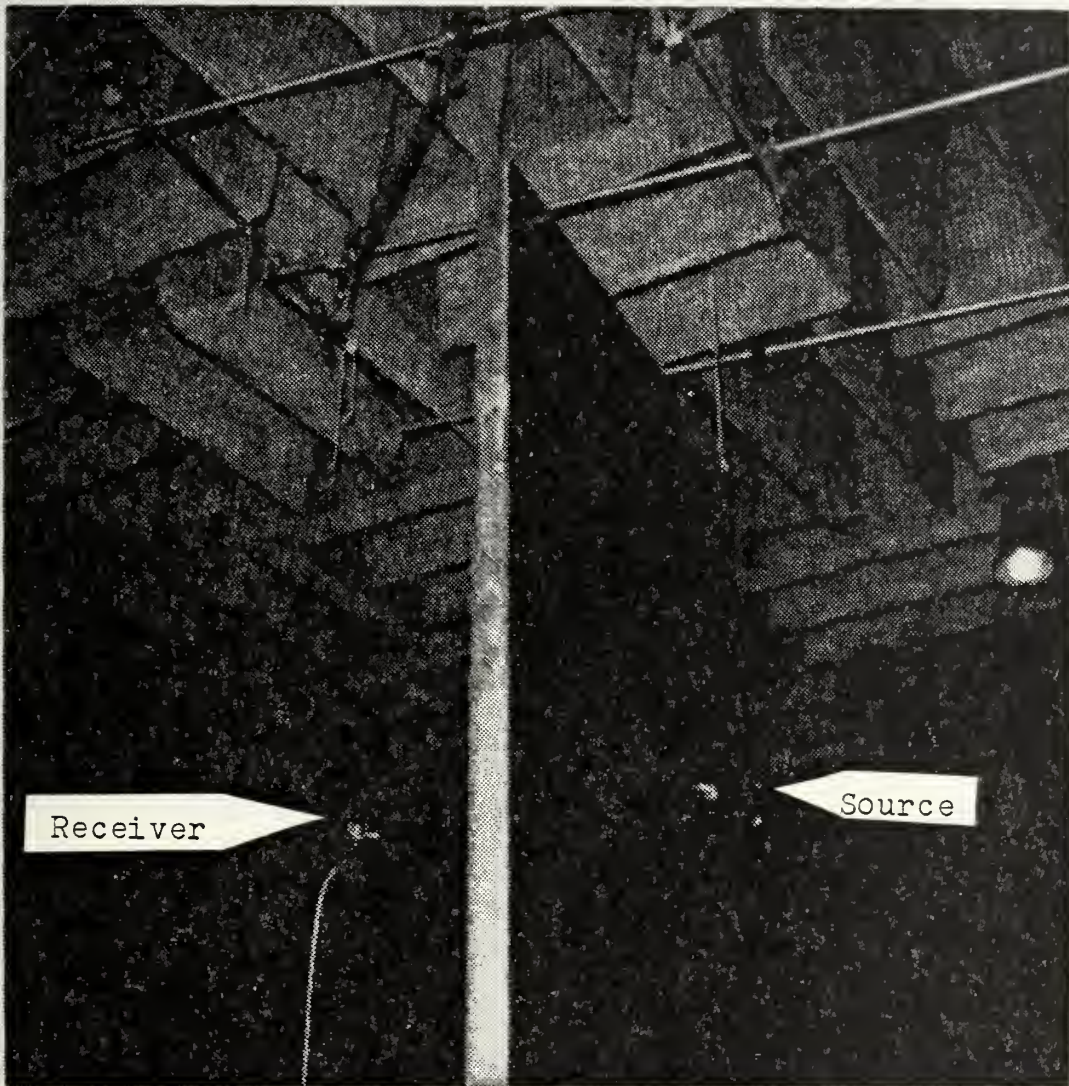
Figure 14. Typical Anechoic Chamber Measurement Apparatus.

59

objects were also supported from below. The source and re-
ceiver were each attached to a pair of thin stainless steel
wires mounted firmly to the ceiling frame and resiliently
to the wire mesh floor of the chamber. Source and receiver
were positioned in the horizontal by moving the ceiling and
floor attachments and vertically by moving up or down the
wires. Additional support of the signal cables was provided,
as necessary, with nylon line from the ceiling frame.

D. PLATE CONSIDERATIONS

The plate used in the experiment should be as thin and
yet, as rigid and non-transparent as possible. In addition,
it was desirable to keep the overall weight of the plate low
to facilitate handling and suspension within the anechoic
chamber. Aluminum plate .475 cm thick was chosen as a
reasonable compromise. The transmission loss, calculated
using the approach of Reference 12, was greater than 40 dB
at 1.5 kHz, increasing with frequency. This was considered
adequate since no thin plate measurements were planned
where the direct path through the plate was to be substan-
tially less than the diffracted path. For the thick plate
tests the direct path would be short but two plates would be
used and the resulting attenuation would certainly be adequate.
These estimates were verified by examining the received sig-
nal prior to the arrival of the first diffraction to ensure
there was no significant direct path arrival.

60

V. BACKSCATTER EXPERIMENTAL RESULTS

In Figures 5 and 6 it was shown that the B-T and H-K
solutions give dramatically different results for backscatter
near the surface of the rigid half-plane. A simple experi-
ment was performed to determine which solution is correct.
The one inch B+K microphone was used as the source with the
one-half inch B+K microphone used as the receiver. They were
taped together and positioned at a distance of 25 cm from the
edge at various angles as shown in Figure 15. Although the
source and receiver acoustic centers are separated by approxi-
mately 2.5 cm they will be assumed to be coincident.

The transmitted waveform was the half triangle discussed
earlier but the received signal was low pass filtered at
60. kHz vice the 14. kHz shown in Figures 12 and 13, to
achieve a higher frequency response. Each transmitted pulse
actually resulted in three received pulses. The first pulse,
which arrived almost immediately, was the direct source/
receiver path. The second was the reflection from the plate.
while the third was the desired diffraction from the edge.
Unfortunately, the first two pulses were considerably higher
in amplitude than the diffracted pulse. Even with the ability
to exclude the first two pulses in the time domain, the
ringing of the reflected pulse interfered with the analysis
of the diffracted pulse. This limited the geometry to
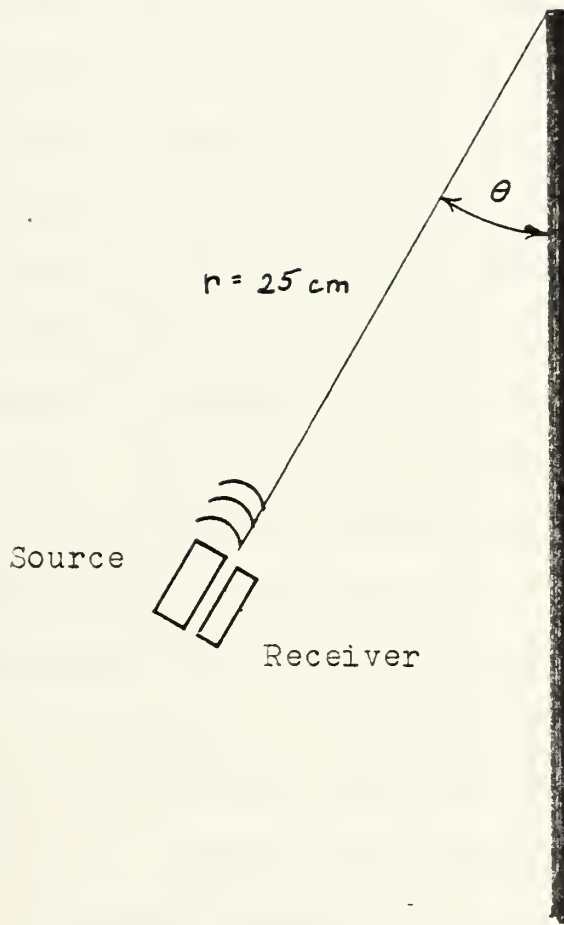
$r = 25$ cm

θ

Source

Receiver

Figure 15. Backscatter Experimental Geometry.

source/receiver locations near the plate, which presented no
particular problem since this was the region of most interest
anyway.

The results of this experiment are presented in Figure 16,
with the free-field pressure at 2r used as the reference.
For the comparison, the theoretical B-T and H-K results are
shown for angles approximating those of the measurements.
(These theoretical results are the same as those presented
in Figures 5 and 6, now plotted as a function of frequency
for specific angles.) The B-T theoretical results are
plotted as a single line since they vary by less than one
dB over the range of angles presented. It is clear that the
measured data tend to agree with the results predicted by the
B-T solution rather than going to zero at the surface of the
plate as in the H-K solution. The considerable scatter in
the measured data, especially near 9 kHz at 30 degrees, is
attributable to interference between the diffraction pulse
and the ringing of the reflected pulse.

The measured data not only favor the B-T solution but
also confirm the presence of a scattered wave near the sur-
face. If this scattered wave also exists on the surface,
as predicted by B-T, (there is no reason to think otherwise)
it points out a serious fallacy in the Kirchhoff assumption.
In order to evaluate the integral in Equation II-25, the
wave field at all points on the surface of integration had
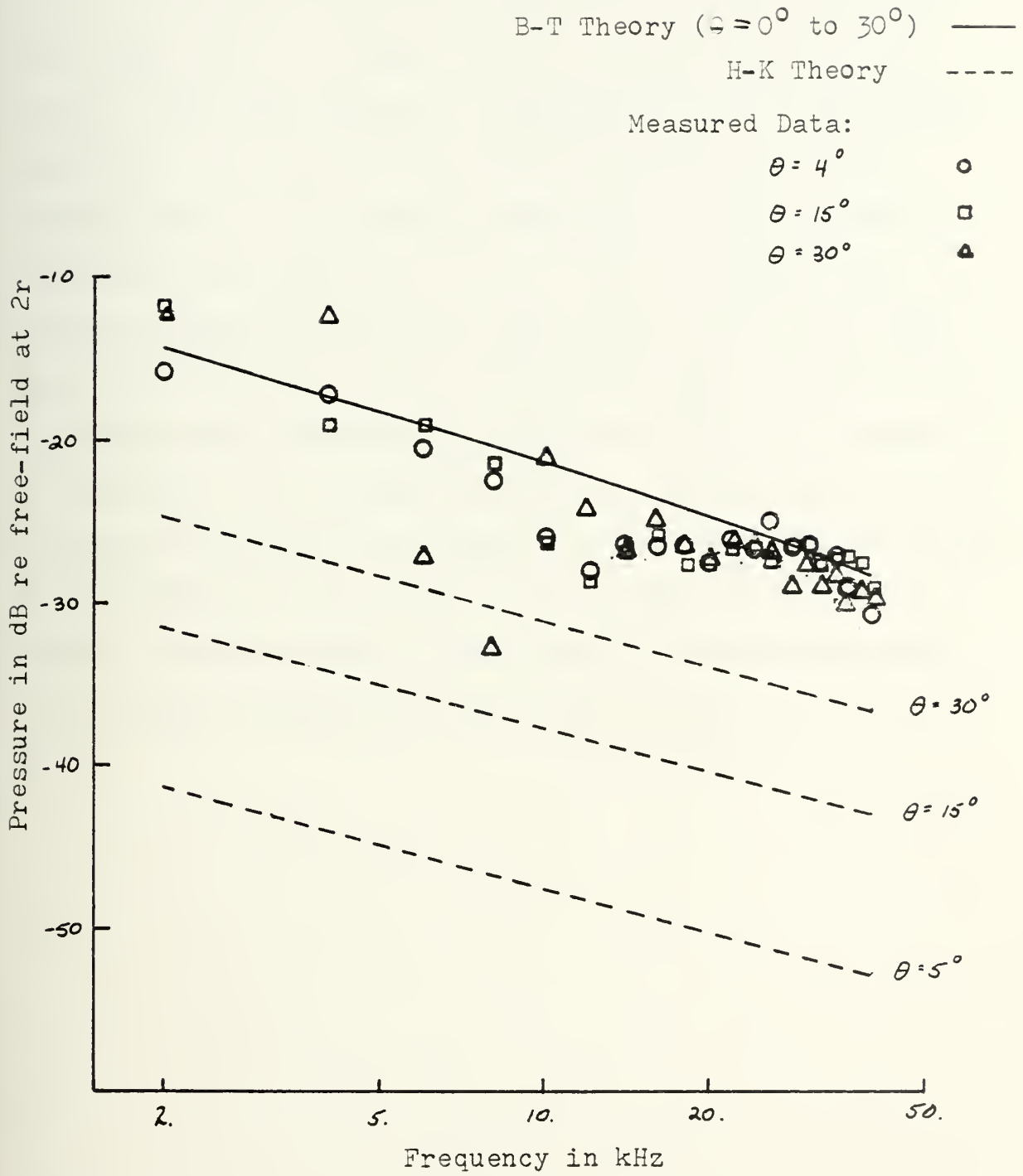to be known. This was accomplished, through the Kirchhoff

Figure 16. Comparison of Measured Backscatter from a Half-plane with Theoretical B-T and H-K Solutions for $r = 25$ cm at various θ's ($\theta = \theta_0$)

assumption, by simply taking the wave field on the surface to be the reflection of the incoming wave. This is equivalent to a boundary condition which forces the diffracted wave field due to the edge to zero at the surface of the plate. When the solution is transformed to the time domain (Equations III-6 and III-7) where the diffracted and reflected terms are considered separately, the diffracted term must go to zero at $\theta = 0°$ in order to satisfy the imposed boundary condition. That this is clearly not the case indicates that the H-K formulation should not be used to estimate the backscattered wave field near the surface of the plate. For forward scattering, the H-K diffraction solution would also be expected to go to zero near the plate. Since Bremhorst's data [Ref. 12] show the presence of a forward scattered wave at the surface, the above argument can probably be applied to this case as well.

VI. <u>FINITE PLATE FORWARD SCATTERING EXPERIMENTAL RESULTS</u>

A. GENERAL

When a rigorous diffraction solution such as Biot-Tolstoy
is applied to the problem of diffraction by a real object,
one must be careful to ensure that the original boundary
conditions are applicable. For a finite barrier, two impor-
tant considerations are whether the barrier is large enough
to be considered infinite in extent and thin enough to ignore
thickness (the double edge). Since the geometry of the half-
plane diffraction problem is such that everything is described
in terms of a cylindrical coordinate system with the origin
at the edge, there is a tendency to think of diffraction as
simply an edge effect. This is the interpretation of the
H-K boundary diffraction wave. This is also the simplist
interpretation of a time domain, impulse solution such as
B-T, where it is easy to visualize an expanding spherical
wavefront intersecting the edge and reradiating acoustic
energy as it "propagates" along the edge. If this were
generally true, one could solve any diffraction problem by
describing the diffracting object in terms of a series of
edges (or, more appropriately, wedges) and adding their con-
tributions. The problem with this approach is that the
original solution assumed the presence of a rigid surface
at some angles $\theta = 0$ and $\theta = \theta_w$ extending to infinity in the

radial and axial directions and an infinite fluid elsewhere
(see Figure 1). When the physical situation approximates this
condition, the diffraction problem can generally be treated
by considering a source at the edge. For an extreme example
where this is not true, one could consider the difference
between the diffraction due to a rigid half-plane and that
due to a large plate shrunk to become a thin wire at the
location of the edge.

A related problem concerns the treatment of barrier cor-
ners. Here the barrier may be "high" enough to consider the
radial dimension to be infinite but its width (the axial, or
z, dimension) is finite. A roadside billboard or a tall
building could be described this way. If the ground is
totally absorbant (no reflections) Medwin [Ref. 8] treats
the diffraction from this type of a barrier by adding the
impulse response of each of the three edges, truncating the
solution for each edge when the wave reaches the corner, to
obtain the total time domain solution. The assumption
implicit here too is that the boundary conditions of the
theoretical B-T solution are sufficiently well approximated
by the actual barrier.

The third major difference between the theoretical B-T
solution and the actual barrier is the double edge caused by
the finite thickness. The theoretical solution is based on
a rigid, infinitely thin screen whereas the actual barrier
is often approximately rigid but of finite thickness.

Some researchers have minimized this problem in their mea-
surements by placing a "knife edge" at the top of the barrier
[cf. Kawai, Ref. 11] but this introduces additional sources
of diffraction where the face of the barrier changes angle.
In any case, the real barrier will always have some finite
thickness dimension and it is desirable to be able to calcu-
late or at least understand the nature of its effect on the
diffracted field.

A series of experiments was performed in order to define
these "finite barrier" effects.

B. FORWARD DIFFRACTION AT A CORNER

Bremhorst [Ref. 12] showed excellent agreement over a
wide frequency range between the B-T infinite plate solution
and pulse measurements on a 3/16" thick plate, provided the
pulse is sampled in such a way as to exclude late arriving
diffracted pulses from other edges. However, discrepencies
between measurements and theory of 5-10 dB were observed at
frequencies approaching 50 kHz with source and receiver near
the plate. The purpose of this experiment was to measure
the diffracted pressure field in the vicinity of the corner
of a plate and compare it to the field predicted by B-T
using Medwin's truncation approach. The present geometry
was chosen to ensure that only the edges intersecting at the
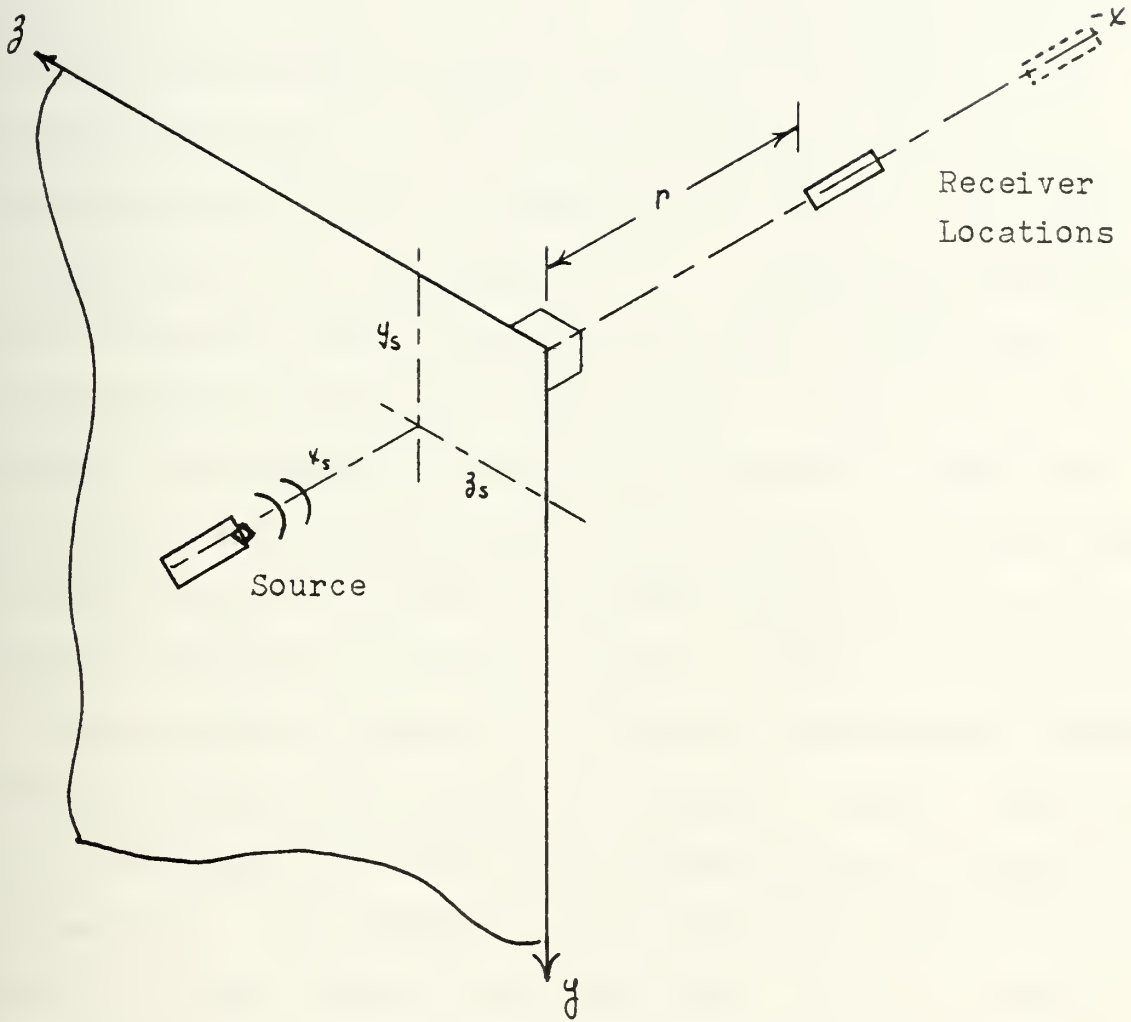corner of interest would contribute to the measurements
(Figure 17).

Figure 17. Corner Diffraction Experimental Geometry.

The source was placed at the coordinates (x_s, y_s, z_s) of 25.5 cm, 8.0 cm, 8.0 cm, respectively. Separate measurements were made using the ½ and 1 inch sources to achieve the widest possible frequency coverage. The receiver was positioned along the x axis $(y_r = 0, z_r = 0)$ at various points between r = 3 cm and r = 45 cm. This geometry was dictated by two considerations; source/receiver directivity and coherent interference. Source and receiver are both to be omnidirectional in the theoretical B-T solution. In order to approximate this adequately, it was considered important that the source appear omnidirectional when viewed from points along a significant portion of the edge near the corner. By orienting the source and receiver in this way all points on the edge between the corner and the point where the least time path crosses the edge were within 2 dB of omnidirectionality up to approximately 30 kHz. The symmetry of the geometry was chosen to eliminate the frequency domain interference pattern created by taking the Fourier transform of a time signal which has two coherent pulses separated by a time delay. The geometry ensures that the diffracted pulses from both edges arrive at the same time. This was accomplished by moving the receiver slightly to maximize the total pulse signal at the nearest and farthest ranges and locating the intermediate measurement points on a straight line between them.

These considerations resulted in a geometry which was somewhat artificial but would allow a relatively simple analysis of the corner effect. The Fourier transformed diffracted pulse data for the 1" and ½" sources are presented in Figures 18 and 19 respectively. The free-field pressure at a range of 28 cm (the distance from source to corner) was used as a reference pressure. Although the measured data using both sources show good agreement in the frequency region where they overlap, their dimensions are large enough to be considered as an effect on the results and are therefore presented separately. The theoretical results from truncating and adding the B-T solutions for the two perpendicular edges is also shown. The agreement between the measurements and this superposition of the truncated components of two cases of B-T theory is seen to be excellent across the entire frequency region.

The theoretical and measured results in Figures 18 and 19 also clearly show the effect of moving closer to the shadow boundary. Because of the geometry shown in Figure 17, decreasing r also moves the receiver nearer to the shadow boundary. The theoretical solution as the receiver approaches the shadow, is shown to approach the delta function form (Appendix A). The measured data clearly show this result, as they approach a flat spectrum for small r, with the more familiar $f^{-\frac{1}{2}}$ frequency dependence observed at larger r.
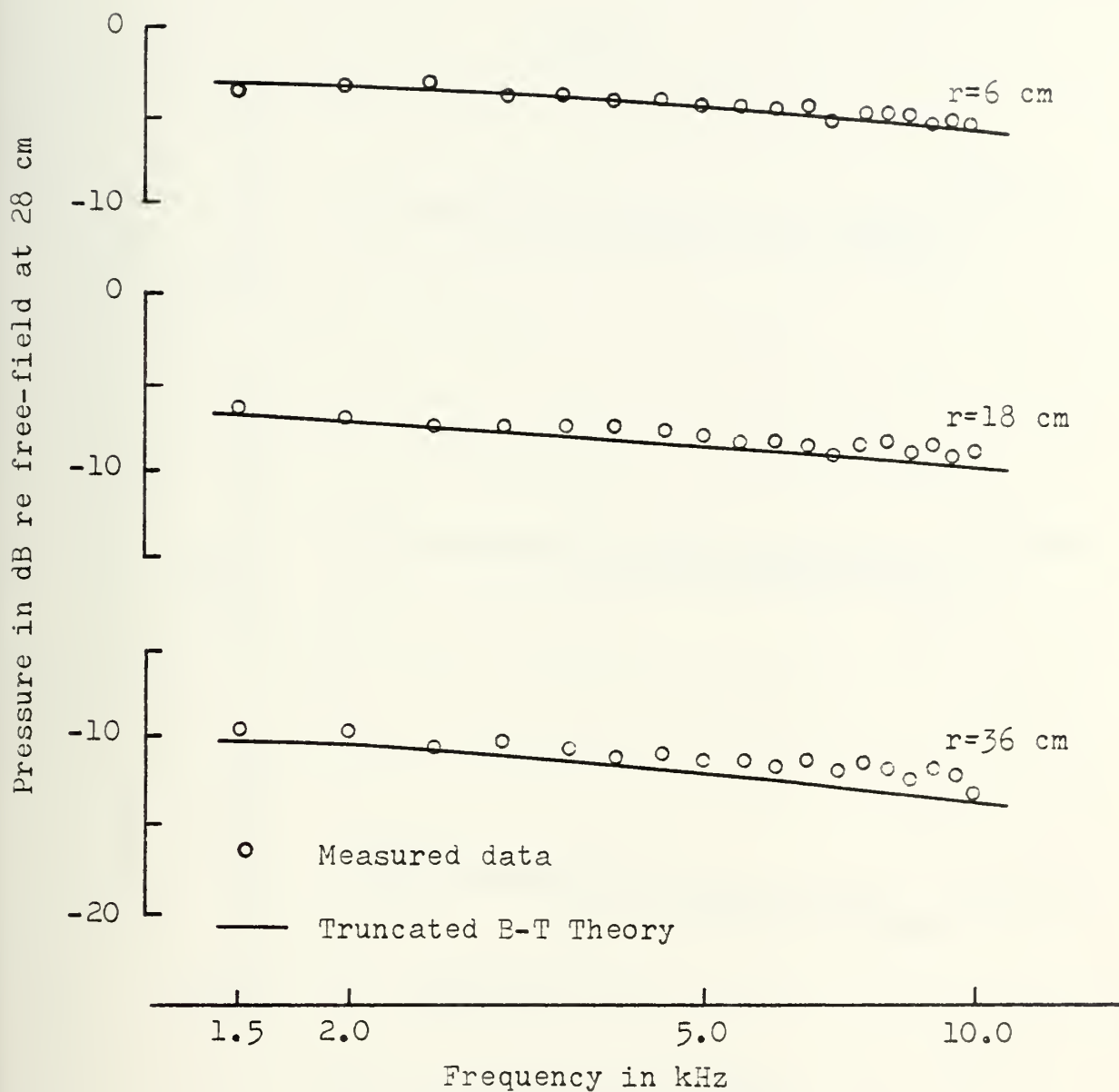
Figure 18. Forward Diffracted Pressure as a Function of Frequency at Various Distances (r) from the Corner, 1" Source (Geometry of Fig. 17).

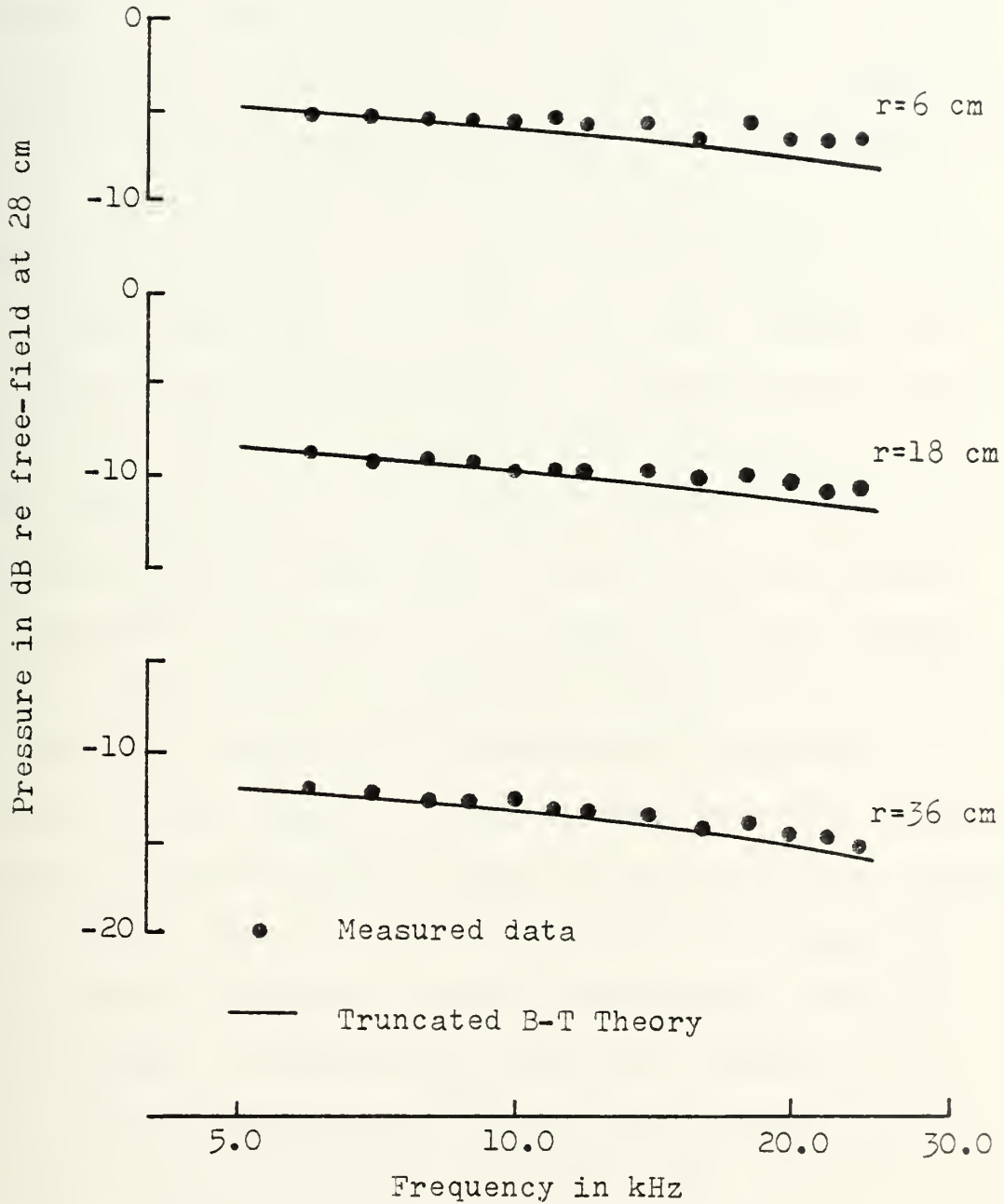Figure 19. Forward Diffracted Pressure as a Function of Frequency at Various Distances (r) from the Corner, $\frac{1}{2}$" Source (Geometry of Fig. 17).

73

In Figure 20, these same measurements are presented as diffracted pressure as a function of range (from the corner) for selected frequencies, once again compared to the sum of "truncated" B-T theoretical solutions. Also presented for comparison are lines of arbitrary level with slopes of -10 log r (cylindrical) and -20 log r (spherical). An apparent source at the corner would be expected to radiate spherically while an infinitely long edge would radiate cylindrically. Because of the geometry the ranges to the corner and to the point on the edge where the least time "ray" crosses are essentially equal so the data may be examined directly for evidence of a spherical divergence from the corner.

The data, as well as theoretical results, of Figure 20 range from a slope of less than 3 dB per double distance near the corner, low frequency, to almost 6 dB per double distance at the highest frequency and largest distance from the corner. In terms of the dimensionless parameter kr (wavenumber times range), it appears that the corner cannot be characterized as a simple spherical or cylindrical source for low values of kr. As kr is increase, the range depen- dence gradually increases to a value approaching 6 dB per double distance. Although the results are somewhat incon- clusive due to limited data, the two line sources, one at each edge, begin to resemble a virtual point source at higher values of kr.
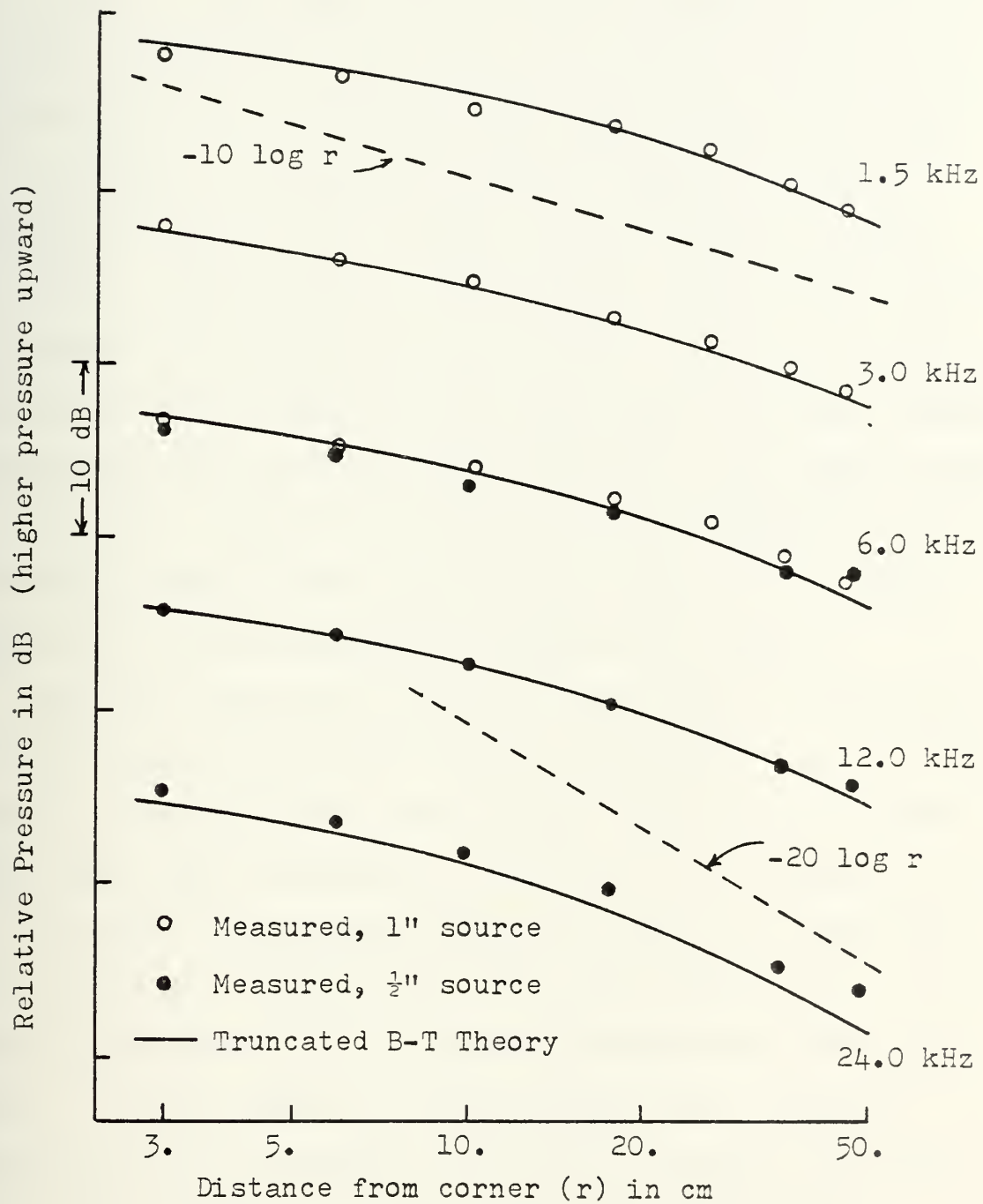
Figure 20. Forward Diffracted Pressure as a Function of Distance from the Corner for Various Frequencies (Geometry of Fig. 17).

An additional experiment was performed to better define
the difference between diffraction by an edge and diffraction
by a corner. The plate used in this experiment was identical
to that used for the corner (Fig. 17) except that the source
and receiver were set up on a long edge, as shown in Figure
21. As before, the measured data are compared to the B-T
calculated results (for a single infinite edge) in Figures
22 and 23. Unfortunately, the agreement between measurements
and theory is not nearly as good in this case as it was for
the corner. The reason for the significant deviation between
measurement and theory at higher frequencies and small ranges
is not known. Figure 24 presents a direct comparison between
corner and infinite edge results, as a function of range,
along with the appropriate B-T theoretical results.

From this comparison it can be seen that the diffracted
pressure field behind the corner is approximately 6 dB higher
than that behind a half-plane (single edge) for the larger
ranges and higher frequencies. As the receiver moves closer
to the plate, the difference between corner and single-edge
data decreases. Furthermore, there does appear to be a fre-
quency dependence in the difference between the corner and
edge at a given range. To better define this frequency
dependence and to estimate the effect of moving away from
the shadow boundary, a final experiment was performed.

Referring to the geometry of Figure 17, the receiver was
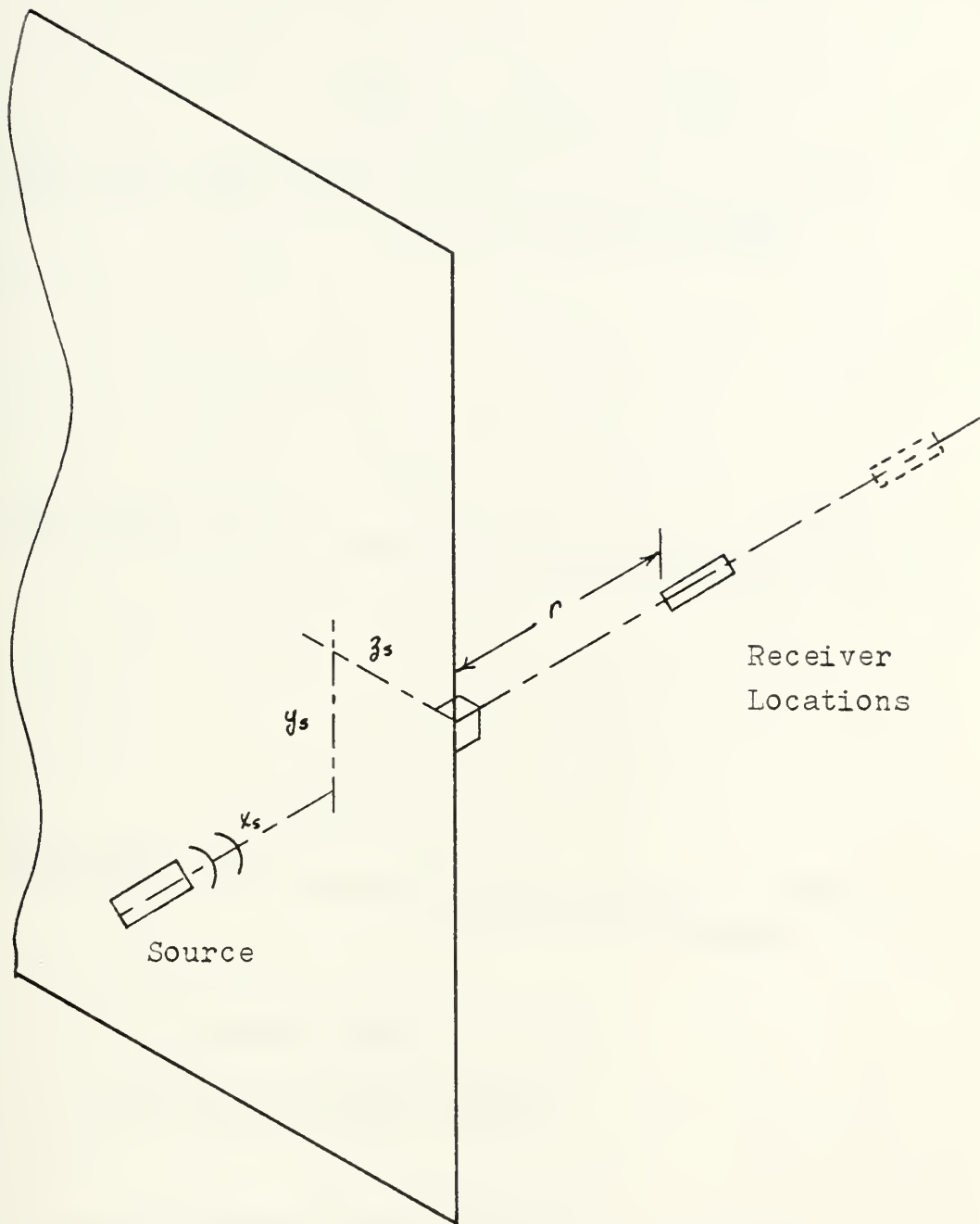placed distances (r) of 18 and 32 cm from the corner on a

76

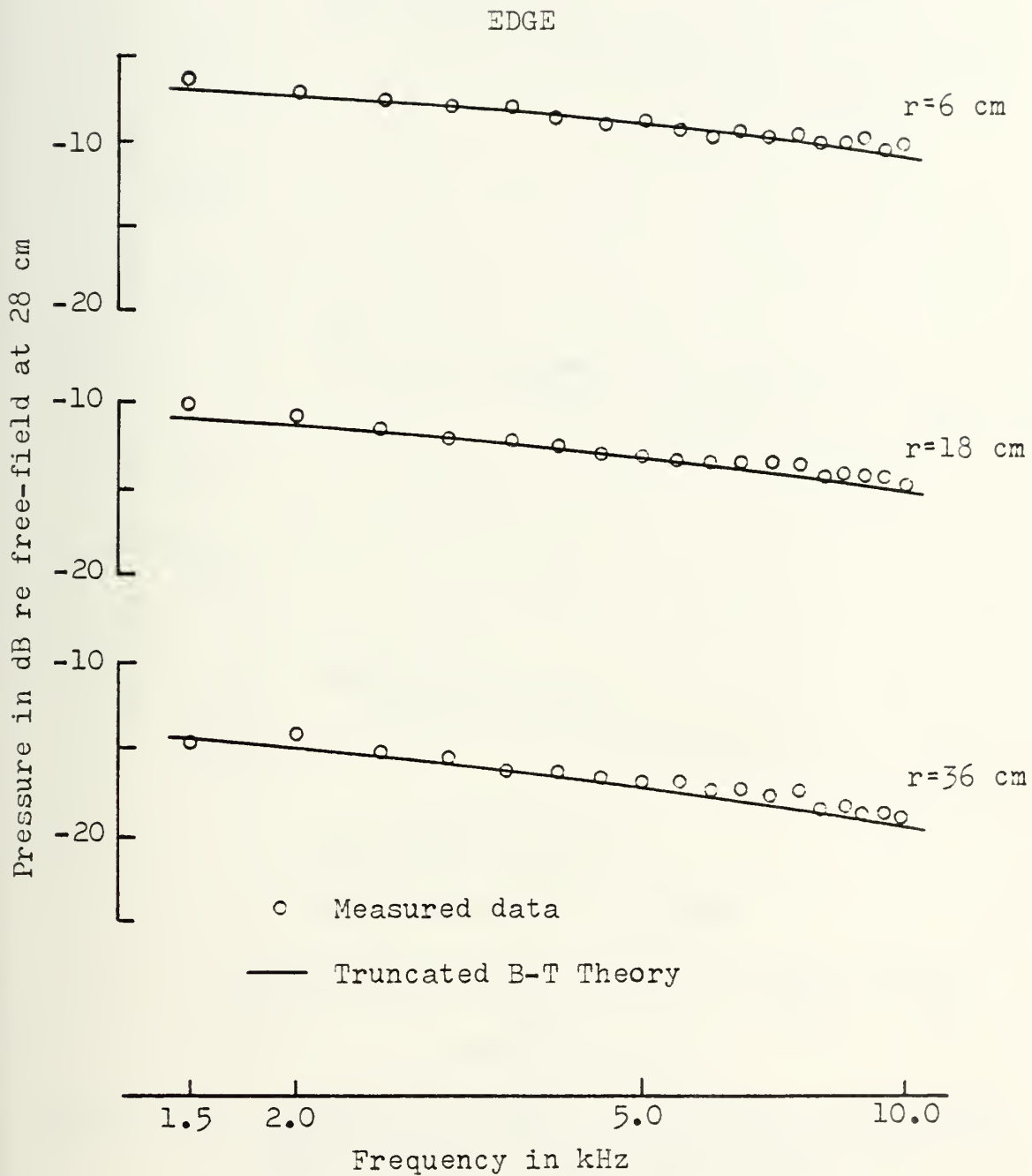Figure 21.   Single Edge Experimental Geometry.

Figure 22. Forward Diffracted Pressure as a Function of Frequency at Various Distances (r) from the Edge, 1" Source (Geometry of Fig. 21).
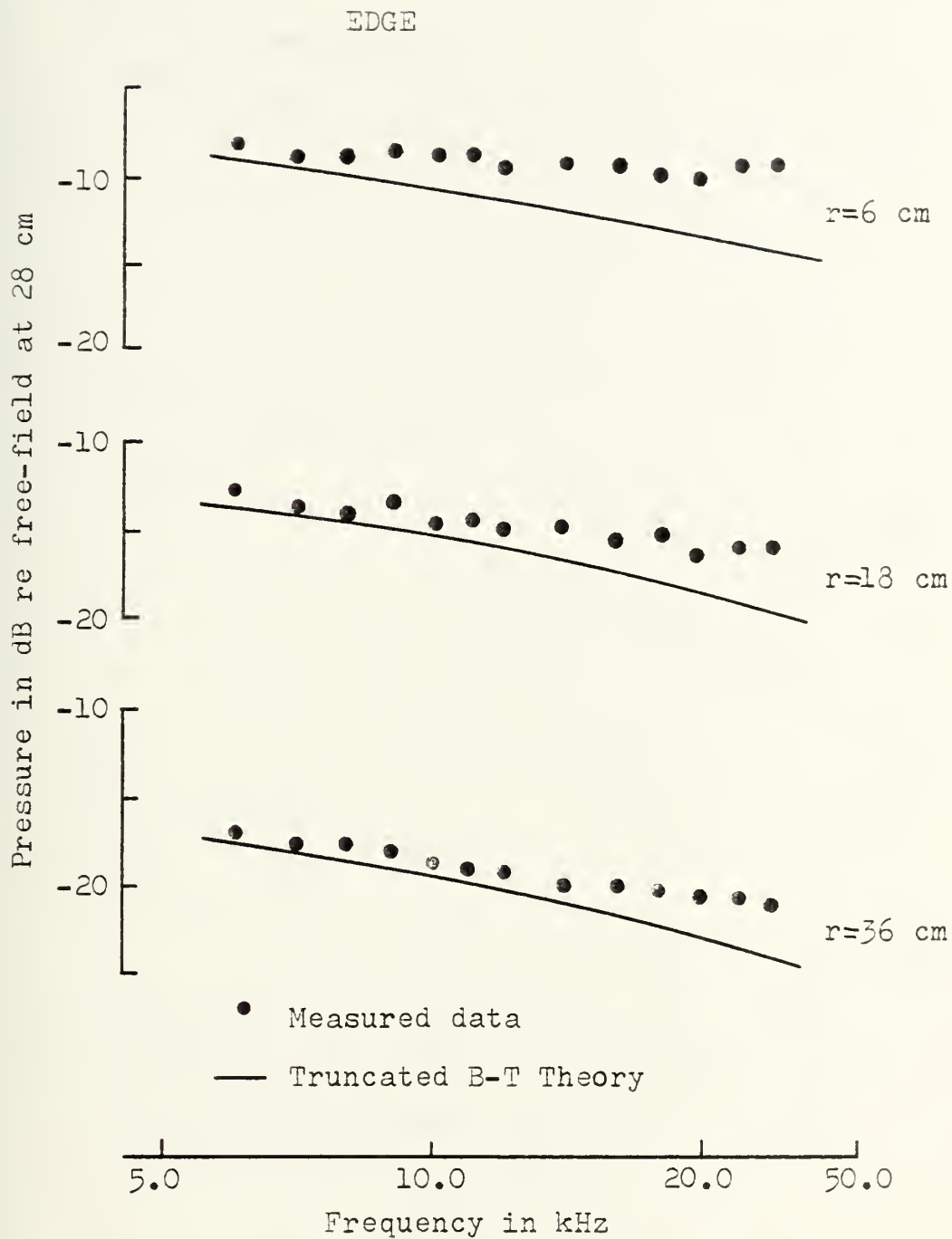
EDGE

Figure 23. Forward Diffracted Pressure as a Function of
Frequency as Various Distances (r) from the
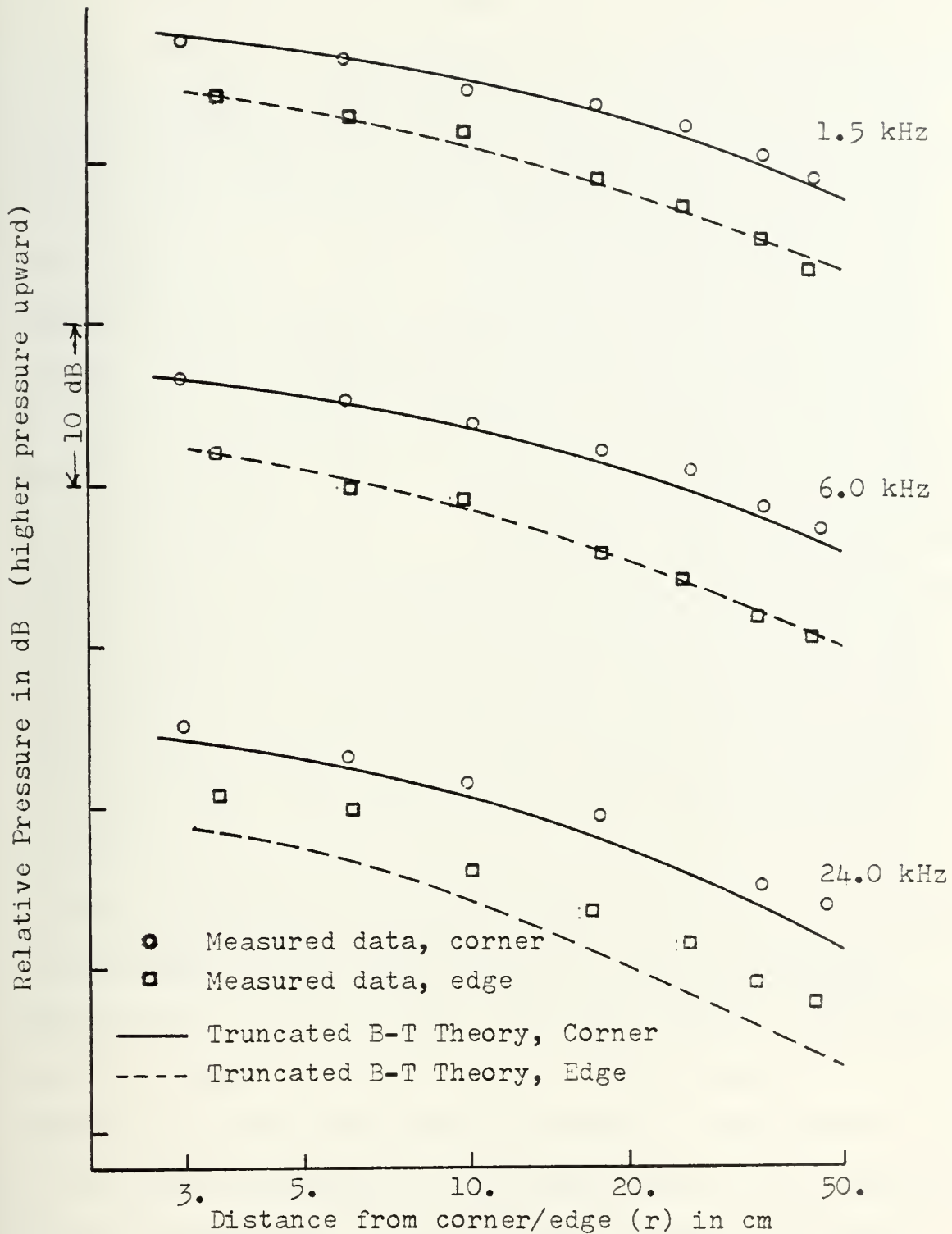Edge, $\frac{1}{2}$" Source (Geometry of Fig. 21).

Figure 24. Comparison of Forward Diffracted Pressure as a Function of Distance (r) for the Corner and the Single Edge for Various Frequencies.

80

line perpendicular to the plate (this is the same geometry as the previous corner measurements). Measurements were also made at distances of 18 and 32 cm from the corner on a 45° line extending into the shadow region "behind" the plate as shown in Figure 25. As before, four identical measurements were made along a single "infinite" edge for comparison. The magnitude of the Fourier transformed data from the corner, divided by the corresponding data from the single edge, are presented in Figure 26. The upper two curves present data taken on the perpendicular line while the lower two are taken on the 45° line (deeper in the shadow). Also shown with the upper curves is the theoretical difference between the corner and edge based on B-T. The general trend indicated by the upper two curves is one of less than a doubling of pressure (due to line sources) at the lower frequencies, increasing to slightly more than double the pressure at the higher frequencies.

When the receiver is moved deeper into the shadow region, the character of the ratio plotted in Figure 26 changes dramatically, as shown by the lower two curves. The monotonic frequency dependence seen near the shadow boundary has been replaced by a more complicated dependence. The average value of the difference appears to be approximately 6 dB, even at the lower frequencies. The detailed frequency dependence will be addressed in the next section. The general conclusion to be drawn from Figure 26 is that the farther the
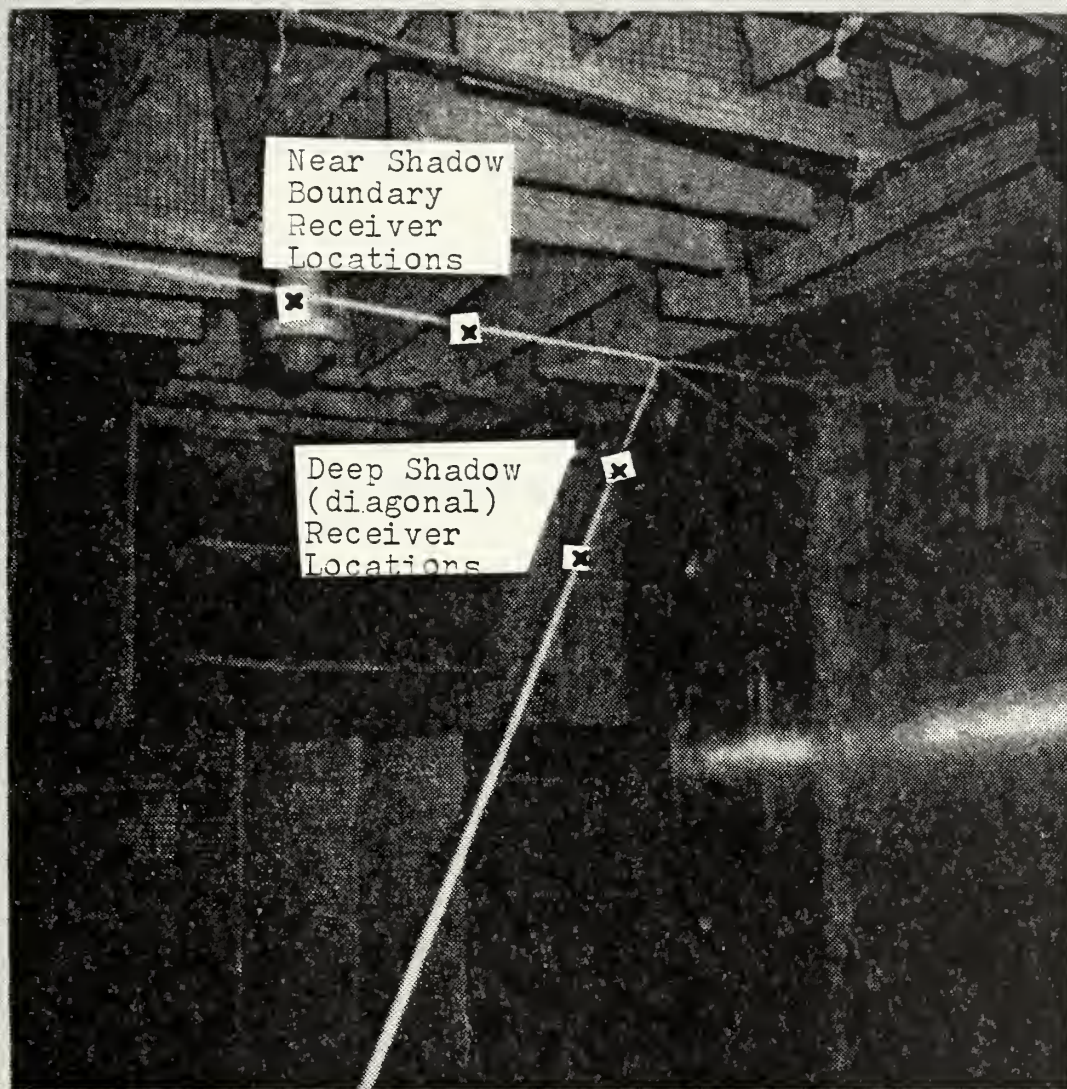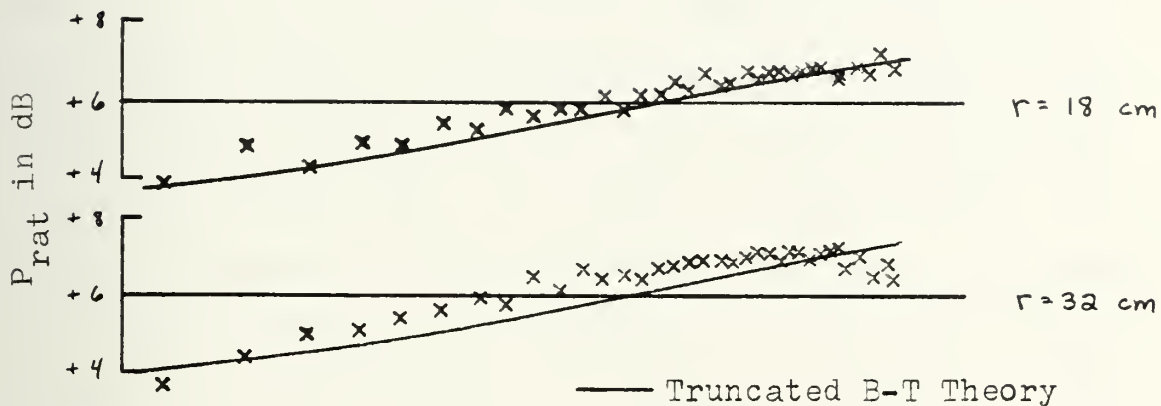
Near Shadow
Boundary
Receiver
Locations

Deep Shadow
(diagonal)
Receiver
Locations

Figure 25. Experiment Geometry for "Near Shadow Boundary"
"Deep Shadow" Forward Diffraction Comparison
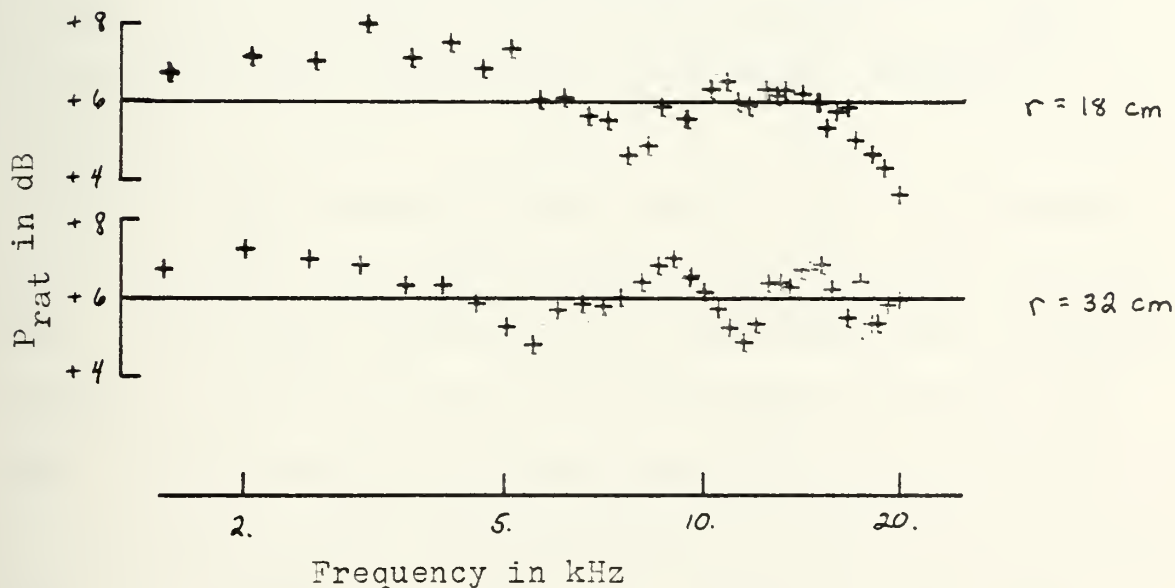Measurements.

82

Figure 26. Comparison of P_{rat} as a Function of Frequency for Receiver Locations in the Deep Shadow and Near the Shadow Boundary (see text).

83

receiver moves into the shadow region, the more the diffrac-
ted pressure field looks like the coherent addition of two
infinite edges, plus a small frequency dependent variation.

In summary, the measurements presented herein show that
the basic approach of adding impulse diffractions from each
edge in the time domain is valid. Near the corner, the
diffracted pressure is less than a simple addition of two
infinite edge diffractions. In this region, the approach
proposed by Medwin [Ref. 8], wherein the time domain solu-
tion is "truncated" at the point where the edge wave reaches
the corner, estimates the diffracted pressure very closely
as shown by Figures 18 and 19. The usual treatment of the
corner as a source of spherically diverging diffracted sound
is not evident in the measured or B-T theoretical results,
at least over the lower range of kr presented. At high
values of kr, the results may be approaching spherical
divergence.

In the high frequency limit, Keller [Ref. 16] predicts
that the corner does produce spherically diverging waves but
that the resulting diffracted field decreases with increasing
frequency much more rapidly than the field produced by an
edge. This characteristic has been used as justification
for disregarding the diffraction at a corner when approaching
practical problems [cf. Ref. 17]. Figure 26 would seem to
indicate that radial distance from the corner and frequency
are not sufficient to determine when to disregard the effects

84

of a corner; one must also consider the relationship of the
receiver location to the shadow boundary. The dimensionless
parameter implied in Medwin's truncation approach is kd where
d is the distance from the corner to the point where the
least time "ray" intersects the edge. No substantiation
for this parameter is offered here, however it does take
into account both distance from the corner and nearness to
the shadow boundary.

C. FORWARD DIFFRACTION BY A STRIP

The next experiment was designed to investigate the be-
havior of diffraction from an "infinite" strip of material
whose width was of the order of a wavelength. Two strips
were actually measured, with widths 10 cm and 4 cm. Given
the measurement capability of 1.5 to 40 kHz, these two strips
provided a total range of ka (a represents the width of the
strip) of 1.09 to 72.8. Source and receiver were located on
a perpendicular line through the center of each strip, as
shown in Figure 27a. The source was 14.5 cm from the strip
for all tests while the receiver was located at distances
from the strip of 9.5, 23.2, 39.5, and 59.5 cm in the case
of the 10 cm wide strip and 9.5, 23.2 for the 4 cm strip.
Once again, this geometry was chosen to eliminate the cohe-
rent interference that would result from different path
lengths around each edge. Identical measurements were also
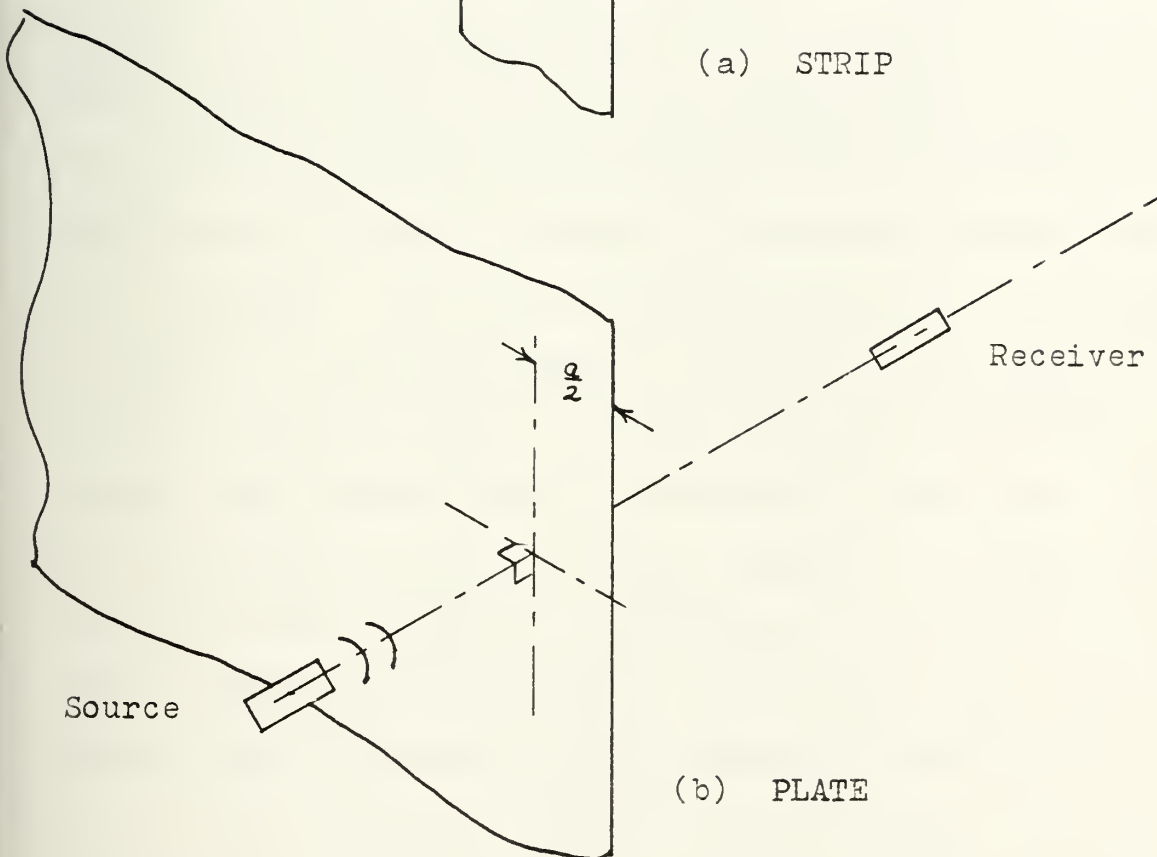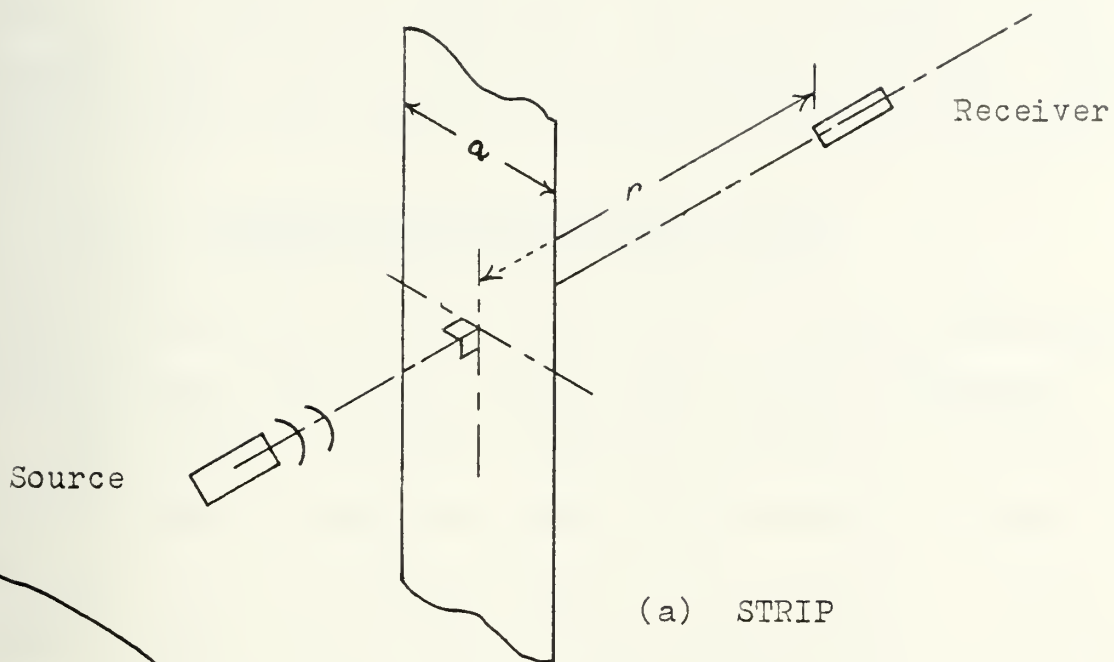performed on a single "infinite" edge as shown in Figure 27b.

85

Figure 27. Strip Diffraction Experimental Geometry.

As long as linear superposition of edge effects holds, the diffracted pressure at any of the measurement points will be double for the strip compared to the corresponding plate (single edge), since there is no truncation involved. With this in mind, all data are presented as the following ratio:

$$P_{rat} = \frac{\text{diffracted pressure behind strip}}{\text{diffracted pressure behind plate}}$$

When superposition holds, there will be a simple doubling of pressure and this ratio will be +6dB at all frequencies.

This ratio, calculated from the measurements on the 10 cm strip and corresponding plate, is presented in Figure 28. The data are not presented above 30 kHz because of limitations in the determination of the perpendicular to the strip (i.e. the path lengths around the two edges could not be equalized well enough to prevent cancellation effects above this frequency). The oscillating pattern in the low frequency portion of the measurements is evident from Figure 28. If this is interpreted as coherent interference between two signals, two features can be extracted from the data. First, this interference pattern does not depend on distance from the strip/plate. Second, by estimating the spacing (in frequency) between adjacent peaks or between adjacent nulls the apparent path difference can be calculated from the relation $d = \lambda = {}^{c}/\Delta f$ in meters. From the data of Figure 28, d is estimated to be 9 cm, quite close to the strip width of 10
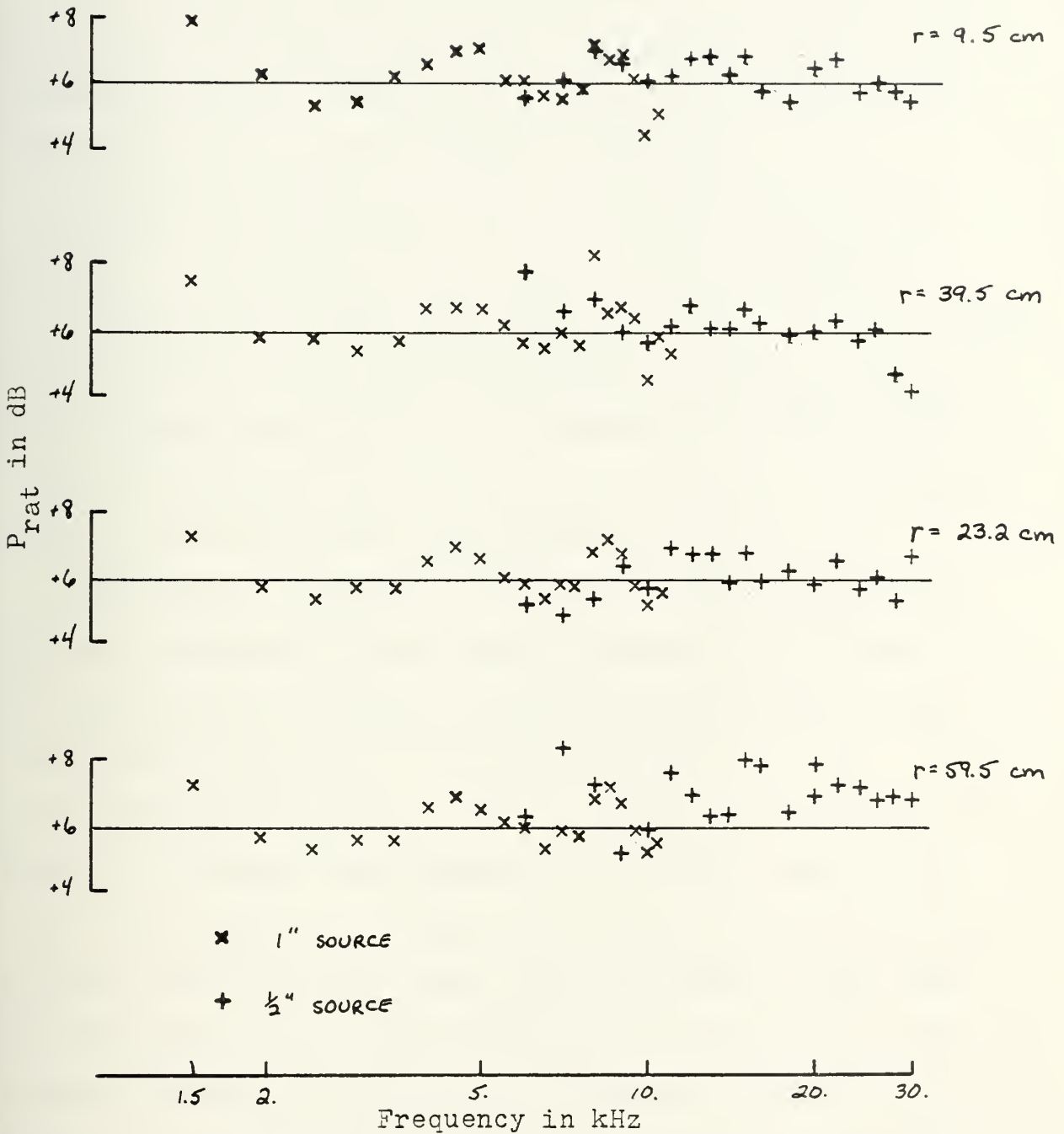
87

Figure 28. Comparison of P_{rat} as a Function of Frequency at Various Distances (r) for the 10 cm Strip (Geometry of Fig. 27).

cm. To verify that strip width is the characteristic dimen-
sion, the experiment was repeated for the 4 cm strip.

The 4 cm strip results are presented in Figure 29. The
strip width from Figure 29 data is estimated to be 4.1 cm,
confirming that the width of the strip is the factor deter-
mining the form of the "interference pattern".

The data measured at 9.5 and 23.2 cm are averaged and
plotted as a function of ka for both strips in Figure 30.
For simplicity, the data from both 1 inch and 1/2 inch sources
were averaged in the overlapping region 6-10 kHz. Figure 30
clearly shows that the frequency dependence is directly re-
lated to the strip width a, with a ka spacing of 2π between
peaks as expected from a simple interference pattern.

The physical explanation offered for this interference
is called secondary diffraction or secondary scattering.
The application of secondary diffraction to the strip is
illustrated in Figure 31. The figure shows only the
interaction at one edge; the mirror image of the process
shown is occurring simultaneously at the other edge. The
solid lines in Figure 31 depict the path of the pulse as it
diffracts over the upper edge, while the dashed lines show
how the diffraction of the same pulse at the opposite edge
generates signals on both sides of the strip which propagate
across the strip and diffract once again at the upper edge.
The doubly diffracted pulse arrives at the receiver at time
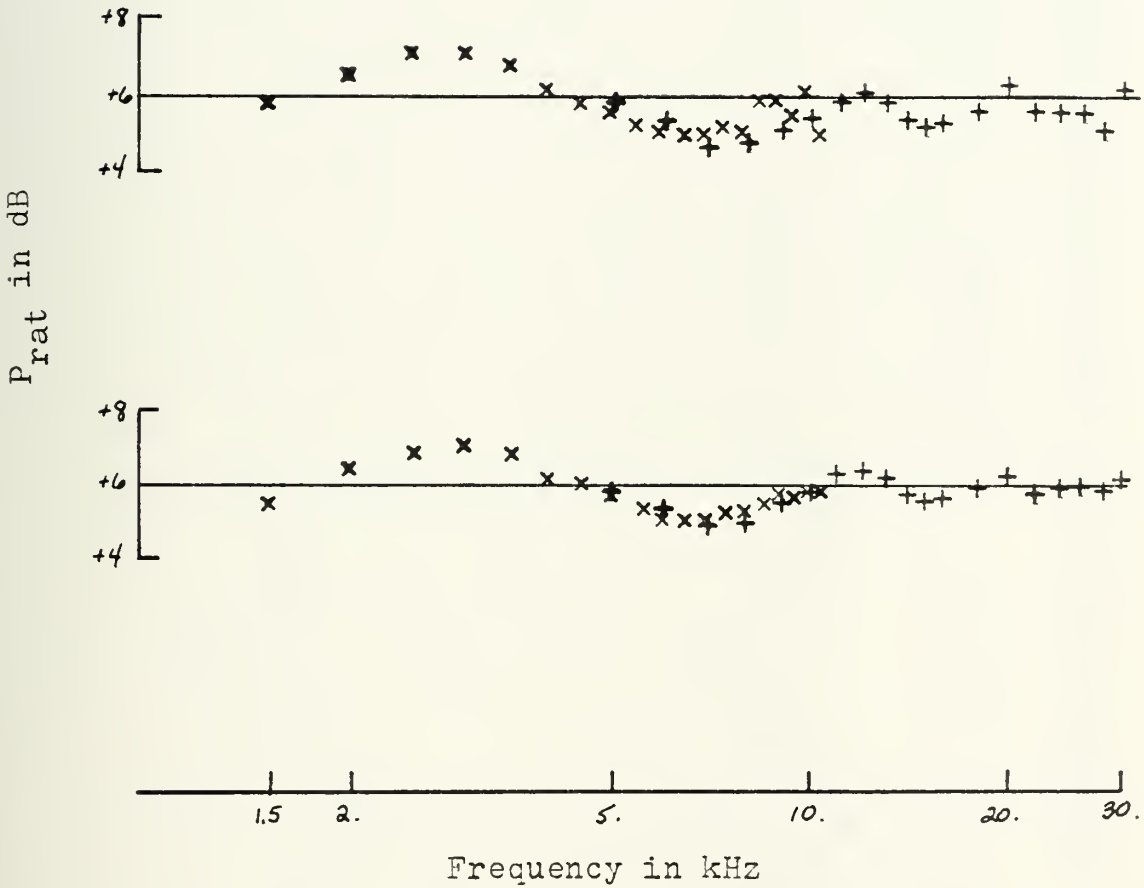equal to the width (a) divided by the propagation velocity

Figure 29.   Comparison of P$_{rat}$ as a Function of Frequency
at Various Distances (r) for the 4 cm Strip
(Geometry of Fig. 27).

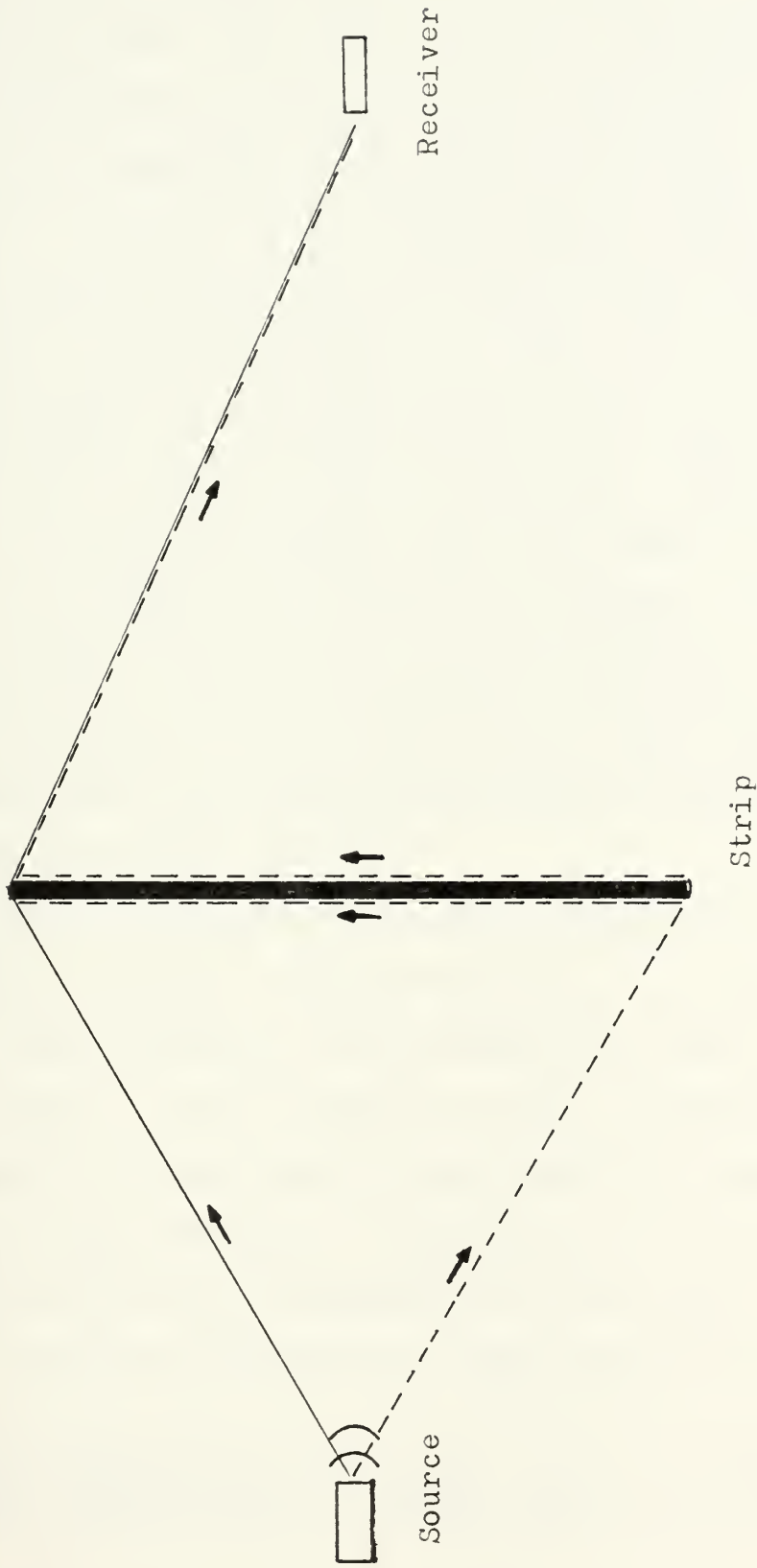Figure 30. Comparison of P_{rat} as a Function of ka for the 4 and 10 cm Strips.

Figure 31.   Secondary Diffraction (Dashed Line) Concept Applied to the Strip.

(c) later than the initial pulse, resulting in the observed

interference pattern. This late pulse would have two dis-

tinct characteristics, arising from the additional diffrac-

tion, which are immediately observable in the measured data

of Figure 30. First, it will be considerably reduced in

amplitude relative to the earlier (single diffraction)

pulse. This is seen in the data as a weak interference

pattern (the peaks are approximately 6 + 1 dB compared to

6 + 6 dB if the two were of equal amplitude). Second, the

difference in amplitude between singly and doubly diffracted

pulses will be greater with increasing frequency since each

diffraction should increase the frequency dependence and

decrease the strength of the diffraction by approximately

$f^{-1/2}$. This causes the decaying amplitude of the interference

pattern with increasing frequency.

A method of calculating the secondary diffraction has

been proposed by Medwin[1] and implemented by Ms. Emily Childs.

The general description of the implementation which follows

is due to Childs.[2] When a spherical pulse intersects an

edge, a boundary or edge wave is generated which appears

to propagate along the edge. Calculating the B-T time domain

solution in discrete time increments, this edge wave becomes

a series of discrete sources on the edge, each with a

_____

[1] Personal communication to author from Dr. H. Medwin.
[2] Personal communication to author from Ms. E. Childs.

characteristic amplitude and phase. Extending this to a two edge system (the thin edged strip in this case), these discrete sources on the first edge (now called secondary sources) each diffract at the second edge and contribute to the diffracted field at the receiver. The proper amplitude is assigned to each secondary source through a system of virtual receivers located at the second edge. The phase of each source is taken into account by performing the entire calculation in the time domain. Figure 32 presents the results of this theoretical calculation in terms of P_{rat} for each strip at a receiver distance of 23.2 cm., compared to the measured data from Figure 30. Two theoretical curves are presented for each strip; one which considers the secondary diffraction on both sides of the strip (double secondary path) and one which considers secondary diffraction only on one side (single secondary path). Although the double secondary path is the intuitively correct interpretation, the measured data obviously agree with the single path approach. One possible explanation is that in using the double path interpretation, each path should be reduced in amplitude by 1/2 (the diffracted pressures along the paths on either side of the strip are of equal amplitude but opposite sign). Keller [Ref. 16] describes a similar phenomenon for the thin slit in an opaque plane using the Geometrical Theory of Diffraction.
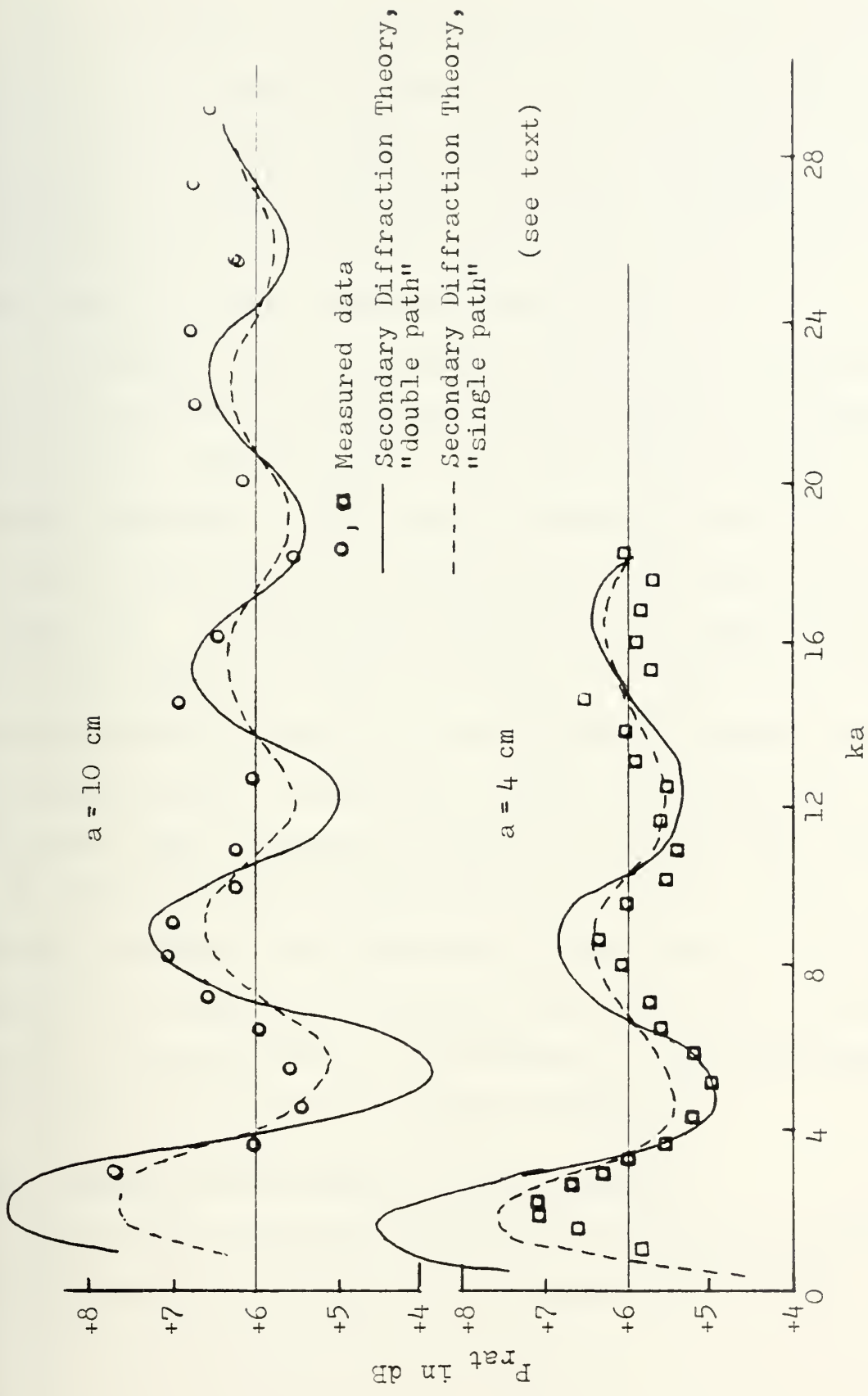
Figure 32. Comparison of Measured and Theoretical P_{rat} as a Function of ka for the 4 and 10 cm Strips.

95

At this point it is also appropriate to point out that the use of secondary diffraction in the preceding explanation of the interference pattern would not be possible with the Helmholtz-Kirchhoff approach, since the scattered or diffracted field on the plate would be zero. There would be no way the pulse could propagate between edges.

It appears that the secondary diffraction explanation can also be applied to the somewhat more complicated geometry of the corner. Recalling Figure 26, there was a detailed frequency dependence in the results, especially where the receiver was deep in the shadow region (the lower curves of Figure 26). Consider now a corner with one edge horizontal and one vertical as shown in Figure 17. There will be a pulse that travels from source to receiver by diffracting over the horizontal edge. In addition, a pulse also diffracts at the vertical edge, propagates across the plate near the corner, and diffracts over the horizontal edge to the receiver. Unlike the strip, the difference in path length of the two pulses is a function of distance from the corner, an effect which can be observed as a difference in the interference patterns in the two lower curves of Figure 26.

D. FORWARD DIFFRACTIONS BY A THICK BARRIER

The usual theoretical approach to solving the problem of diffraction by a plate is to consider it to be an

infinitely thin, rigid half-plane. However, a real barrier
which significantly attenuates the direct path of sound must,
of necessity, have a thickness which is a significant frac-
tion of a wavelength at high frequency. In Reference 12,
Bremhorst presented data which showed the diffracted pressure
at various points in the shadow of a 3/16" thick steel plate.
In particular, Figures 37 through 46 of Reference 12 showed
that the measured diffracted pressure was generally less
than that predicted by B-T, especially near the surface of
the plate (on the shadow side). Bremhorst attributed this
to the finite thickness of the plate. To confirm this
hypothesis, an experiment was performed using two barriers
of different thickness.

The variable thickness was achieved by placing a piece
of aluminum stock of the appropriate thickness between two
3/16" aluminum plates and machining the resulting "edge"
smooth and square. Damping material was placed in the gap
between the plates to attenuate the direct path. An example
of the thick edge can be seen in the photograph of Figure
14. Thicknesses of 2.2 and 3.5 cm were evaluated utilizing
the geometry shown in Figure 33. Measurements were made at
$\theta = 300°$ and 345°, where there was considerable disagreement
between Bremhorst's measurements and B-T theory. The measured
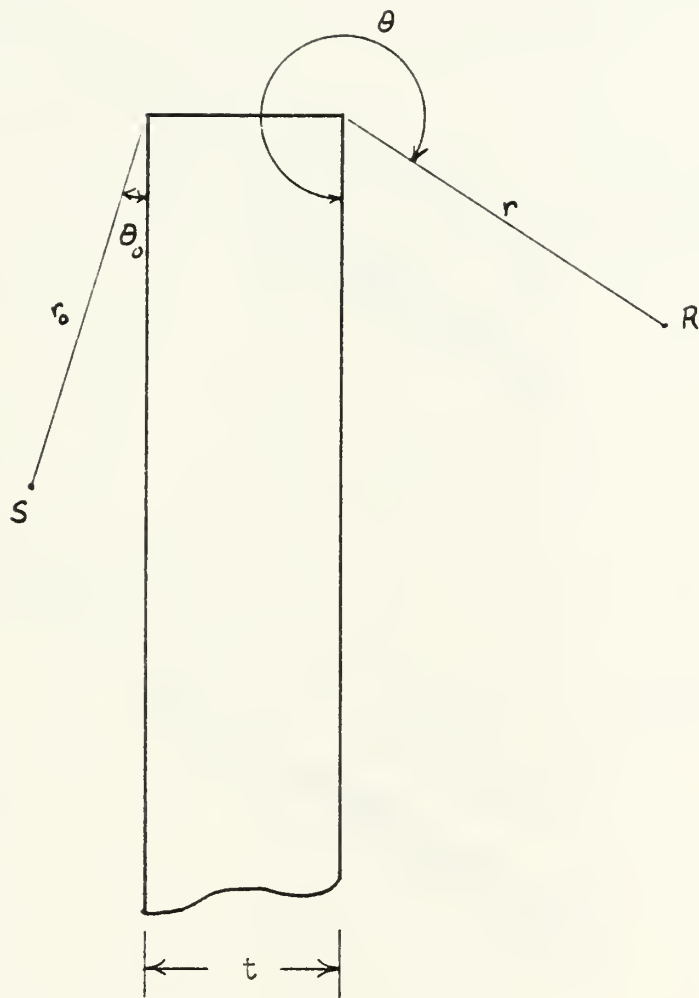data are shown in Figure 34, compared to the Bremhorst's
results and the B-T theory.
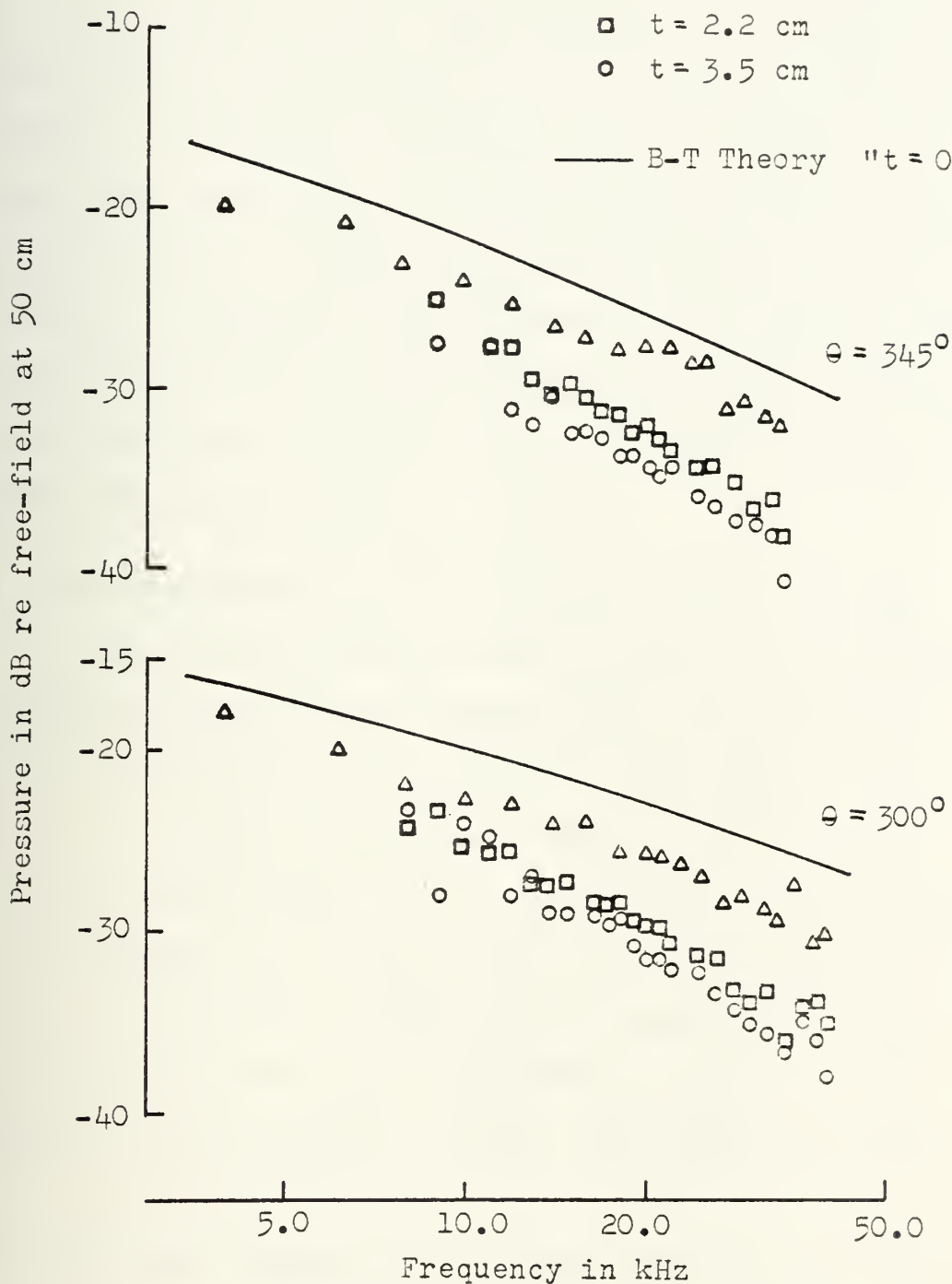
Figure 33.   Thick Barrier Measurement Geometry.

Figure 34. Forward Diffracted Pressure as a Function of Frequency for Various Thickness (t) Plates, $\theta_o = 15^o$, $r = r_o = 25$ cm.

The data presented in Figure 34 indicate that barrier thickness is an important parameter in determining the diffracted pressure field, especially when the thickness is on the order of one wavelength (10-15 kHz for the thick barriers tested). It has been suggested by Medwin [3] that this thickness can be handled by a secondary diffraction calculation based on the B-T theory, as discussed earlier for the thin strip, by considering the thickness to be a double edge. This has not been verified at this time, although the thickness does appear to explain the discrepancy between Bremhorst's data and the B-T theory.

E. FORWARD DIFFRACTION BY A BARRIER ON A RIGID BASE

A typical noise control barrier consists of a plane screen or plate mounted perpendicular to a flat base, as shown in Figure 35. The total pressure field at the receiver, if it is in the shadow region, consists of the source signal arriving via multiple paths. The usual approach to solving this problem is to consider that for the top edge there are four geometrically distinct paths, each involving one diffraction at the top of the barrier, made up of all possible combinations of source, receiver, and images of source and

_____

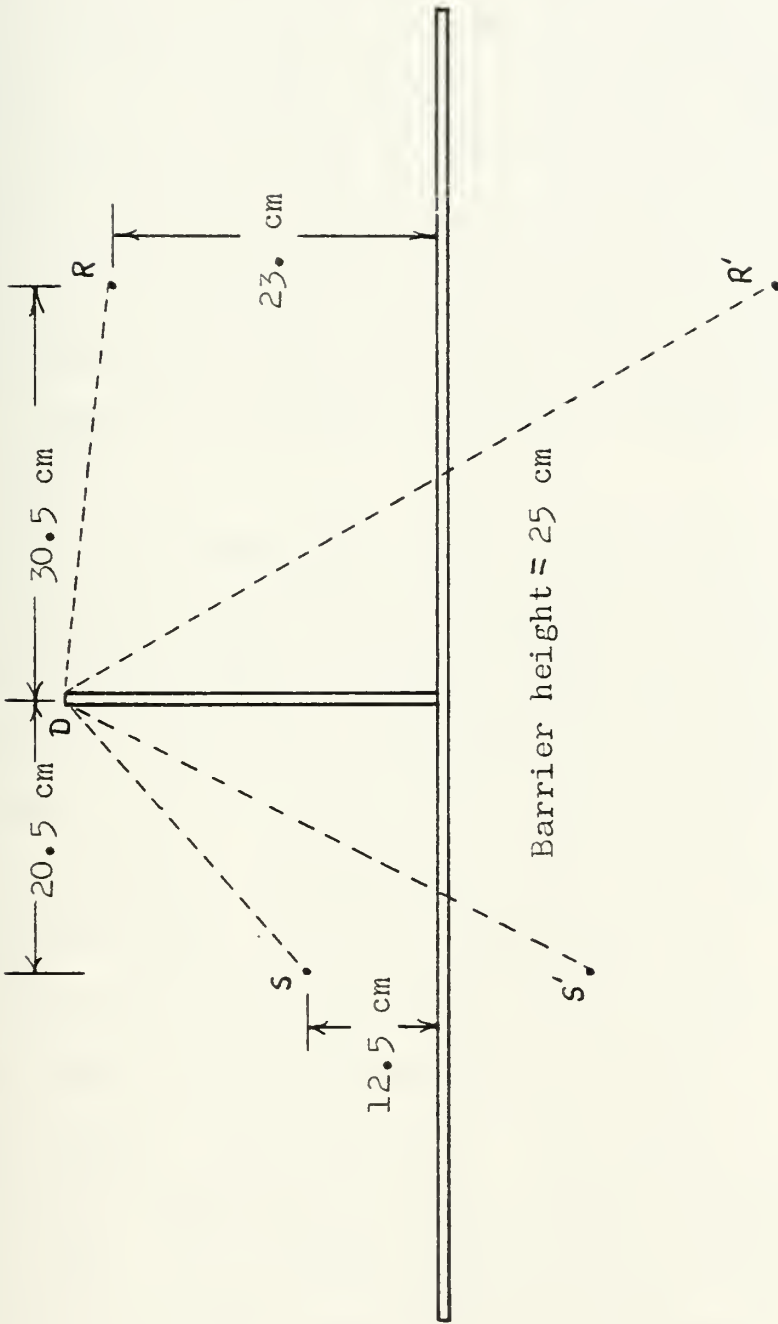[3] Personal communication to the author by Dr. H. Medwin.

100

Figure 35.   Geometry of Barrier on Rigid Base.

receiver in the base, as shown in Figure 35. Using the no-
tation of Figure 35, these paths are denoted as SDR, S'DR,
SDR', S'DR'. It should be pointed out that S' and R' here
are true images as used in optics and acoustics to describe
reflection from a plane surface. The term "image" is also
used by authors in the noise control field [cf. Ref. 5] in
conjunction with the "image of the source in the barrier",
as discussed in section II. This usage is considered here
to be inappropriate and will always be set apart by quotation
marks ("image") to prevent confusion with the more common
term (image).

To test the hypothesis that the four paths described
above adequately characterize propagation from source to
receiver in this case, a simple experiment was performed.
A barrier with base was constructed of 3/16 inch aluminum
plate with an overall width of 120 cm and barrier height of
25 cm in the basic configuration shown in Figure 35. Source
and receiver (both 1/2" B+K microphones) were positioned so
that each of the four paths would have a different length,
and each path would intersect the axis of the microphone
at approximately the same angle. This would allow at least
a qualitative comparison of the relative strengths of the
various paths. Use of the pulsed source of earlier experi-
ments would allow the identification, in the time domain,
of each path by its characteristic propagation time.

Similarly, undesirable paths such as backscatter from the edges of the finite base and diffraction around barrier sides would have propagation times longer than the longest (S'DR') path of interest and could be eliminated in the time domain. The results of this experiment are shown in Figure 36, compared to the calculated arrival times of each of the four paths. It is clear from these results that the four paths constructed from the source, receiver and their images in the base are the dominant paths in this basic barrier configuration. If any other paths exist, they must be of relatively low level or coincide with one or more of the four basic paths. The path due to the "image of the source in the barrier" as discussed by Isei [Ref. 5] would coincide with the SDR and SDR' paths of Figure 36. The relative amplitude of the various paths also behave as expected, with the later arrivals (longer paths) having lower amplitudes.

The strengths of the various paths were examined by varying the geometry slightly. By increasing the barrier height to 42 cm and changing the receiver location (Figure 37), the separation in time between the paths was increased engough to allow a separate spectrum analysis of each pulse. The data of Figure 38, taken with the source/receiver oriented to insonify/receive both SDR and S'DR paths equally (approximately), show the separation between the two pulses, and the general trend in their amplitudes. As expected, the S'DR pulse appears to be an exact replica of the SDR pulse.

Figure 36. Total Received Time Domain Signal Due to the
Four Paths of Barrier on Base (Geometry of
Fig. 35).
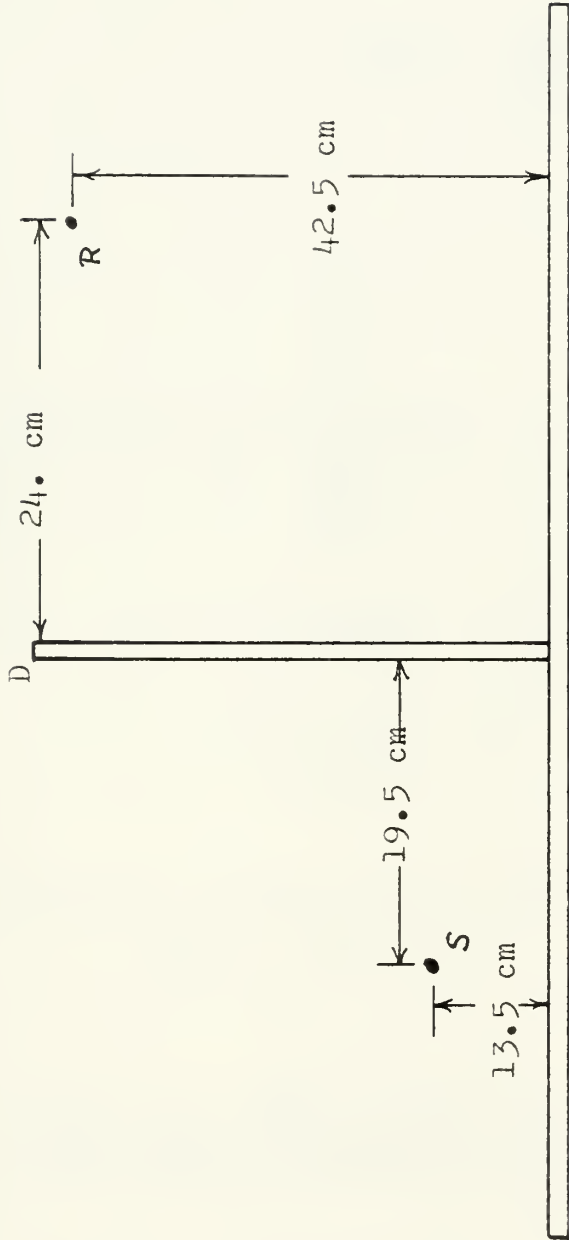
Barrier Height = 42 cm

Figure 37. Geometry of Barrier on Rigid Base, Tall Barrier.

Figure 38.   Received Time Domain Signal Due to the SDR and S'DR paths (Geometry of Fig. 37).

The actual strength of each path was measured by "pointing" the source in the direction of the path of interest (the receiver always pointed toward the edge, D) and Fourier transforming only the received pulse corresponding to that path. This was done for both the SDR and S'DR paths. The data, normalized by the free field pressure at the receiver with the barrier _and_ base removed, (source/receiver pointed at each other) are presented in Figure 39. Also presented for comparison are the B-T infinite half-plane theoretical results for each path. The agreement between theory and measurements shown in Figure 39 is excellent, indicating that the diffracted field at the receiver due to SDR and S'DR paths may be computed separately, using the geometry of the source and the image of the source in the base. The total diffracted pressure at the receiver may then be obtained by adding the contributions of each path.

It is important to note that the theoretical results in Figure 39 were obtained from the _complete_ form of the B-T infinite half-plane solution. The complete theoretical solution for the diffracted field at R in Figure 35 consists of the sum of four terms. Isei [Ref. 5] approaches the same problem by adding the contributions of six different paths, as shown in Figure 3 of Reference 5. It appears that he has used the solution due to Macdonald in a form which is separated into "real" and "image" components as discussed in section II and is applying these separately to the six paths.
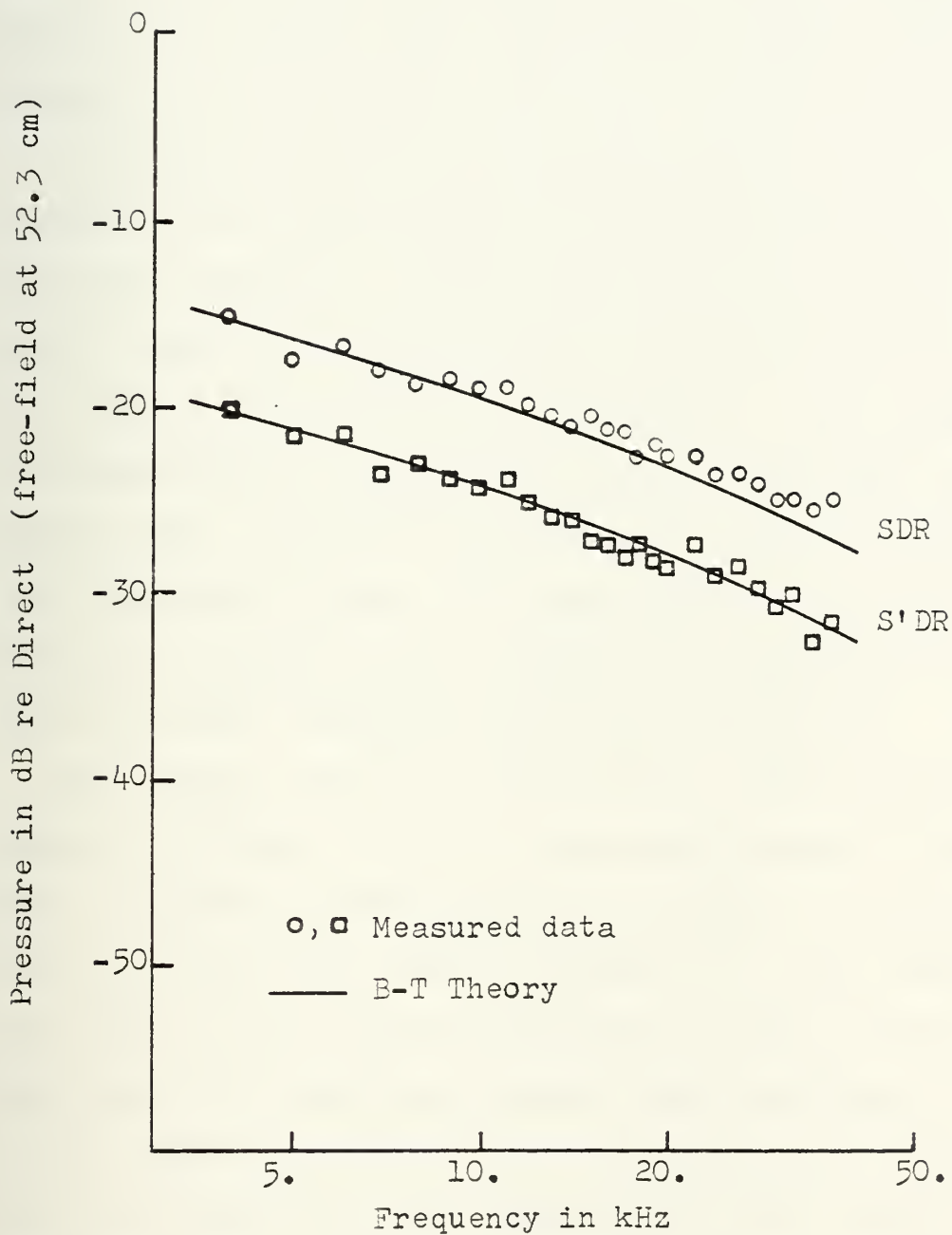
107

Figure 39. Diffracted Pressure as a Function of Frequency for the SDR and S'DR Paths Compared to the B-T Theory (Geometry of Fig. 37).

Figure 39 shows that the correct approach is to apply the complete solution (e.g. in Macdonald's solution this would be the sum of the "real" and "image" source components) to each of the four paths to obtain the correct diffracted field. One need not consider the "image of the source in the barrier" because it is an integral part of the complete solution.

In addition to the four paths described earlier, it is possible to have an additional path which propagates from the source, diffracts at the intersection of the barrier and base B, then diffracts over the top edge of the barrier to the receiver, shown in Figure 40 as SBDR. This assumes a non-perpendicular intersection of barrier and base since Tolstoy [Ref. 7] shows that there will be no diffraction from a 90° "interior" corner. The theoretical prediction of this diffracted pressure at the receiver was approached in the same way as for the thin strip, discussed earlier.

The geometry shown in Figure 40 was constructed of 3/16" aluminum, as before, with the source and receiver located as shown. The SDR and SBDR paths (see Figure 40) can be seen directly in the time domain in Figure 41. (The relative amplitudes are only approximate due to source directivity.) Once again, the source was pointed toward the path of interest and the received pulse was analyzed separately. The frequency spectrum of the SBDR pulse, normalized by the direct, free-field pressure, is shown in Figure 42. Also shown is the

109
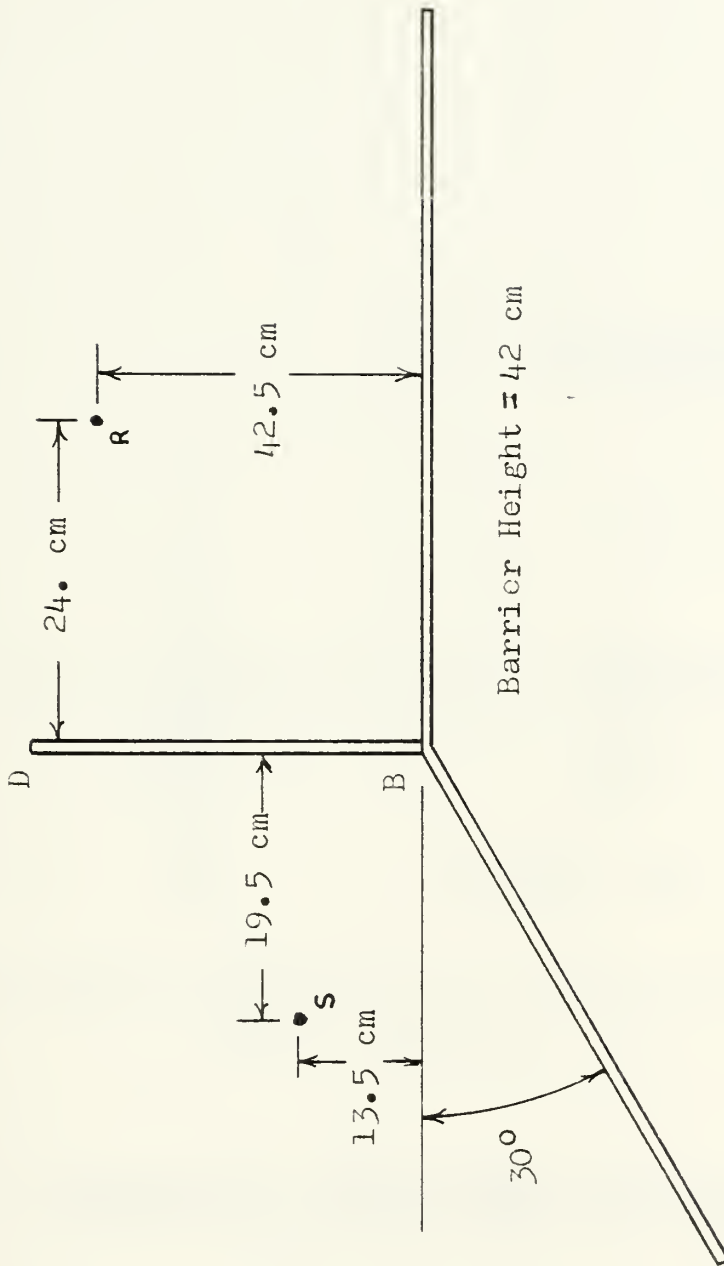
Figure 40. Geometry of Barrier on Angled Base.
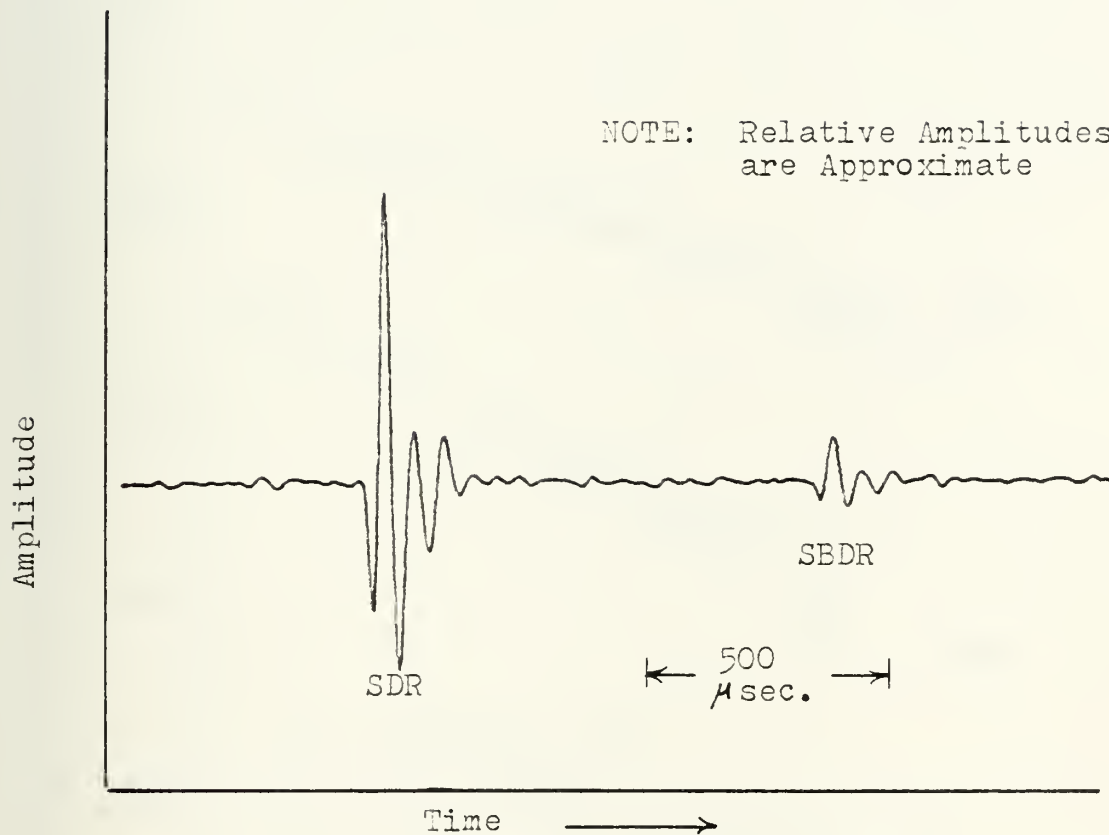
Figure 41. Received Time Domain Signal Due to the SDR
and SBDR Paths (Geometry of Fig. 40).
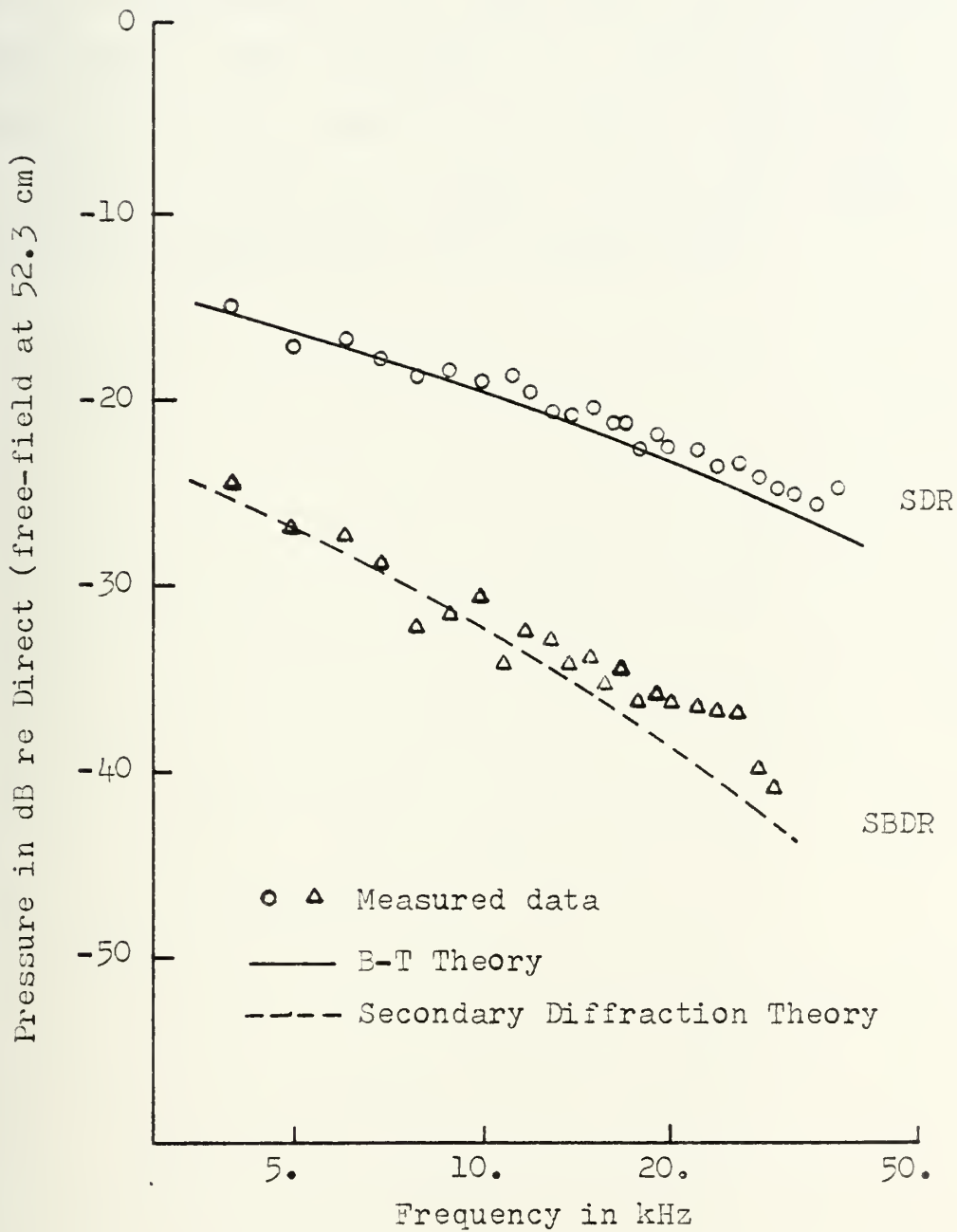
Figure 42. Diffracted Pressure as a Function of Frequency
for the SDR and SBDR Paths Compared to the B-T
Theory and Secondary Diffraction Theory,
respectively (Geometry of Fig. 40).

112

theoretical result from the secondary diffraction program.
For comparison, the SDR path data and theory from Figure 39
are also presented. (The SDR geometry is identical to the
previous experiment.) The additional diffraction in the
SBDR path is seen in the data as a different frequency depen-
dence as well as a lower overall level. When the B-T theory
is used as a basis for secondary diffraction, there is
excellent agreement with the measured data.

VII. CONCLUSIONS

The exact impulse diffraction solution of Biot and
Tolstoy (B-T) has been compared to the exact CW diffrac-
tion solution of Macdonald for forward scattering and to
the impulse solution to the Helmholtz equation (H-K) for
backscatter using the Kirchhoff approximation. For back-
scatter from an infinite edge, B-T and H-K have been found
to reduce to a similar although analytically different time
domain form. Comparison of B-T and H-K in the frequency
domain showed substantial disagreement, except for geometries
where the diffracted pulse was close to the reflected pulse
in time, where both solutions approached the same value.
Backscatter near the plate was found to be grossly under-
estimated by the H-K solution, due to the boundary condition
used by Kirchhoff to simplify the integral. The backscattered
pressure near the surface predicted by B-T was confirmed by
laboratory measurement.

Macdonald and B-T solutions for forward diffraction from
a plate were both found to be in good agreement with the
experiment. Both solutions can be expressed as the sum of
a term containing the source/receiver angles as $(\theta - \theta_0)$ and a
term containing $(\theta + \theta_0)$. These terms were originally identi-
fied by Macdonald as the "real" and "image" source terms.
The concept of "image of the source in the barrier", as used

114

in the noise control literature, is found to be a mis-
interpretation of Macdonald's solution. For a barrier on
a rigid base, the diffracted pressure due to the real source
and the true image source (the image of the source in the
base) were measured separately and both were found to agree
with the complete (both $\theta - \theta_0$ and $\theta + \theta_0$ terms) B-T solution.

The solution of finite barrier problems was found to
be facilitated by the time domain, impulse nature of the B-T
solution. Measurements of forward diffraction near a plate
corner show that Medwin's proposed approach of truncating
the B-T time domain solution to account for the corner accu-
rately predicts the diffracted field. Experimental results
do not agree with simple spherical radiation from the corner
over most of the range of kr between 1 and 150. Limited
data do show a trend toward spherical divergence as kr
approaches 150. Measurements of the forward diffraction by
a thin strip confirm the presence of secondary diffraction,
i.e., waves that first diffract at one edge, propagate across
the surface of the strip, and diffract again at the other
edge. The time domain B-T solution is shown to be a useful
starting point in characterizing this secondary diffraction.
At high frequencies, forward diffraction loss by a plate of
finite thickness is found to be considerably greater than
the theoretical prediction, for an infinitely thin screen.
It appears that this may also be explained by the double
edge creating secondary diffraction with an additional
diffraction contribution at the second edge.

115

APPENDIX: A

APPROXIMATION OF THE BIOT-TOLSTOY SOLUTION
NEAR THE SHADOW BOUNDARY

Since the B-T solution is a delta function impulse solution, it is expected that it will approach the delta function form for limiting cases where the receiver is approaching the boundary between "illuminated" and "shadow" regions, herein referred to as the shadow boundary. As this limit is approached, the early time portion of the diffracted pulse will increasingly dominate the solution, creating a difficult numerical calculation problem. To better understand this problem, the solution will be approximated for the following conditions:

A. $\theta_w = 2\pi$ (thin plate)

B. $\theta = \theta_o + \pi + \varepsilon$ (receiver in the shadow region, ε small)

C. $t - \tau_o \to 0$ from the positive side (early diffracted pulse)

For $\theta_w = 2\pi$, the complete solution can be written as

$$p(t) = - \frac{S\rho c}{8\pi^2} \{\beta\} [rr_o \sinh Y]^{-1} [\exp(-Y/2)] \qquad (A-1)$$

where

$$Y = \text{arg cosh} \left[\frac{c^2 t^2 - (r^2 + r_o^2 + z^2)}{2rr_o}\right] \qquad (A-2)$$

and β is a four term sum written symbolically as

116

$$\beta = \frac{\sin\left[\frac{1}{2}(\pi \pm \theta \pm \theta_0)\right]}{1 - 2\exp\left(-\frac{1}{2}Y\right)\cos\left[\frac{1}{2}(\pi \pm \theta \pm \theta_0)\right] + \exp(-Y)} \qquad (A-3)$$

For the early diffracted pulse

$$\Delta t = t - \tau_0 \rightarrow 0$$

Medwin [Ref. 8] shows that when $\frac{\Delta t}{\tau_0} \ll 1$, the factor containing $\sinh Y$ can be approximated as

$$(rr_0 \sinh Y)^{-1} \cong (2\, t_0 c^2 rr_0)^{-\frac{1}{2}}$$

(This same result for the specific case of backscatter was shown in section III.) This factor goes to infinity as Δt approaches zero and is generally assumed to be the factor that determines the time dependence of $p(t)$ under these circumstances. Time dependence also enters A-1 through the $\exp(-Y/2)$ term but this will be ignored because this function only varies between 1 and zero and is relatively constant for Y (and therefore Δt) approaching zero.

The β term contains both time and geometry dependence in a rather complex way. The approach here will be to separate the β into four terms and examine each one in the limit as both Y and ε approach zero. (Y is directly, although not linearly, related to Δt. The expansion of arg cosh is not trivial and so the limiting procedure here will be with respect to Y rather than t.) The β term can be written as $(\beta_{++} + \beta_{+-} + \beta_{-+} + \beta_{--})$ with the subscripts referring to the various combinations as shown in Table (A-1).

TABLE A-1

TERM	COMBINATION OF π, θ, θ_o	SUBSTITUTION OF $\theta = \theta_o + \pi + \varepsilon$
β_{++}	$\pi + \theta + \theta_o$	$2\pi + 2\theta_o + \varepsilon$
β_{+-}	$\pi + \theta - \theta_o$	$2\pi + \varepsilon$
β_{-+}	$\pi - \theta + \theta_o$	$-\varepsilon$
β_{--}	$\pi - \theta - \theta_o$	$-(2\theta_o + \varepsilon)$

Using the usual, first order approximations for sine and cosine of small angles, these terms can be approximated by the following

$$\beta_{++} \cong - \frac{\sin \theta_o + \varepsilon/2 \cos \theta_o}{1 + 2 \exp(-Y/2)[\cos\theta_o - \varepsilon/2 \sin \theta_o] + \exp(-Y)}$$

$$\beta_{+-} \cong - \frac{\varepsilon/2}{1 + 2\exp(-Y/2) + \exp(-Y)} \qquad\qquad (A-4)$$

$$\beta_{-+} \cong - \frac{\varepsilon/2}{1 - 2\exp(-Y/2) + \exp(-Y)}$$

$$\beta_{--} \cong - \frac{\sin \theta_o + \varepsilon/2 \cos \theta_o}{1 - 2\exp(-Y/2)(\cos \theta_o + \varepsilon/2\sin \theta_o) + \exp(-Y)}$$

With these first order approximations, the behavior of each β term can be examined at $Y = 0$

$$\beta_{++}\Big|_{Y=0} \cong - \frac{\sin \theta_o + \varepsilon/2 \cos \theta_o}{2(1 + \cos \theta_o - \varepsilon/2 \sin \theta_o)}$$

$$\beta_{--}\Big|_{Y=0} \cong - \frac{\sin \theta_o + \varepsilon/2 \cos \theta_o}{2(1 - \cos \theta_o - \varepsilon/2 \sin \theta_o)}$$

$$\beta_{+-}\Big|_{Y=0} \cong - \frac{\varepsilon}{8}$$

$$\beta_{-+}\Big|_{Y=0} \cong \text{(denominator goes to zero)}$$

From this first order analysis, it is seen that three of the four β terms have the potential of dominating the $p(t)$ solution at small values of Y. These terms will now be examined to second order in the denominator. (The numerator contains no difference terms and so the first order

approximation for small ε will be retained for simplicity.)

Considering β_{-+}, the following approximations are used

$$\cos\left(-\varepsilon/2\right) \cong 1 - \frac{\varepsilon^2}{8}$$

$$\exp\left(-Y\right) \cong 1 - Y + \frac{Y^2}{2}$$

to obtain

$$\beta_{-+} \cong -\frac{2\varepsilon}{Y^2 + \varepsilon^2 - \frac{Y\varepsilon^2}{2} + \frac{Y^2\varepsilon^2}{8}}$$

Neglecting terms higher than second order in the small

quantities Y and ε,

$$\beta_{-+} \cong -\frac{2\varepsilon}{Y^2 + \varepsilon^2(1-Y/2)} \tag{A-5}$$

which approaches a finite value as Y approaches 0,

$$\lim_{Y \to 0} \beta_{-+} = -\frac{2}{\varepsilon}$$

Using an identical approach yields the following results

for β_{++} and β_{--}:

$$\lim_{Y \to 0} \beta_{++} = -\frac{\sin\theta_o + \varepsilon/2 \cos\theta_o}{2(1+\cos\theta_o + \varepsilon^2/8 \cos\theta_o - \varepsilon/2\sin\theta_o)} \tag{A-6}$$

$$\lim_{Y \to 0} \beta_{--} = -\frac{\sin\theta_o + \varepsilon/2\cos\theta_o}{2(1-\cos\theta_o + \varepsilon^2/8\cos\theta_o - \varepsilon/2\sin\theta_o)} \tag{A-7}$$

A detailed analysis of the β_{++} and β_{--} terms was not

done, however, they assume the following maximum values at

$Y = 0$:

$$\beta_{++} = \frac{2}{\varepsilon} \quad \text{at} \ \theta_o = \pi \ ; \ Y = 0$$

$$\beta_{--} = -\frac{2}{\varepsilon} \quad \text{at} \ \theta_o = 0; \ Y = 0$$

Since these limiting values are the same as for the β_{-+} term and will be less for other values of θ_o, it is concluded that the β_{-+} term will dominate β for the early diffracted pulse.

For comparison, the $(rr_o \sinh Y)^{-1}$ term can also be approximated for Y approaching zero as

$$(rr_o \sinh Y)^{-1} = \frac{1}{rr_o}(Y + \frac{Y^3}{6} + \ldots)^{-1} \cong \frac{1}{rr_o Y} \qquad (A-8)$$

Comparing Equations A-8 and A-5 leads to the conclusion that the $rr_o \sinh Y$ factor will determine the time dependence of the early diffracted pulse only when ε^2 is much greater than Y^2 and Y is much less than 1.

In terms of the basic diffraction problem geometry, this means that as the receiver approaches the shadow boundary from inside the shadow (ε approaches zero), the time region over which the $(rr_o \sinh Y)^{-1}$ factor will determine the time dependence of $p(t)$ becomes very small. This region must be determined, based on the geometry, before an analytical plus digital approach such as outlined by Medwin [Ref. 8] can be employed. This is illustrated in Figures A-1, A-2 which show the behavior of $(\sinh Y)^{-1}$ and β_{-+} as a function of Y for two values of ε. Since the B-T solution contains the product of these terms, one can be assumed to be the factor which determines the time dependence only when the slope of the other

121
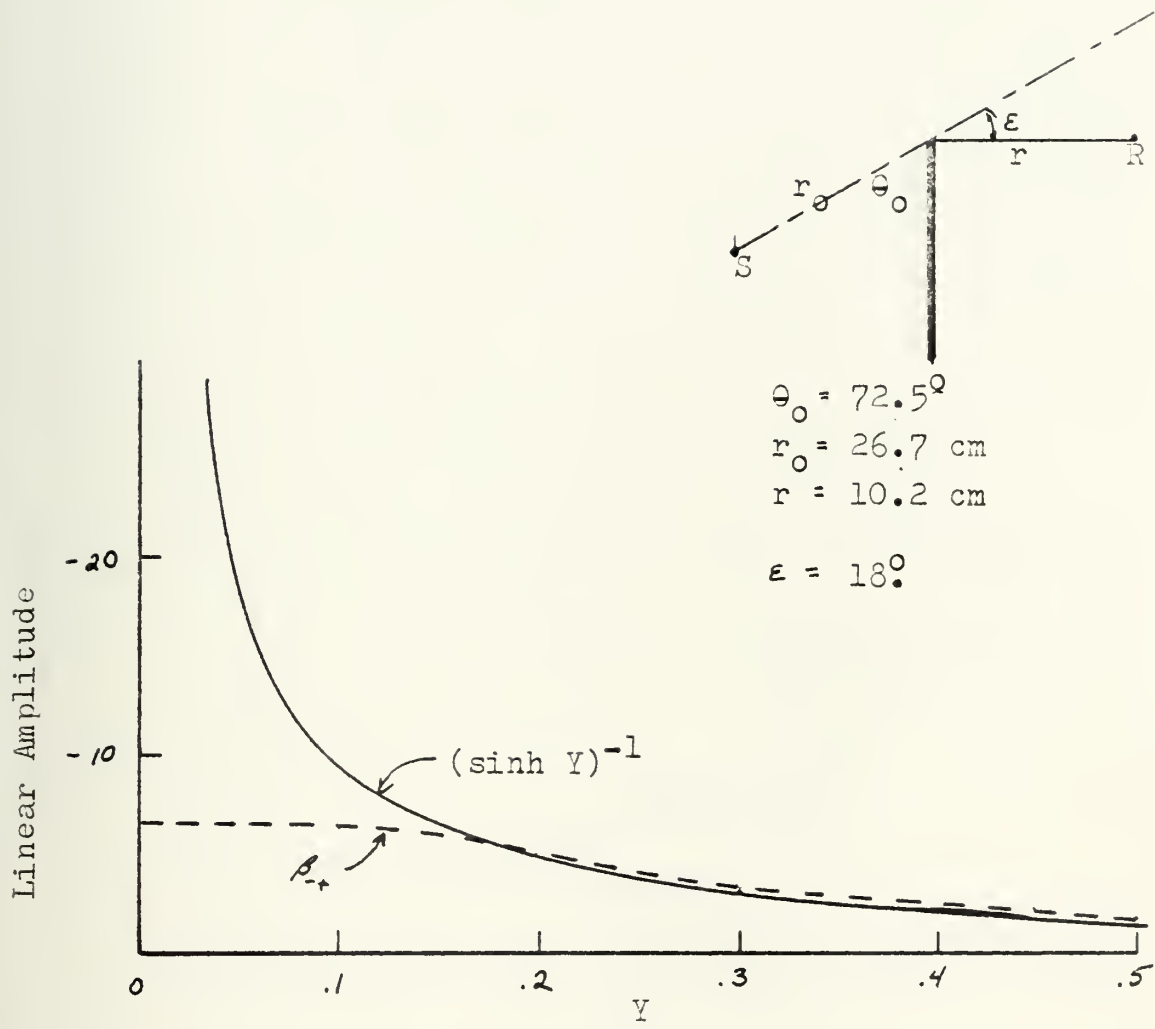
Figure A-1 Behavior of the B-T Solution Near the Shadow Boundary, $\varepsilon = 18°$.
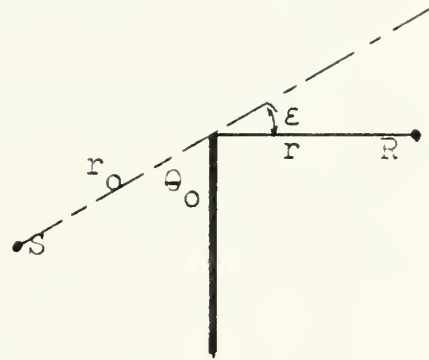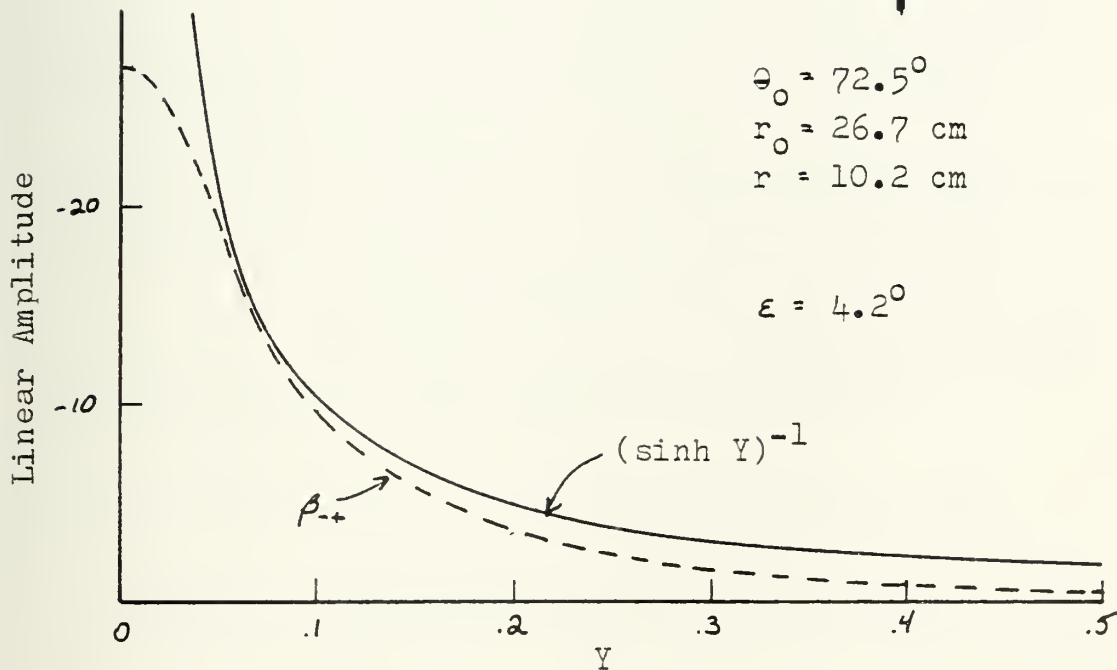
Figure A-2 Behavior of the B-T Solution Near the Shadow Boundary, $\varepsilon = 4.2°$.

123

approaches zero. Based on this, the $(\sinh Y)^{-1}$ term would dominate below approximately $Y = .1$ for $\varepsilon = 18°$ and below $Y = .01$ for $\varepsilon = 4.2°$.

LIST OF REFERENCES

1. Sommerfield, A., *Mathematische Annalen*, v. 47, p. 317, 1896.

2. Carslaw, H. S., *Proceedings of the London Mathematical Society*, v. 30, p. 121, 1899.

3. Macdonald, H. M., "A Class of Diffraction Problems", *Proceedings of the London Mathematical Society*, v. 14, p. 410, 1915.

4. Biot, M. A. and Tolstoy, I., "Formulation of Wave Propagation in Infinite Media by Normal Coordinates with an Application to Diffraction", *The Journal of the Acoustical Society of America*, v. 29, p. 381, 1957.

5. Isei, T., Embleton, T. F. W., and Piercy, J. E., "Noise Reduction by Barriers on Finite Impedance Ground", *The Journal of the Acoustical Society of America*, v. 67, p. 46, 1980.

6. Baker, B. B. and Copson, E. T., *The Mathematical Theory of Huygen's Principle*, 2nd ed., Oxford. 1950.

7. Tolstoy, I., *Wave Propagation*, McGraw-Hill, 1973.

8. Medwin, H., "Shadowing by Finite Noise Barriers", *The Journal of the Acoustical Society of America*, (to be published in the April 1981 issue).

9. Watson, G. N., *A Treatise on the Theory of Bessel Functions*, 2nd ed., The Macmillan Company, 1945.

10. Clay, C. S. and Medwin, H., *Acoustical Oceanography: Principles and Applications*, John Wiley and Sons, 1977.

11. Kawai, T., Fujimoto, K., and Itow, T., "Noise Propagation Around a Thin Half-Plane", *Acustica*, v.38, p. 313, 1977.

12. Bremhorst, J. H., *Impulse Wave Diffraction by Rigid Wedges and Plates*, M. S. Thesis, Naval Postgraduate School, Monterey, CA., 1978.

13. Bowman, J. J., Senior, T. B. A., and Uslenghi, P. L. E., *Electromagnetic and Acoustic Scattering by Simple Shapes*, North-Holland Publishing Co., Amsterdam, 1969.

14.   Decker, W., Backscatter from a Composite Rough Surface,
      M. S. Thesis, Naval Postgraduate School, Monterey, CA.,
      Dec. 1980.

15.   Frederiksen, E., "Condenser Microphones Used as Sound
      Sources", Bruel and Kjaer Technical Review, No. 3,
      1977.

16.   Keller, J. B., "Diffraction by an Aperture", Journal
      of Applied Physics, v. 28, p. 426, 1957.

17.   Hutchins, D. L., and Kouyoumjian, R. G., "Calculation of
      the Field of a Baffled Array by the Geometrical Theory
      of Diffraction", The Journal of the Acoustical Society
      of America, v. 45, p. 485, 1969.

INITIAL DISTRIBUTION LIST

No. Copies

1. Library, Code 0142   2
   Naval Postgraduate School
   Monterey, California 93940

2. Department Chairman, Code 61   2
   Department of Physics and Chemistry
   Naval Postgraduate School
   Monterey, California 93940

3. Professor H. Medwin, Code 61Md
   Department of Physics and Chemistry   6
   Naval Postgraduate School
   Monterey, California 93940

4. Professor K. Woehler, Code 61Wh
   Department of Physics and Chemistry   1
   Naval Postgraduate School
   Monterey, California 93940

5. Professor C. S. Clay   1
   University of Wisconsin
   1215 W. Dayton Street
   Madison, Wisconsin 53706

6. Gary M. Jebsen   1
   Code 1932
   David Taylor Naval Ship R&D Center
   Bethesda, MD 20084

7. Director of Defense Research and Engineering   1
   Office of the Secretary of Defense
   Washington, D.C. 20301
   ATTN: Office, Assistant Director (Research)

8. Professor I. Tolstoy   1
   Knockvennie, Castle Douglas
   S. W. SCOTLAND

9. Professor K. Gray, Code 62Gy   1
   Department of Electrical Engineering
   Naval Postgraduate School
   Monterey, California 93940

10.   Defense Technical Information Center   2
      Cameron Station
      Alexandria, Virginia 22314

11.   Director   6
      Naval Research Laboratory
      Washington, D.C. 20375
      ATTN: Library, Code 2620

12.   Office of Naval Research
      Arlington, Virginia 22217
      ATTN: (Code 480)   3
      ATTN: (Code 460)   1
      ATTN: (Code 102-OS)   1
      ATTN: (Code 102IP)   6

13.   Dr. M. Sevik   1
      Code 19
      David Taylor Naval Ship R&D Center
      Bethesda, MD 20084

14.   Mr. J. F. O'Donnell   1
      Code 193
      David Taylor Naval Ship R&D Center
      Bethesda, MD 20084

15.   Dr. W. G. Neubauer, Code 8132   1
      Naval Research Laboratory
      4555 Overlook Avenue
      Washington, D.C. 20375

16.   Dr. J. Piercy   1
      Physics Division
      National Research Council
      Ottawa, Ontario K1A OS1
      CANADA

17.   Dr. S. Hayek   1
      Pennsylvania State University
      224 Hammond
      University Park, PA 16802

18.   Dr. Tony F. W. Embleton   1
      Department of Physics
      National Research Council
      Montreal Road
      Ottawa, Ontario K1A OS1
      CANADA

No. Copies

19.   Ms. Emily Childs   1
      Code 61
      Department of Physics and Chemistry
      Naval Postgraduate School
      Monterey, California 93940